

Islamic University of Gaza

High Studies Deanship

Faculty of Engineering

Civil Engineering Department

Design and Rehabilitation of Structures



الجامعة الإسلامية - غزة

عمادة الدراسات العليا

كلية الهندسة

قسم الهندسة المدنية

تصميم وتأهيل المنشآت

نمذجة تأثير أحمال الانفجار على مبنى خرساني باستخدام برنامج LS-DYNA

Numerical Modeling of Blast Loads effects on a Reinforced Concrete Structure Using LS-DYNA Software

Submitted by:

Mahmoud L. R. Shaheen

Supervised by:

DR. Eng. Mohammed Arafa

DR. Eng. Mamoun Alqedra

A thesis submitted in partial fulfillment of the requirement for degree of Master of Science in Civil Engineering

Design and rehabilitation of structures

2015

إقرار

أنا الموقع أدناه مقدم الرسالة التي تحمل العنوان:

نمذجة تأثير أحمال الانفجار على مبنى خرساني باستخدام برنامج LS-DYNA

Numerical Modeling of Blast Loads effects on a Reinforced Concrete Structure Using LS-DYNA Software

أقر بأن ما اشتملت عليه هذه الرسالة إنما هو نتاج جهدي الخاص، باستثناء ما تمت الإشارة إليه
حيثما ورد، وإن هذه الرسالة ككل أو أي جزء منها لم يقدم من قبل لنيل درجة أو لقب علمي أو
بحثي لدى أي مؤسسة تعليمية أو بحثية أخرى.


DECLARATION

The work provided in this thesis, unless otherwise referenced, is the
researcher's own work, and has not been submitted elsewhere for any
other degree or qualification

Student's name:

اسم الطالب/ة: محمود لطفي شاهين

Signature:

التوقيع: 

Date:

التاريخ: 10 نوفمبر 2015



نتيجة الحكم على أطروحة ماجستير

بناءً على موافقة شئون البحث العلمي والدراسات العليا بالجامعة الإسلامية بغزة على تشكيل لجنة الحكم على أطروحة الباحث/ محمود لطفي رشيد شاهين لنيل درجة الماجستير في كلية الهندسة قسم الهندسة المدنية- تصميم وتأهيل المنشآت وموضوعها:

نمذجة تأثير أحمال الانفجار على مبنى خرساني باستخدام برنامج LS-DYNA Numerical Modelling of Blast Loads effects on a Reinforced Concrete Structure Using LS-DYNA Software

وبعد المناقشة العلنية التي تمت اليوم الثلاثاء 14 محرم 1437هـ، الموافق 2015/10/27م الساعة الواحدة ظهراً بمبنى القدس، اجتمعت لجنة الحكم على الأطروحة والمكونة من:

.....	مشرفاً و رئيساً	د محمد حسني عرفة
.....	مشرفاً	د. مأمون عبد الحميد القدرة
.....	مناقشاً داخلياً	د. مازن طه أبو الطيف
.....	مناقشاً خارجياً	د. مصطفى ماهر الطيب

وبعد المداولة أوصت اللجنة بمنح الباحث درجة الماجستير في كلية الهندسة/ قسم الهندسة المدنية- تصميم وتأهيل المنشآت.

واللجنة إذ تمنحه هذه الدرجة فإنها توصيه بتقوى الله والبروم طاعته وأن يسخر علمه في خدمة دينه ووطنه.

والله ولي التوفيق،،،

نائب الرئيس لشئون البحث العلمي والدراسات العليا

أ.د. عبدالرؤف علي المناعمة

Dictation

To my beloved mother, Allah bless her soul

To my father

To my wife and daughters

To my brothers and sisters,

To my friends,

For their endless support

Acknowledgments

I thank almighty Allah for giving me patience, strength, and determination to accomplish this work.

I also would like to express my sincere appreciation to my supervisors, Dr. Mohammed Arafa and Dr. Mamoun AlQedra for their guidance and strong support throughout the duration of this thesis.

Deep thanks and gratitude are due to my father, Mr. Lotfy Shaheen and my mother for their infinite support and encouragement.

I would like to express my thanks to my wife for her patience and support during the time in which this work was done and to my daughters for bringing joy to my life.

I also thank my brothers, sisters, and my friends for their encouragement.

Abstract

Explosions near buildings can cause catastrophic damages on the building external and internal frames, and most important can cause injuries and loss of life to the occupants of these buildings. Due to these extreme conditions, efforts have been made in the last few decades to develop methods to evaluate the pressure loads generated from explosions and the structural response to these loads and to enhance the design of the structures to withstand it. Experiments on explosions can be very expensive, dangerous and time consuming compared to simulation using finite element analysis software.

This study aims at modeling and analyzing a reinforced concrete structure under blast loading using finite element software LS-DYNA. The simulated structure consists of four columns supporting one way ribbed slab, designed to withstand regular loads. It was modeled using LS-Prepost and analyzed using LS-DYNA. The concrete and steel were represented using solid volume elements. The material models of concrete and steel were carefully chosen to represent the actual behavior of both materials.

The verification of the developed model was carried out by comparing its deflection and spalling results with those obtained by reliable field experimental tests. The verification process indicated a close agreement between the results of the developed model and those obtained from actual experiments.

Consequently, the verified model was utilized to study the effect of blast loading on a 3×3 m single story building, where the blast was in the middle of the building. The model was analyzed for two milliseconds. The blast wave reached the slab first then reached the columns causing deflection. The effect of increasing concrete strength was studied. The deflection of the structure was decreased slightly when higher strength concrete was used, and the concrete withstood higher stresses. The effect of changing the blast location was also investigated.

المخلص

الانفجارات بالقرب من المباني يمكن أن تحدث أضراراً بالغة لأجزاء المبنى من الداخل والخارج، والأهم من ذلك أنها يمكن أن تحدث إصابات لساكلي هذه المباني قد تصل إلى فقدان الحياة. لذلك وبسبب هذه الأحمال غير التقليدية، كثير من الجهد تم بذله في العقود القليلة الماضية لتطوير طرق لتقدير الأحمال الناتجة عن الانفجارات وكذلك تقدير مدى استجابة المنشآت لها، وذلك لتحسين تصميم المباني لتحملها. التجارب على الانفجارات مكلفة بشكل كبير وفيها الكثير من الخطورة ومستهلكة للوقت مقارنة بمحاكاتها على برامج التحليل الإنشائي باستخدام طريقة العناصر المحددة.

هذا البحث يهدف إلى نمذجة وتحليل مبنى خرساني معرض لأحمال الانفجارات باستخدام برنامج التحليل بالعناصر المحددة LS-DYNA.

النموذج عبارة عن مبنى يتكون من أربع أعمدة يرتكز عليها سقف والمبنى مصمم لتحمل الأحمال العادية. تم عمل النموذج باستخدام برنامج LS-Prepost وتم تحليله باستخدام برنامج LS-DYNA. تم استخدام عناصر سداسية منتظمة لتمثيل الخرسانة، وتم استخدام عناصر سداسية وثمانية غير منتظمة لتمثيل حديد التسليح. تم اختيار نماذج مواد للخرسانة والحديد بدقة حتى تمثل التصرف الحقيقي لكلا المادتين.

تم التحقق من كفاءة النموذج بواسطة مقارنة نتائج انحناء وتقنت الخرسانة من اختبارات موثقة لعمود يتعرض لانفجار مع نتائج نمذجة العمود نفسه باستخدام LS-DYNA. نتائج التحليل كانت متقاربة جداً مع نتائج الاختبارات.

تم استخدام النموذج لدراسة تأثير أحمال الانفجار على مبنى خرساني من طابق واحد أبعاده 3 × 3 متر. وتم تحليل النموذج لمدة جزئين من الثانية. وصلت موجة الانفجار الى المبنى وعناصره وتحركت خلالها مسببة انحناءات واضحة. بعد ذلك تم دراسة أثر زيادة قوة الخرسانة على نتائج التحليل والتي تسببت بتقليل الانحناءات قليلاً وكذلك زادت قدرة الخرسانة على تحمل الاجهادات، وكذلك تم دراسة أثر تغيير مكان الانفجار على نتائج التحليل.

Table of contents

Dictation	I
Acknowledgments	II
Abstract.....	III
المخلص	IV
Table of contents	V
List of Tables	VIII
List of Figures	X
List of Abbreviations and Symbols.....	XIV
Chapter 1: Introduction.....	1
1.1 Background.....	1
1.2 Problem statement	2
1.3 Aim and objectives.....	2
1.4 Methodology	2
1.5 Contents of thesis	3
Chapter 2: Literature Review	4
2.1 Overview	4
2.2 Explosions.....	4
2.2.1 Unconfined explosions	4
2.2.2 Confined explosions.....	5
2.3 Shock wave phenomena	6
2.4 TNT equivalency.....	8
2.5 Prediction of blast wave parameters.....	9
2.6 Dynamic response of structures to blast loads.....	11
2.7 Modeling techniques for blast loads.....	13
2.7.1 Empirical blast method.....	13
2.7.2 Multi Material Arbitrary Lagrangian Eulerian (MM-ALE) method....	13
2.7.3 Coupling of empirical and MM-ALE method	14
2.8 Previous studies.....	14

2.9	Summery.....	18
Chapter 3: Finite Element Modeling Using LS-DYNA		19
3.1	Finite Element Method.....	19
3.2	Modeling using LS-DYNA.....	20
3.2.1	Modeling of steel reinforcement.....	21
3.2.2	Modeling of concrete	23
3.3	Materials modeling.....	24
3.3.1	Concrete material model.....	24
3.3.2	Steel material model.....	28
3.3	Methods of including rebar in reinforced concrete.....	28
3.3.1	Smeared reinforcement.....	28
3.3.2	Shared nodes method	29
3.3.3	Penalty methods	29
3.4	Modeling of blast loads	29
Chapter 4: Model Validation		33
4.1	Introduction.....	33
4.2	Experimental test data	33
4.2.1	LS-DYNA model	34
4.2.2	Experimental test results.....	37
4.2.3	The FE analytical results	37
Chapter 5: Numerical Model Applications.....		40
5.1	Introduction.....	40
5.2	Model structure geometry.....	40
5.2.1	Structure reinforcement details	42
5.2.2	Building the model in LS-Prepost.....	43
5.3	Internally blasted model	45
5.3.1	Stress distribution at the columns	45
5.3.2	Stress distribution at the RC slab	47
5.3.3	Deflections of columns.....	52
5.3.4	Deflections of slab members	54
5.4	Effect of concrete strength on the behavior of the structure.....	58

5.4.1	Stress distribution of the columns with concrete strength of 58 MPa .	58
5.4.2	Stress distribution at the 58 MPa compressive strength concrete slab.	60
5.4.3	Deflection of columns with 58 MPa compressive strength concrete...	63
5.4.4	Deflection of slab members with 58 MPa concrete Strength	65
5.5	Effect of changing the explosion location	68
5.5.1	Stress distribution of externally blasted columns	69
5.5.2	Stress distribution of the slab members.....	72
5.5.3	Deflections of columns.....	80
5.5.4	Deflection of slab members	82
Chapter 6: Conclusion and recommendations		87
6.1	Modeling RC structure under blast loading.....	87
6.2	Conclusions.....	87
6.3	Recommendations	88
References.....		89

List of Tables

Table 2.1: Heat of detonation of common explosives.....	9
Table 2.2: TNT equivalent mass factors.....	9
Table 3.1: SECTION_SOLID keyword parameters	23
Table 3.2: Material models for concrete in LS-DYNA.....	24
Table 3.3: MAT_CSCM_CONCRETE parameters.....	27
Table 3.4: MAT_PIECEWISE_LINEAR_PLASTICITY parameters.....	28
Table 3.5: Statistics of three blast-modeling methods	31
Table 3.6: LOAD_BLAST_ENHANCED keyword parameters	32
Table 4.1: Concrete model parameters values for the verification model.....	35
Table 4.2: Reinforcement steel model parameters values for the verification model	35
Table 4.3: Blast load parameters values for verification model	35
Table 4.4: Statistics of verification model.....	37
Table 5.1: Steel material model parameters values for the case study.....	44
Table 5.2: Concrete material model parameters values for the case study.....	44
Table 5.3: Blast loading parameters values for the case study	44
Table 5.4: Statistics of the case study.....	44
Table 5.5: Comparison of column maximum tension stresses between columns with 29 MPa and 58 MPa compressive strength concrete	58
Table 5.6: Comparison of column maximum compression stresses between columns with 29 MPa and 58 MPa compressive strength concrete.....	59
Table 5.7: Comparison of the tension stresses in the 58 MPa and 29 MPa strength concrete slab members	61
Table 5.8: Comparison of the compression stresses in the 58 MPa and 29 MPa strength concrete slab members	62
Table 5.9: Comparison of the Von-Mises stresses between the 29 MPa and 58 MPa strength concrete slab members	63
Table 5.10: Comparison of the deflection in the 58 MPa and 29 MPa strength concrete columns.....	65
Table 5.11: Comparison of the deflection values for the 58 MPa and 29 MPa concrete strength slab members	67
Table 5.12: Maximum stresses value for externally blasted columns.....	72

Table 5.13: Externally blasted slab members tension stresses	75
Table 5.14: Externally blasted slab members compression stresses	78
Table 5.15: Externally blasted slab members Von-Mises stresses	79
Table 5.16: Maximum deflection values for externally blasted slab members	86

List of Figures

Figure 2.1: (a) Free air burst, (b) Air burst, (c) Surface burst	5
Figure 2.2: (a) Fully vented explosion, (b) Partially confined explosions, (c) Fully confined explosions	6
Figure 2.3: Interaction of air blast with a structure	7
Figure 2.4: Free air burst pressure - time variation	7
Figure 2.5: Idealized pressure - time variation	8
Figure 2.6: Blast wave parameters for positive phase free air blast wave	11
Figure 2.7: (a) SDOF system, (b) Blast loading	12
Figure 2.8: Strain rates for several loading conditions	12
Figure 2.9: Stress-strain curves of concrete at different strain rates	13
Figure 3.1: Simple finite elements: (a) line elements, (b) plane elements, (c) volume elements	20
Figure 3.2: Steel bar modeling: (a) volume tube before meshing, (b) elements of steel bar with nodes, (c) irregular hexahedral and pentahedral elements	22
Figure 3.3: Steel bars and stirrups modeling (a) creating, (b) meshing	22
Figure 3.4: Concrete modeling and meshing	23
Figure 3.5: Concrete model yield surface in two dimensions	26
Figure 3.6: Concrete model yield surface in three dimensions	26
Figure 3.7: Strain softening and modulus reduction for the model	27
Figure 3.8: Effective plastic strain versus yield stress for material type 24	28
Figure 3.9: Schematic of empirical method in LS-DYNA	30
Figure 3.10: MM-ALE modeling method in LS-DYNA	30
Figure 3.11: Coupling of empirical and MM-ALE method in LS-DYNA	31
Figure 4.1: Dimensions and reinforcement details of column 3A	33
Figure 4.2: Field test setup	34
Figure 4.3: Boundary conditions and the location of the explosive	36
Figure 4.4: Deflection and spall of test column	37
Figure 4.5: Blast wave propagation through the column at: (a) 0.21 milliseconds, (b) 0.60 milliseconds	38
Figure 4.6: Pressure profile for the column point of contact with the blast wave	38

Figure 4.7: Isoperimetric view of the verification model with the deflection	39
Figure 4.8: Maximum deflection in the direction of the blast versus time	39
Figure 5.1: Schematic of the structure and the location of explosive	40
Figure 5.2: Slab dimensions in meters (a) top view, (b) section A-A.....	41
Figure 5.3: Columns Dimensions in meters: (a) Front view, (b) Side view	41
Figure 5.4: Slab reinforcement details: (a) Main beam (B.1) detailing, (b) Secondary beam (B.2) detailing, (c) Section A-A details.....	42
Figure 5.5: Columns reinforcement details	43
Figure 5.6: Blast wave pressure on slab and columns.....	45
Figure 5.7: Columns tension stresses	46
Figure 5.8: Column compression stresses	46
Figure 5.9: Column maximum Von-Mises stress	47
Figure 5.10: Stresses of a failed column element	47
Figure 5.11: Slab members tension x -stresses	48
Figure 5.12: Slab members tension y -stresses	49
Figure 5.13: Slab members tension z -stresses	49
Figure 5.14: Slab members compression x -stresses	50
Figure 5.15: Slab members compression y -stresses	50
Figure 5.16: Slab members compression z -stresses	51
Figure 5.17: Slab members Von-Mises stresses	52
Figure 5.18: Contours of x -axis deflection	52
Figure 5.19: Columns x -axis deflection.....	53
Figure 5.20: Contours of y -axis deflection	53
Figure 5.21: Columns y -deflection.....	54
Figure 5.22: Slab members maximum x -axis deflections.....	54
Figure 5.23: Contours of x -axis deflection for slab members.....	55
Figure 5.24: Slab members maximum y -axis deflections.....	55
Figure 5.25: Contours of y -axis deflection for slab members.....	56
Figure 5.26: Slab members minimum z -axis deflections	56
Figure 5.27: Slab members maximum z -axis deflections.....	57
Figure 5.28: Contours of z -deflection for slab members	57

Figure 5.29: Column with 58 MPa compressive strength concrete Von-Mises stresses	59
Figure 5.30: Stresses of a failed element in the column with 58 MPa concrete compressive strength	60
Figure 5.31: 58 MPa strength concrete structure contours of x -deflection	64
Figure 5.32: Structure with 58 MPa concrete strength contours of y -displacement ..	64
Figure 5.33: Contours of x -axis deflection for slab members with 58 MPa strength concrete.....	65
Figure 5.34: Contours of y -displacement for slab members with 58 MPa concrete strength	66
Figure 5.35: Contours of z -displacement for slab members with 58 MPa concrete strength	66
Figure 5.36: Schematic of the structure and the location of external explosion.....	68
Figure 5.37: External blast wave pressure on structure.....	68
Figure 5.38: Front columns tension stresses	69
Figure 5.39: Front columns compression stresses	69
Figure 5.40: Front columns Von-Mises stresses.....	70
Figure 5.41: Rear columns tension stresses	70
Figure 5.42: Rear columns compression stresses.....	71
Figure 5.43: Rear columns Von-Mises stresses	71
Figure 5.44: Stresses of a failed element in the front column	72
Figure 5.45: Externally blasted slab members tension x -stresses	73
Figure 5.46: Externally blasted slab members tension y -stresses	74
Figure 5.47: Externally blasted slab members tension z -stresses	74
Figure 5.48: Externally blasted slab members compression x -stresses.....	76
Figure 5.49: Externally blasted slab members compression y -stresses.....	76
Figure 5.50: Externally blasted slab members compression z -stresses	77
Figure 5.51: Externally blasted slab members Von-Mises stresses	79
Figure 5.52: Externally blasted front columns deflection	80
Figure 5.53: Externally blasted front columns deflection contours: (a) in x -direction, (b) in y -direction.....	81
Figure 5.54: Externally blasted rear columns deflection.....	81

Figure 5.55: Externally blasted rear columns deflection contours: (a) in x -direction, (b) in y -direction	82
Figure 5.56: Externally blasted slab members maximum x -deflections.....	83
Figure 5.57: Externally blasted slab x -deflection contours	83
Figure 5.58: Externally blasted slab members maximum y -deflections.....	84
Figure 5.59: Externally blasted slab y -deflection contours	84
Figure 5.60: Externally blasted slab members maximum z -axis deflections.....	85
Figure 5.61: Externally blasted slab members minimum z -deflections	85
Figure 5.62: Externally blasted slab z -deflection contours.....	86

List of Abbreviations and Symbols

ALE	Arbitrary Lagrangian Eulerian
CSCM	Continuous Surface Cap Model
DOT	Department of Transportation
FEA	Finite Element Analysis
FEM	Finite Element Method
F_m	Idealized explosion maximum force
FRP	Fiber Reinforced Polymers
H_{exp}^d	The heat produced in the detonation of the chosen explosive
H_{TNT}^d	The heat produced in the detonation of TNT explosive
HSC	High Strength Concrete
I	Idealized shock wave positive phase impulse
i_s	Shock wave positive incident impulse
i_s^-	Shock wave negative incident impulse
MM-ALE	Multi Material Arbitrary Lagrangian Eulerian
NCHRP	National Cooperative Highway Research Program
NSC	Normal Strength Concrete
P_{so}	Shock wave positive peak over pressure
P_{so}^-	Shock wave negative peak over pressure
R	Actual distance between the explosion and the affected object
RC	Reinforced Concrete
SDOF	Single Degree of Freedom
t_A	Shock wave front arrival time
t_d	Idealized shock wave positive phase duration
TNT	Trinitrotoluene
t_o	Shock wave positive phase duration
t_o^-	Shock wave negative phase duration
W	Explosive weight
W_{exp}	Weight of the chosen explosive
W_{TNT}	Weight of TNT explosive
Z	Scaled distance between the explosion and the affected object

Chapter 1: Introduction

1.1 Background

A bomb explosion in or near a structure can cause disastrous damages on the structure and on the internal objects, and most important can cause injuries and loss of life to occupants due to direct blast or structure collapse and fragments. Efforts have been made in the past few decades to develop methods to predict blast loading, predict the structural response to such extreme loads, and design the structure to resist or to withstand these loads and to prevent progressive collapse (Almusallam et al. 2010).

An explosion is the result of a very rapid release of a large amount of energy; this release is caused by physical, chemical, or nuclear events (Baker et al. 1983).

When an explosion takes place, the expansion of the hot gases produces a pressure wave in the surrounding air called the shock wave, which moves away from the center of the explosion with the velocity of sound and a very high pressure in front of the wave. The hot gases and the high-pressure causes the wave to speed up to some level. After a short period, the pressure behind the front drops below the ambient pressure causing a partial vacuum in a negative phase. The front of the blast waves weakens as it progress far from the explosion center, and its velocity drops so its peak pressure, and can be treated as a sound wave (Ngo et al. 2007).

Development of finite element analysis (FEA) software tools helps a lot in the field of dynamic loads and especially blast loads, because experimental tests of blast loads on structures are very expensive and dangerous. There are many FEA Software tools available for simulation of dynamic loads such as ABAQUS, Dyna3D, AUTODYN, ANSYS, LS-DYNA, etc. In this work, LS-DYNA software is used.

LS-DYNA is a general-purpose finite element code for analyzing the large deformation static and dynamic response of structures, including structures in contact with fluids (LS-DYNA 2014). LS-DYNA contains a large library of material models and functions to link these materials. The user interface software for preprocessing and post-processing is LS-Prepost. LS-Prepost uses keywords to define material models parameters and all other functions.

1.2 Problem statement

Blast loads on structures would cause large damages especially if they are close to the main structural elements such as columns or main beams. Therefore, blast loads and its effects should be understood to design the main structural elements to withstand such loads. Using FEA software tools to model and understand the response of reinforced concrete (RC) structures under blast loading is very helpful in terms of time and cost. Further more it is very safe compared to experimental approaches.

1.3 Aim and objectives

The aim of this work is to study and numerically simulate the effect of air blast loads on a RC structure. The following objectives are set to achieve the aim of the study:

1. Develop a computer model to simulate a RC structure and the blast loads using LS-DYNA.
2. Perform a case study to determine the blast effects on the deformation and the stresses of the RC structure.
3. Determine the effect of concrete strength on the response of the RC structure.
4. Determine the effect of changing the charge location on the response of the RC structure.

1.4 Methodology

To complete this work the following steps were conducted:

Step 1: Literature review from books, papers and researches, which related to “modeling of Blast Loads on Structures”, including blast phenomena and structural response to dynamic loads.

Step 2: Study carefully LS-DYNA software and the material models for concrete and reinforcement steel implemented in it.

Step 3: Carry out a validation and verification for the model.

Step 4: Carry out numerical cases.

Step 5: Discuss the obtained results

Step 6: State recommendations and conclusion.

1.5 Contents of thesis

This thesis consists of five chapters, which are arranged in a logical sequence for the reader to follow. Chapter 2 discusses explosions types, the shock wave parameters, how to predict them and the dynamic response of concrete structures to blast loads and also discusses the techniques of numerically modeling blast loads. At the end of this chapter, some of the latest researches done in the field of blast loads prediction and simulation are listed. Chapter 3 discusses finite element method, a brief introduction about LS-DYNA software, material models description for concrete and steel reinforcement, the methods of including rebar in concrete, and the techniques of modeling blast loads on structure. Chapter 4 contains the verification model geometry and results compared to the results of experimental tests, the geometry and reinforcement details of the case study, and the results of the analysis of the case study, then studying the effect of changing concrete strength and changing the charge location on the results. And finally, chapter 5 contains the conclusion on the analysis results and the recommendations.

Chapter 2: Literature Review

2.1 Overview

Structures subjected to extreme loads including blast loads are difficult to study experimentally, and the evaluation of the damages caused by blast loads is hard to conduct. Existing RC structures mostly are not designed to resist extreme loads and since the response of these structures to such loads is unknown, it is necessary to find ways to evaluate and predict it.

Using FEA software in predicting damages caused by blast loads is widely used in the present days, this is because of the variety of material models, the ease of accessing them and changing parameters, the ability to simulate problems that is very hard to conduct in laboratories, the costless efforts compared to laboratories, and the safety of using FEA software.

2.2 Explosions

An explosion is a pressure disturbance caused by the sudden release of energy in the form of flash and high sound (Dusenberry 2010). The produced pressure moves away from the explosion center in the form of a wave called shock wave, or blast wave. The source of explosions could be physical, chemical or nuclear. Physical explosions include the sudden failure of a cylinder of compressed gas and the mixing of two liquids with different temperatures. Chemical explosions could be the rapid release of energy caused by the reaction between two materials like the rapid oxidation of the fuel, some materials needs a shock to react and release energy. Nuclear explosion is the most dangerous explosions and results from the formation of new nuclei by redistribution of the protons and neutrons inside the nuclei of a material.

Explosions can be categorized based upon the confinement of the explosive charge to the following types: (Army et al. 1990)

2.2.1 Unconfined explosions

In this group the shock wave reaches the structure directly with or without reflection and amplification as shown in Figure 2.1, the unconfined explosions are divide into:

2.2.1.1 Free air burst explosions

The explosion takes place far above the building so that the blast wave propagates away from the explosion center and strikes the structure directly without reflection and amplification of the initial shock wave.

2.2.1.2 Air burst explosions

The explosion takes place above the building so that the produced shock wave reaches the ground surface and reflects before reaching the structure.

2.2.1.3 Surface burst explosions

The explosion takes place on or near the ground so that the produced shock wave reflects and amplifies and merged with the reflected wave to reach the structure.

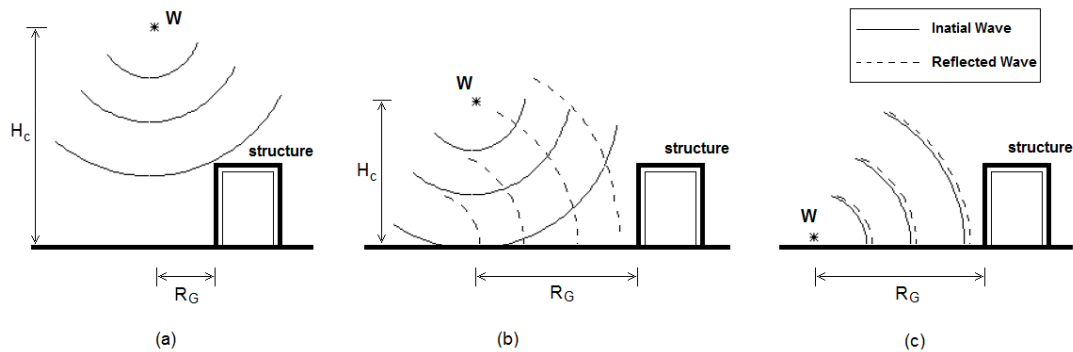


Figure 2.1: (a) Free air burst, (b) Air burst, (c) Surface burst (Karlos and Solomos 2013)

2.2.2 Confined explosions

In this group, the charge detonates inside a fully or partially closed structure as in Figure 2.2. The inside surfaces of the structure reflect and amplify the produced shock wave many times so that the value of the pressure increased to higher values, the confined explosions can be divided to (Koccaz et al. 2008):

2.2.2.1 Fully vented explosions

In fully vented explosion, the explosive charge detonates in a structure with one or more opened surfaces. The initial shock wave reflects and amplifies by the closed surfaces and vents to the atmosphere from the opened surfaces.

2.2.2.2 Partially confined explosions

In partially confined explosion, the explosive charge detonates in a structure with limited size openings. The initial wave is amplified by the surfaces and vents to atmosphere from the openings after a period.

2.2.2.3 Fully confined explosions

In full confined explosion, the explosive charge detonates in a total or near total closed structure.

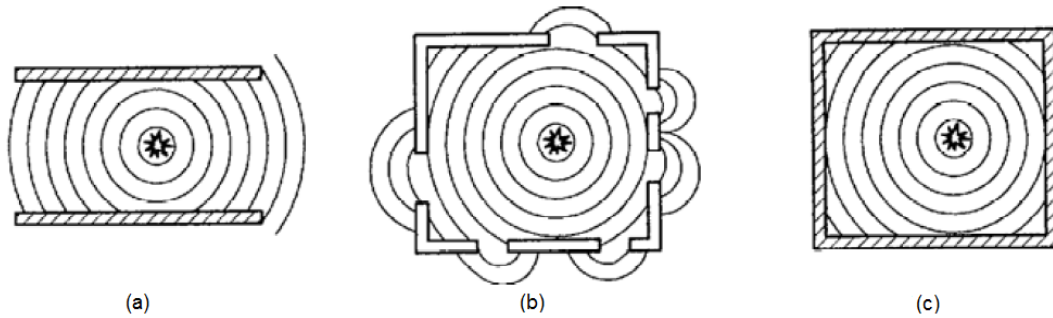


Figure 2.2: (a) Fully vented explosion, (b) Partially confined explosions, (c) Fully confined explosions (Koccaz et al. 2008)

2.3 Shock wave phenomena

The rapid release of energy generated from the detonation of an explosive charge causes a sudden increase in the pressure in the surrounding medium, like air. This pressure increase translate radially in the air in the form of a wave called shock wave. The shock wave moves away from the center of explosion in a velocity greater than the velocity of sound with a maximum pressure at the shock front, the maximum pressure is called the peak over pressure. When blast waves face an obstruction, they will reflect to amplitudes higher than their initial values. The reflection is a function of the strength of the blast and the angle of incident of the shock wave front (Marchand and Alfawakhiri 2004). Figure 2.3 shows the interaction of air blast with a structure.

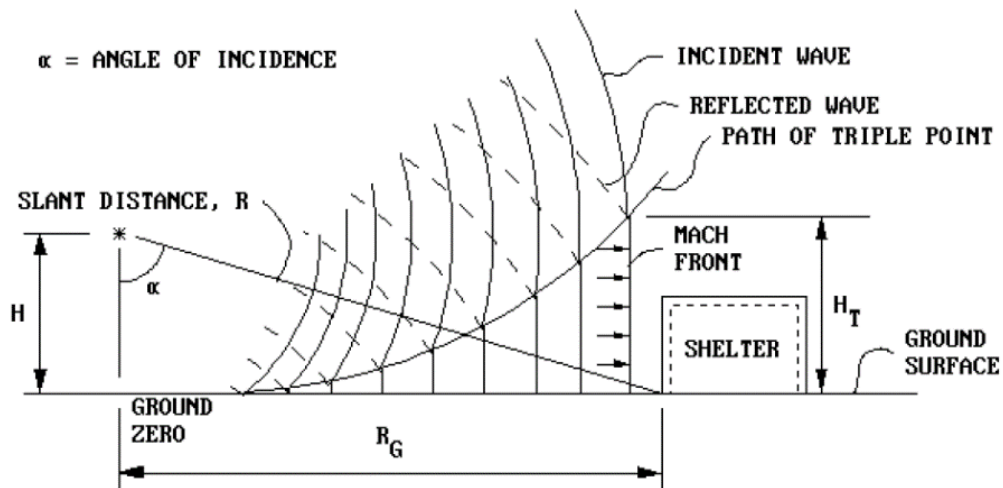


Figure 2.3: Interaction of air blast with a structure (Marchand and Alfawakhiri 2004)

The front of the blast wave weakens as it moves away from the center of the explosion, until its velocity drops to be under the velocity of sound. At any point far from the explosion center, the shock front reaches the point at time (t_A), with a maximum over pressure (P_{so}). The pressure then decreases to reach the ambient atmosphere pressure in a positive phase with duration (t_o) followed by a negative phase with duration (t_o^-) longer than the positive phase, with a maximum negative pressure (P_{so}^-) in the form of suction wave, as shown in Figure 2.4.

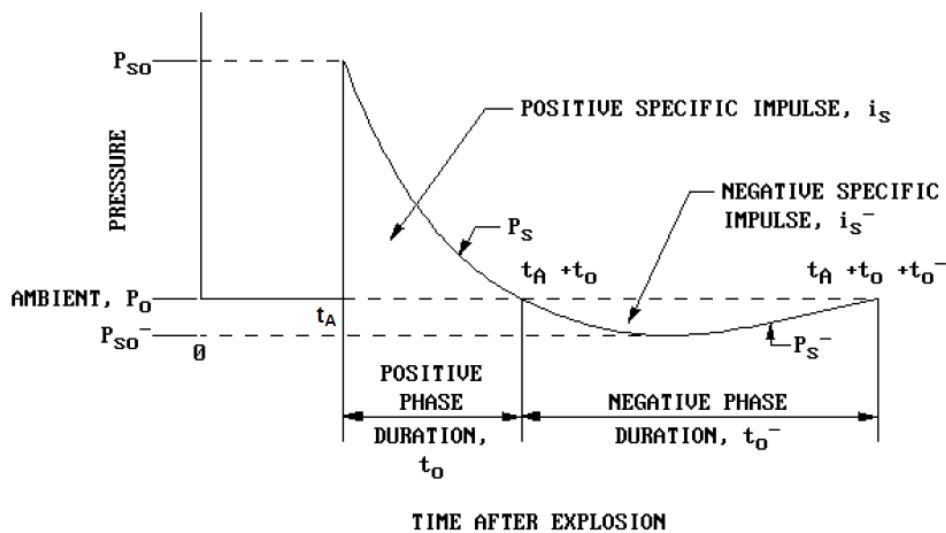


Figure 2.4: Free air burst pressure - time variation (Army et al. 1990)

The integrated area under the pressure time curve is the incident impulse detonated (i_s) for the positive phase and (i_s^-) for the negative phase, which is an important parameter in the design because it relates to the total force (per unit area) that is applied on a structure due to the blast (Karlos and Solomos 2013).

For design purposes and for the ease of using blast wave parameters, the pressure time curve is idealized as shown in Figure 2.5.

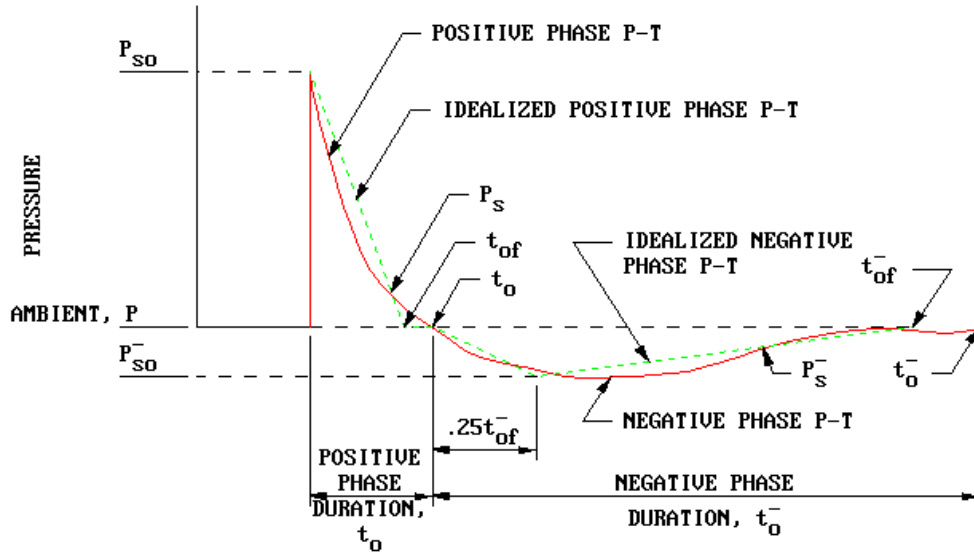


Figure 2.5: Idealized pressure - time variation (Army, Navy et al. 1990)

2.4 TNT equivalency

The wide variety of materials to produce explosions has led to the chosen of one material to represent all explosives for all the necessary calculations of blast parameters. Trinitrotoluene (TNT) was chosen because of its stable characteristics compared to other explosives. An equivalent TNT weight is computed according to equation (1) that links the weight of the TNT to the weight of the chosen explosive by the ratio of the heat produced in the detonation (karlos and solomos 2013).

$$W_{TNT} = W_{exp} \frac{H_{exp}^d}{H_{TNT}^d} \quad (1)$$

Where, W_{TNT} is the weight of TNT explosive, W_{exp} is the weight of the chosen explosive, H_{exp}^d is the heat produced in the detonation of the chosen explosive, and H_{TNT}^d is the heat produced in the detonation of TNT explosive. Table 2.1 introduces a list of common explosives and the heat of the detonation of each one.

Table 2.1: Heat of detonation of common explosives (Karlos and Solomos 2013)

Name of explosive	Heat of Detonation (MJ/Kg)
TNT	4.10 – 4.55
C4	5.86
RDX	5.13 – 6.19
PETN	6.69
PENTOLITE 50/50	5.86
NITROGLYCRIN	6.30
NITROMETHANE	6.40
NITROCELLULOSE	10.60
AMON./NIT (ANFO)	1.59

Table 2.2 shows some predetermined TNT equivalent mass factors (Dusenberry 2010). These factors can be used to determine the weight of TNT that produce the same blast wave parameters as the other explosive of certain weight.

Table 2.2: TNT equivalent mass factors (Dusenberry 2010)

Name of explosive	TNT equivalent mass factor
TNT	1.00
C4	1.37
RDX	1.10
PETN	1.27
PENTOLITE 50/50	1.42
NITROGLYCRIN	1.00
NITROMETHANE	1.00
NITROCELLULOSE	0.50
AMON./NIT (ANFO)	0.87

2.5 Prediction of blast wave parameters

Blast wave parameters have been the focus of a number of studies in the last decades. The blast parameters were usually calculated in terms of scaled distance (Z). The most commonly used scaling approach is called cube root scaling method or the Hopkinson-Cranz scaling first introduced by Hopkinson in 1915 then independently by Cranz in 1926. Thin law states that “*self-similar blast waves are produced at identical scaled distance when two explosive charge of similar geometry and of the same explosive, but of different sizes, are detonated in the same atmosphere*” (Baker, Cox et al. 1983). The

scaled distance is computed by dividing the standoff distance from the charge to the point of interest by the cube root of the charge weight,

$$\text{(Scaled Distance) } Z = \frac{R}{W^{\frac{1}{3}}} \quad (2)$$

Where R is the actual Distance from the explosion and W is the charge weight.

The estimation of peak overpressure due to spherical charge based on scaled distance was introduced in a number of studies all based on empirical data from conducted experiments (Ngo, Mendis et al. 2007), and it was introduced in Brode (1955) as:

$$P_{S0} = \frac{6.7}{Z^3} + 1 \text{ bar} \quad (P_{S0} > 10 \text{ bar}) \quad (3)$$

$$P_{S0} = \frac{0.975}{Z} + \frac{1.455}{Z^2} + \frac{5.85}{Z^3} - 0.019 \text{ bar} \quad (0.1 \text{ bar} < P_{S0} < 10 \text{ bar}) \quad (4)$$

Another expression to estimate peak over pressure was introduced in Gibson (1994) as:

$$P_{S0} = \frac{797 \left[1 + \left(\frac{Z}{4.5} \right)^2 \right]}{\sqrt{1 + \left(\frac{Z}{0.048} \right)^2} \sqrt{1 + \left(\frac{Z}{0.32} \right)^2} \sqrt{1 + \left(\frac{Z}{1.35} \right)^2}} \quad (5)$$

A publicly available manual published by the Department of Defense in USA (Army et al. 1990), contains the relationships among charge weight, stand of distance and the blast wave parameters in the form of figures and tables. The blast wave parameters in this manual is calculated in terms of scaled distance, once the scaled distance is known we can use it to get the blast wave parameters from the specified curves in Army, Navy et al. (1990). In this research, the focus is only on free air blast positive phase. Figure 2.6 introduces the parameters for positive phase of free air blast in American units.

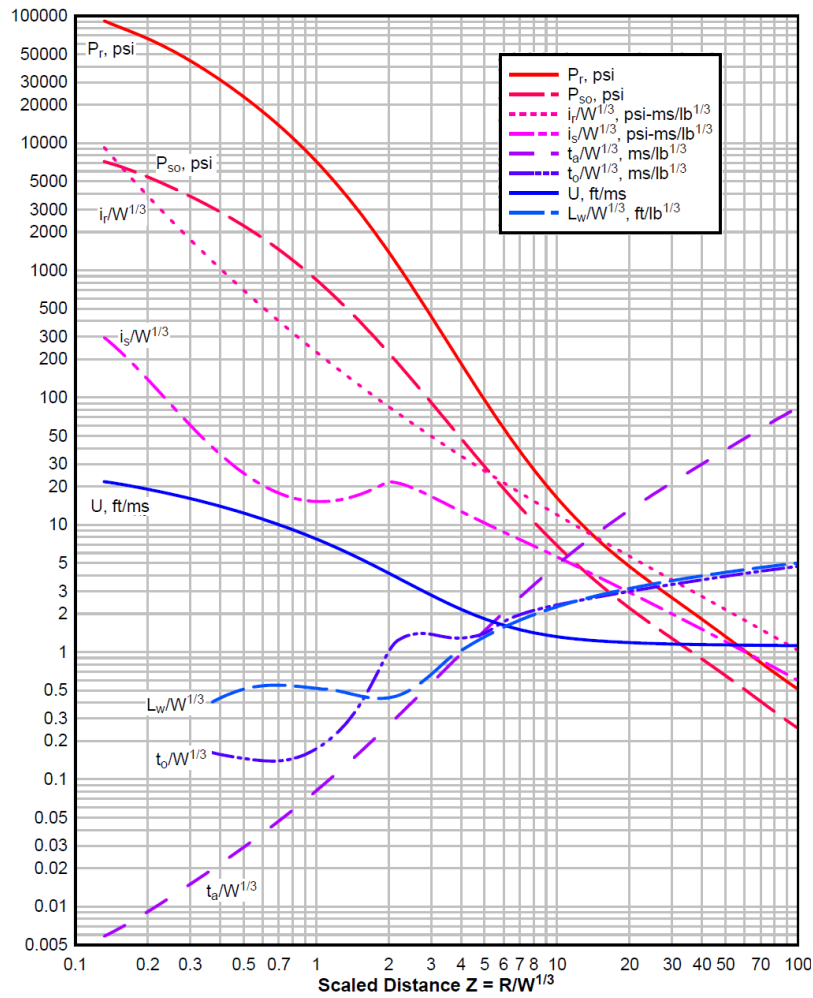


Figure 2.6: Blast wave parameters for positive phase free air blast wave (Army et al. 1990)

2.6 Dynamic response of structures to blast loads

A structure subjected to an external explosion will be affected by the blast wave, and normal pressures will be applied to its exposed surfaces. The response of a structure under explosion loading depends on various factors such as the shape of the structure, the relative location of the blast from the structure, the geometry of the area between the structure and the detonation point, the opening of the structures etc. (karlos and Solomos 2013).

Analyzing the dynamic response of concrete structures subjected to blast loads is very complex due to several reasons including, the effect of high strain rates, the nonlinearity of concrete, the uncertainty of blast loads calculations and the time dependent deformations of structures. Therefore, a number of assumptions has been

proposed and widely accepted to simplify the analysis of blast loads on structures. The first assumption is idealizing the structure as a single degree of freedom (SDOF) system. The structure is replaced by an equivalent system of one concentrated mass and one weightless spring representing the resistance of the structure against deformation. The second assumption is idealizing the blast load positive phase as a triangle with maximum force (F_m) and duration (t_d) as shown in Figure 2.7 (b) (Ngo et al. 2007).

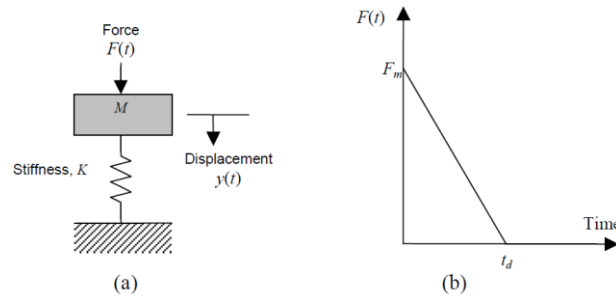


Figure 2.7: (a) SDOF system, (b) Blast loading (Ngo et al. 2007)

The area under the triangle of the idealized blast loading is the blast impulse (I)

$$I = \frac{1}{2} F_m t_d \quad (6)$$

Material behavior under high strain rates is different from in static loads because a material under rapid loadings is unable to deform at a normal rate as in static loadings. Figure 2.8 shows a typical range of strain rates for several loading conditions (Ngo et al. 2007).

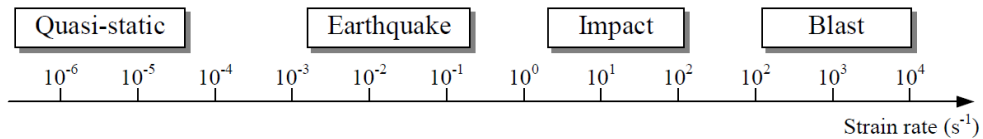


Figure 2.8: Strain rates for several loading conditions (Ngo et al. 2007)

The rapid loading creates an enhancement in the stress level of the yielding. As a result, a structural member will increase its strength in excess of their static capability (Jayasooriya et al. 2009). Strength magnification factors as high as 4 in compression and up to 6 in tension for strain rates in the range: $10^2 - 10^3$ / sec have been reported (Grote et al. 2001). Figure 2.9 illustrates the stress-strain curves of concrete at different stress rates.

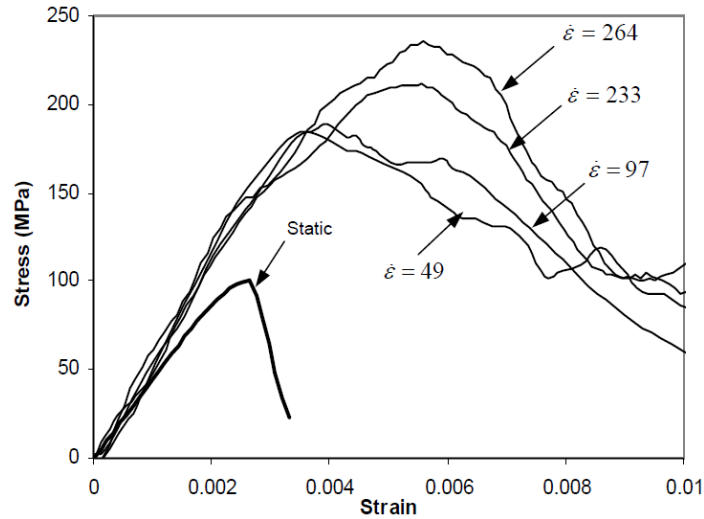


Figure 2.9: Stress-strain curves of concrete at different strain rates (Ngo et al. 2004)

2.7 Modeling techniques for blast loads

The blast loads could be modeled by several means varying from simple calculation of the pressure produced from an explosive charge and applying the pressure to structural member, to complicated technique of modeling the charge as a material and modeling the air domain around the charge and the structure.

2.7.1 Empirical blast method

The air blast pressure is computed empirically with data from Army, Navy et al. (1990), and the pressure is directly applied to the structural elements. This method requires modeling of concrete and steel elements only, modeling of air domain and explosives as materials is not required. This method is very effective, requires less time, and can be done using moderate computer specifications.

2.7.2 Multi Material Arbitrary Lagrangian Eulerian (MM-ALE) method

In this method, explosive and air domain should be modeled in addition to concrete and reinforcement. The explosive charge is detonated within the air domain and the shockwave is transferred through air to contact the structure. The elements number in this method is very high, which requires a lot of time for processing and analyzing and needs a computer with very high specifications.

2.7.3 Coupling of empirical and MM-ALE method

This method is a coupling of empirical and MM-ALE Methods. The air domain is modeled and minimized. The blast pressure is modeled using the empirical method and applied to the air then transferred through air domain to contact the structure. This method requires less time than MM-ALE method and gives almost the same results.

In this study the coupling of empirical and MM-ALE method will be used.

2.8 Previous studies

Several investigations have been conducted to study the effect of explosions on buildings, and to simulate and model blast loads.

- Shugar et al., (1992) used ABAQUS and DYNA3D (early version of LS-DYNA) to model and analyze three different types of RC structures subjected to blast loads; a cylindrical missile test cell, flat slabs with variable shear steel, and a soil covered roof slab. The results of the analysis were accurate when compared to SDOF method for design and compared to experimental tests. The concrete material models implemented in the software caused the simulation to terminate permanently.
- Remennikov, (2003) studied and compared some of the currently available analytical and numerical techniques of predicting blast loads. The limitations of each method were identified. Then he studied a simple case of a single building subjected to blast load using AUTODYN finite element software. The results of the analysis results were good when compared to analytical methods.
- Le Blanc et al., (2005) used LS-DYNA to compare two ways of subjecting a structure to blast load, the first was using a load model implemented in LS-DYNA keyword, and the second was a user-defined load based on empirical model created by Army, Navy et al. (1990). The user defined load model for blast evaluation leads to more accurate and conservative results when used for surface blast loads. However, the load model in the LS-DYNA leads to very good results when used to model air blast loads.
- Ngo et al., (2007) modeled and analyzed a ground floor column of a multistory building using LS-DYNA. The modeling consisted of two types of concrete,

Normal Strength Concrete (NSC) and High Strength Concrete (HSC), and two types of ties detailing, 400 mm spacing for ordinary detailing and 100 mm spacing for seismic detailing, with decreasing the dimensions of the HSC Column. The analysis showed that the effect of shear reinforcement is significant. The ultimate lateral displacement at failure increased by using 100 mm ties about 50%.

- Razaqpur et al., (2007) tested eight doubly reinforced concrete panels with welded steel mesh. Half of the specimens were additionally reinforced with Fiber Reinforced Polymers (FRP) on each face. The specimens are subjected to an explosive charge in the air, and then the tests data were recorded for each test specimen. Some of the specimens are modeled using a software developed by the US army based on empirical formulas from experiments, called CONWEP (Army, Navy et al. 1990). The results obtained from the software analysis were in reasonable agreement with the experimental data.
- Almusallam et al., (2010) investigated a typical eight-story building subjected to blast loadings using the finite element software LS-DYNA. The building was a RC framed structure with concrete core for lifting shafts designed with ACI-318 building code. The beams and columns were represented by beam elements and the concrete core was represented by shell elements in the analysis. The concrete strength was 40 MPa and the yield strength of steel was 500 MPa. A material model implemented in LS-DYNA that was capable of representing plain concrete, reinforcement bars and concrete with smeared reinforcement was used. The loads applied in the analysis were gravity loads as a ramp loading function and blast loads using inbuilt function in LS-DYNA. The results of the analysis indicated that, the columns directly facing the blast were severely damaged due to fragmentation of concrete and rapture of steel bars and eventually lost their load bearing capacity. Due this loss, the gravity loads caused partial collapse of the structure.
- Borrvall & Riedel, (2011) defined a concrete model implemented in LS-DYNA and all its parameters. The defined concrete model was used to model a square RC plate with $125 \times 125 \times 23.5$ cm dimensions and 0.1% reinforcement ratio subjected to close 1.25 kg explosive at 10 cm distance. The rebar was modeled using beam elements along the mesh lines coupled to concrete. The results obtained from the

analysis were acceptable compared to previous experimental results on a RC plate with the same parameters, with some comments needs further studying related to the behavior of the model in tension.

- Morales et al., (2011) designed an experimental set-up for testing planner reinforced concrete elements under blast loads, in which four slabs were tested in the same time in each detonation. The set-up consisted of a steel frame to support the four slabs, and the explosive charge were hanged in the middle of the frame to insure that the load distributed equally to the slabs. There were 12 slabs to test, six of them were normal strength concrete, and the other six were high strength concrete. The slabs were $500 \times 500 \times 80$ mm in dimension reinforced with a mesh of 6mm diameter steel bars spaced 150mm in both directions. The response of the slabs to blast loads where nearly the same, the slabs failed due to tensile stresses on the rear slab side, and failed due to shear on the corners. Using the experimental data from the previous experiments, a numerical model was developed using the FEA software LS-DYNA, solid elements ware used to model the concrete and the support steel plates and the steel rebar was modeled using beam elements and connected with the concrete using the common nodes. Two different material models were used to simulate concrete. The results of the analysis showed similarity using the two material models in the crack pattern. In the two cases, the numerical results are very similar to the experimental results.
- Moutoussamy & Herve, (2011) studied the penalty method for connecting steel reinforcement to concrete by modeling several RC beams and frames with different reinforcement ratios. The results of the modeling were compared to calculated theoretical values of the deflection and resultant forces. For the modeled beams the values of yielding were close by 2% to 10% to the theoretical values. For the modeled frames, the numerical results for crack opening were close by 1% to theoretical results and the values of the yielding were close by 1% for normal case to 20% for under reinforcement case, this deviation was explained by the fact that the compressed section is too small so the stress distribution was not true.
- Tai et al., (2011) modeled a RC Plates subjected to blast pressure wave using LS-DYNA, and compared the results of different mesh sizes to results obtained from

empirical equation. The comparison showed that finer meshing gives results that were more accurate. They also investigated the effects of different explosive amount, different reinforcement ratio and different standoff distances on the plate.

- Puryear et al., (2012) used LS-DYNA to model and analyze a RC column with different parameters, such as charge weight, standoff distance and column geometry. The results of the analysis were compared to test data from a series of blast tests supporting National Cooperative Highway Research Program (NCHRP), Report 645 (Williamson, Bayrak et al. 2010). The modeling and the analysis yields good results compared to NCHRP 645 tests.
- Tabatabaei & Volz, (2012) modeled a previous experimental test in LS-DYNA to compare three different methods of simulation of blast loads on structures. These three methods are empirical blast method, arbitrary Lagrangian Eulerian (ALE) method, and coupling of empirical and ALE Method. The test specimen was 184 × 184 cm concrete panel reinforced to resist blast loads based on Army, Navy et al. (1990) subjected to 36kg of TNT detonated at 168 cm above the center of the panel. The results of the analysis showed that, coupling of the empirical and ALE is the most suitable method.
- Wu et al., (2012) studied three concrete models implemented in LS-DYNA. The three material models were used in modeling and analyzing structures subjected to different dynamic loads. A comparison with available tests data showed the most suitable material among the three materials to represent concrete subjected to dynamic loads.
- Pereira et al., (2013) investigated three concrete material models implemented in LS-DYNA. A concrete bar subjected to a pulse load was modeled to study the three material models. The results obtained then compared and, the most suitable material model to represent the concrete behavior identified.
- Schwer, (2014) described the various methods of including rebar in reinforced concrete and assessed the effectiveness of these methods through a comparative numerical example of concrete slab loaded in axial extension, under self-weight and subjected to air blast loading using LS-DYNA with comparison to experimental results. The concrete was modeled with solid elements and the reinforcement was

modeled with beam elements. The methods described was smeared reinforcement, shared nodes and penalty methods. The analysis showed that, using any of the described methods provided acceptable results for the axial extension and self-weight load case. However, for the blast-load case, the smeared reinforcement was inadequate and the suitable method was the penalty method.

2.9 Summery

Many of the previous studies used LS-DYNA to model different concrete elements subjected to blast loads and verified their works by comparing it with experimental results. The results of the modeling were promising and satisfying and were very close to the experimental results. But modeling a structural unit consisting of several elements were not investigated.

Using finite element software like LS-DYNA saves time and money and gives more flexibility in changing different parameters of a study. LS-DYNA is easy to use and have a huge material library allowing the user to choose from it whatever it is suitable for his study.

Chapter 3: Finite Element Modeling Using LS-DYNA

3.1 Finite Element Method

The modern development of the finite element method (FEM) began in the 1940s in the field of structural engineering. The finite element method is a numerical method for solving problems of engineering and mathematical physics. Typical problem areas of interest in engineering and mathematical physics that are solvable by use of the finite element method include structural analysis, heat transfer, fluid flow, mass transport, and electromagnetic potential. (Logan 2007).

The finite element method was able to solve complicated structural problem to some level, but not very complicated ones until the invention of computers.

The finite element analysis method requires the following major steps (Madenci & Guven 2006):

- Discretization of the domain into a finite number of subdomains (elements).
- Selection of interpolation functions.
- Development of the element matrix for the subdomain (element).
- Assembly of the element matrices for each subdomain to obtain the global matrix for the entire domain.
- Imposition of the boundary conditions.
- Solution of equations.
- Additional computations (if desired).

Depending on the geometry and the physical nature of the structural member, it can be discretized by using line, plane, or volume elements.

Line element are simple two-nodded or higher line elements typically used to represent a bar or beam element. Plane elements are Simple two-dimensional elements with corner nodes typically used to represent plane stress/strain. Volume elements are Simple three-dimensional elements typically used to represent three-dimensional stress state. Figure 3.1 illustrates finite element types.

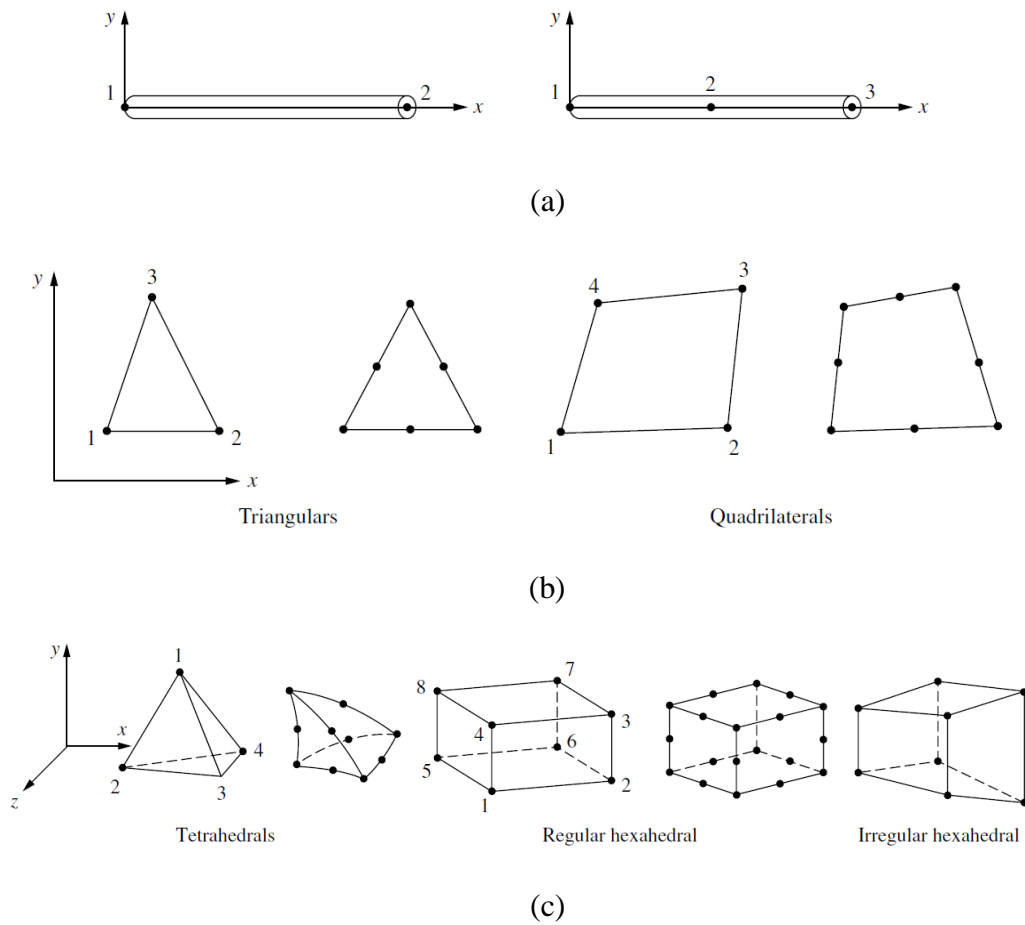


Figure 3.1: Simple finite elements: (a) line elements, (b) plane elements, (c) volume elements (Logan 2007)

3.2 Modeling using LS-DYNA

LS-DYNA originated in 1976 as DYNA3D and DYNA2D at Lawrence Livermore National Laboratory. The early application was mainly for stress analysis of structures subjected to impact loading. The first version contained trusses, membranes and a choice of solid element. In 1976, super computers were much slower than today's PCs, which made analyzing very time consuming.

From 1976 to 1988 new versions of DYNA3D were released with enhancements in material models and element types, and during this period the computers enhanced and became faster and easier to use. At the end of 1988, Livermore Software Technology Corporation was found to continue the development of DYNA3D as a commercial version called LS-DYNA3D, which was later shortened to LS-DYNA with new many enhanced capabilities.

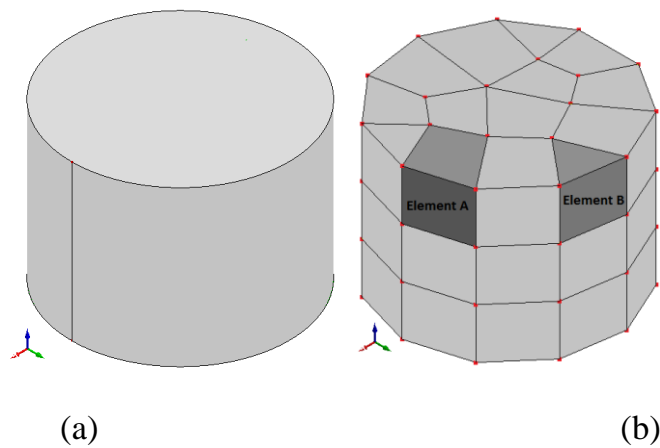
The latest version of LS-DYNA R7.0 2014 has an improved user interface, a huge library of material models; the ability of implementing a user defined material model, and much more capabilities (LS-DYNA 2014).

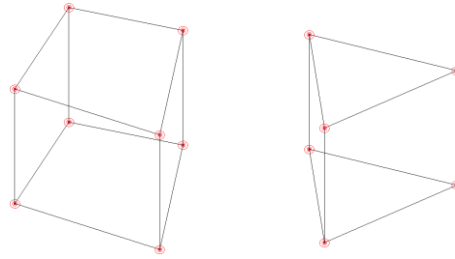
LS-DYNA is a general-purpose finite element software for numerically solving a wide variety of structural engineering problems. LS-DYNA element library consists of a huge variety of element types. For the numerical simulation of RC structure, irregular hexahedral and pentahedral elements has been used for steel reinforcement and regular hexahedral elements has been used for concrete.

3.2.1 Modeling of steel reinforcement

Plane or volume elements can be used to model steel reinforcement in LS-DYNA. Modeling steel by using plane elements is easy to use and the model will have less elements than using volume elements, so their analysis does not need much time. Using volume elements to model steel is a better choice because they reflect the behavior of steel more effectively.

In this research, the steel bars were first modeled in LS-Prepost as volume tubes. The elements created using the auto meshing function. Auto meshing function requires entering size of the element. The size of the element is the average length of the element in all directions. The auto meshing function selects the appropriate element shape with the defined size and generate it. For the steel bars the auto meshing resulted in using irregular hexahedral with 8 nodes and pentahedral elements with 6 nodes as shown in Figure 3.2. Each node has 3 degrees of freedom.

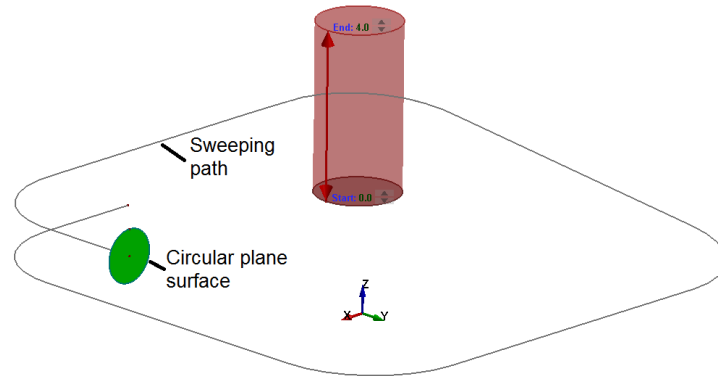




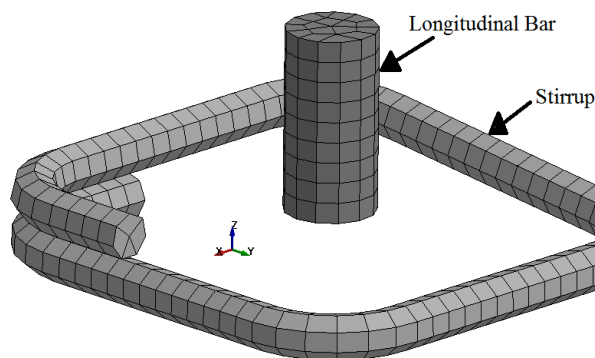
(c)

Figure 3.2: Steel bar modeling: (a) volume tube before meshing, (b) elements of steel bar with nodes, (c) irregular hexahedral and pentahedral elements

The stirrups was modeled as solids generated from sweeping a circular plane surface along a curve bath representing the bend steel with the hoops. Figure 3.3 shows the creating and the meshing of steel stirrups and bars.



(a)



(b)

Figure 3.3: Steel bars and stirrups modeling (a) creating, (b) meshing

3.2.2 Modeling of concrete

Concrete was modeled and meshed in one step by using shape mesher function in LS-Prepost. Regular hexahedral element was used for concrete with 8 nodes, each node with 3 degree of freedom as shown in Figure 3.4.

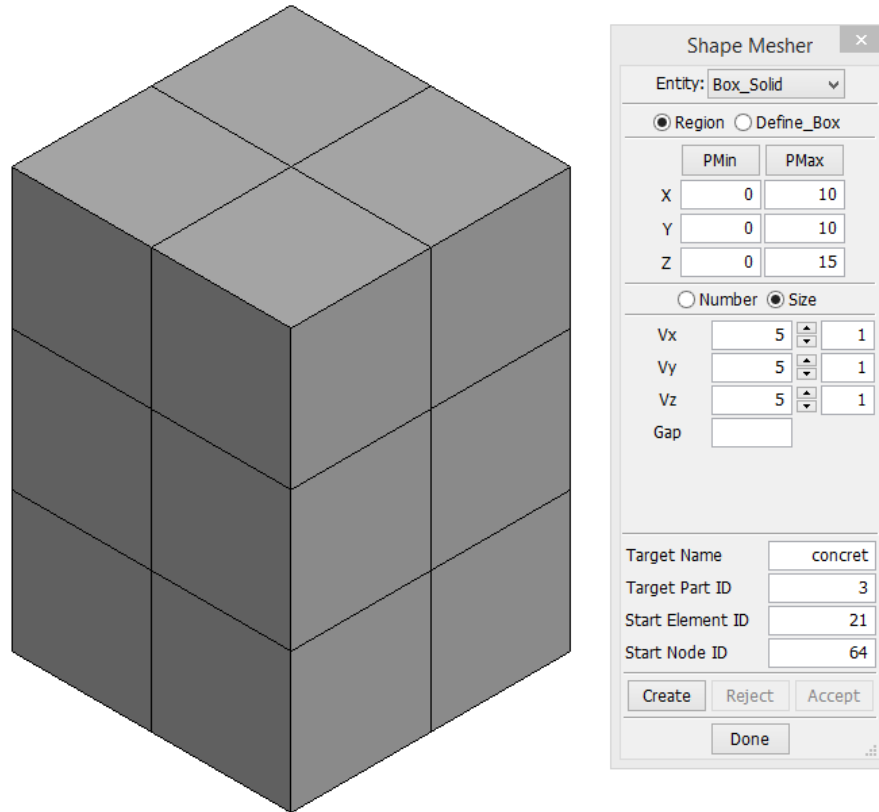


Figure 3.4: Concrete modeling and meshing

The properties of the elements for steel reinforcement and concrete were defined using the keyword SECTION_SOLID in LS-Prepost. The parameters of the keyword are shown in Table 3.1.

Table 3.1: SECTION_SOLID keyword parameters

Parameter	LS-DYNA Symbol	Value	Value Explanations
Title of the section	TITLE	Solid	
Section ID	SECID	1	Required to be linked to parts
Element formulation	ELFORM	1	Constant stress solid element
Ambient element type	AET	0	Not required for this ELFORM

3.3 Materials modeling

3.3.1 Concrete material model

A wide variety of material models for concrete exist in LS-DYNA library, some of the models are specialized and some of them are for general modeling of concrete. Table 3.2 contains a list of some materials models of concrete and its properties.

Table 3.2: Material models for concrete in LS-DYNA (LS-DYNA 2014)

Material Type No.	LS-DYNA name	Description
016	MAT_PSEUDO_TENSOR	This model has been used to analyze buried reinforced concrete structures subjected to impulsive loadings.
072	MAT_CONCRETE_DAMAGE	This model is an update of material type 16.
072R3	MAT_CONCRETE_DAMAGE_REL3	A newer version of material type 72. The most significant user improvement provided by Release III is a model parameters generation capability, based on the unconfined compression strength of the concrete.
084	MAT_WINFRITH_CONCRETE	This model is a smeared crack, smeared rebar model for general modeling of concrete
159	MAT_CSCM_CONCRETE	This is a smooth model and is available for solid elements. Its most important property is the automatic generation of model parameters based on few inputs.
172	MAT_CONCRETE_EC2	The material model can represent plain concrete only, reinforcement steel only, or a smeared combination of concrete and reinforcement. The model includes concrete cracking in

		tension and crushing in compression. It can be used only for shell and beam elements.
272	MAT_RHT	This model is used to analyze concrete structures subjected to impulsive loadings. It can be used for solid elements

The concrete in this research was modeled as solid elements using material type 159 (MAT_CSCM_CONCRETE) where fewer inputs parameters for the concrete model is required.

Continuous Surface Cap Model (CSCM) was developed in 1990s, and was sponsored by the department of transportation (DOT) in the United States of America to be available in LS-DYNA in 2005 under the name MAT_CSCM_CONCRETE to be aimed for road side safety analysis (Wu et al. 2012).

CSCM can be categorized as isotropic, plastic damage, and rate dependent model. It considers the Hooke's law to describe elastic behavior. The damage and the plastic response of the materials are related. CSCM considers a cap formulation to describe compaction of the material (Pereira et al. 2013).

The strength of concrete is modeled by a combination of shear failure surface and cap hardening surface in a low to high confining pressure regimes.

The general shape of the yield surface in the meridian plane is shown in Figure 3.5 and Figure 3.6. This surface uses a multiplicative formulation to combine the shear surface with the hardening cap surface smoothly and continuously. The smooth intersection eliminates the numerical complexity of treating a compressive 'corner' region between the failure surface and cap (Murray 2007). That is why this type of model is referred to as a smooth cap model or as a continuous surface cap model (CSCM).

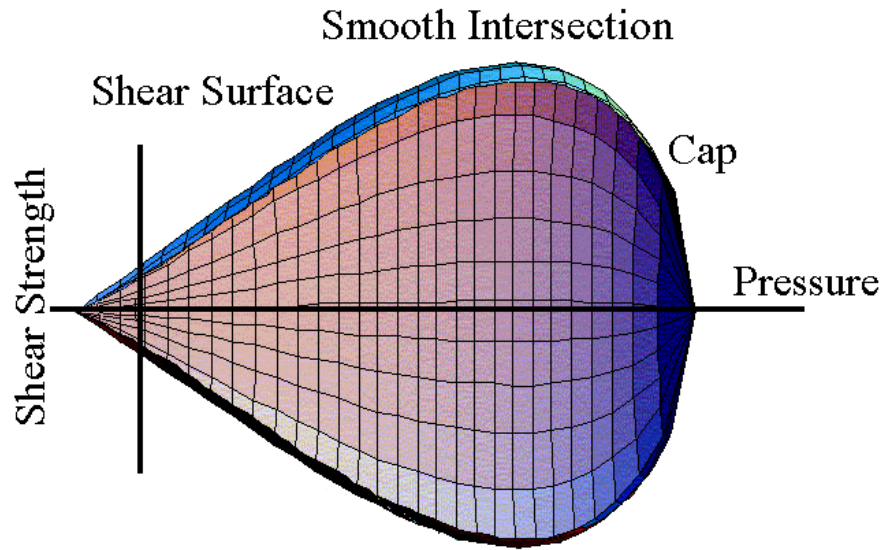


Figure 3.5: Concrete model yield surface in two dimensions (Murray 2007)

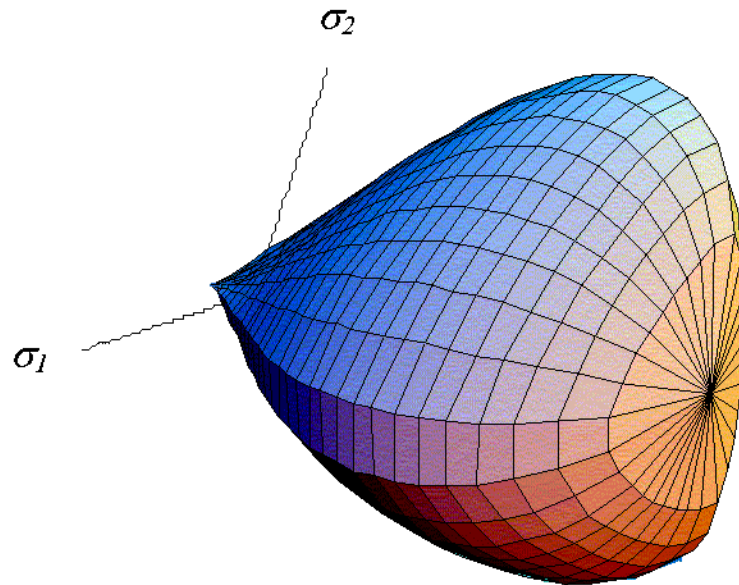


Figure 3.6: Concrete model yield surface in three dimensions (Murray 2007)

The damage formulation models both strain softening, which is a reduction in strength during progressive straining after a peak strength value is reached, and modulus reduction which is a decrease in the unloading/loading slopes as illustrated in Figure 3.7.

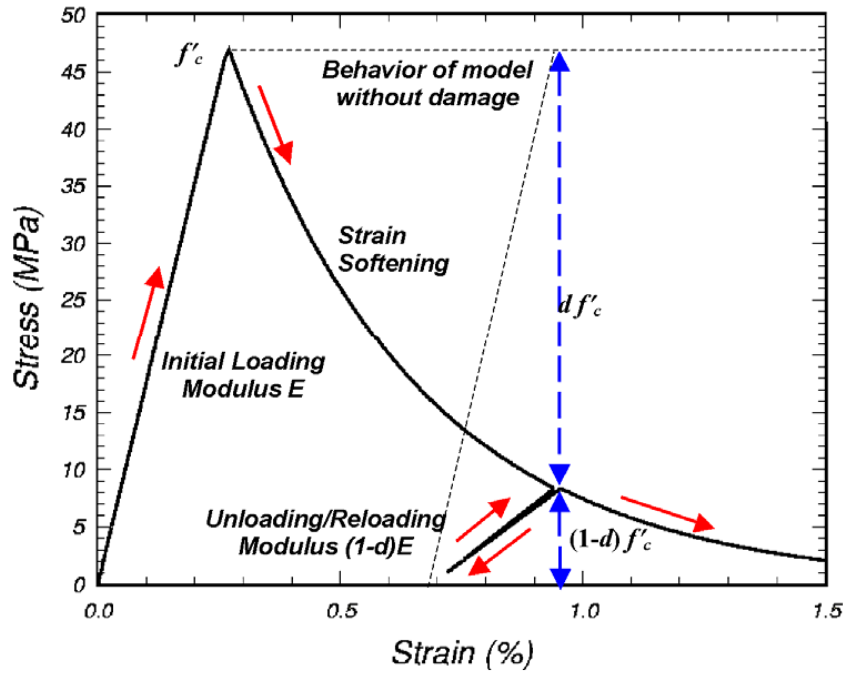


Figure 3.7: Strain softening and modulus reduction for the model (Murray 2007)

MAT_CSCM_CONCRETE in LS-DYNA is provided based on three input specifications: the unconfined compression strength, the aggregate size, and the units. The unconfined compression strength affects stiffness, strength, hardening, and softening. The CSCM is valid for normal compressive strengths from 28 MPa to 58 MPa. The aggregate size affects the brittleness of the softening behavior of the damage formulation (Murray 2004).

Table 3.3 shows the required parameters for the selected material model MAT_CSCM_CONCRETE.

Table 3.3: MAT_CSCM_CONCRETE parameters

Parameter	LS-DYNA Symbol	Unit
Mass Density	RO	Kg/mm ³
Compression Strength	FPC	GPa
Max Aggregate size	DAGG	mm

3.3.2 Steel material model

The steel rebar was modeled using material type 24 (MAT_PIECEWISE_LINEAR_PLASTICITY). This material model represent steel reinforcement behavior, with plastic deformation, strain rate effects, and failure. Figure 3.8 shows the effective plastic strain versus the yield stress for different strain rates.

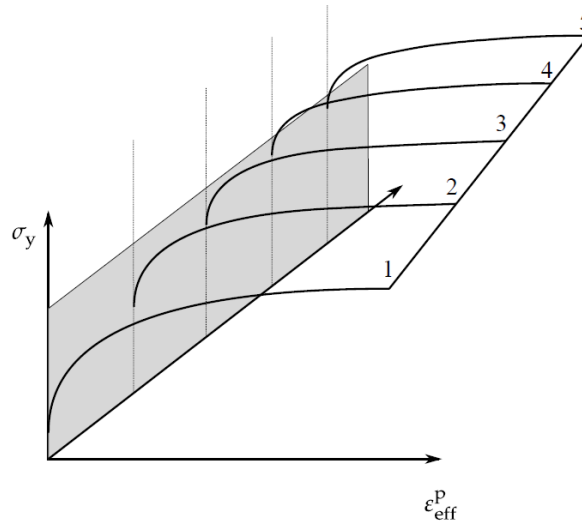


Figure 3.8: Effective plastic strain versus yield stress for material type 24

The material model for steel reinforcement requires inputting mass density, modulus of elasticity, yield stress, and tangent modulus for simple modeling of steel as shown in Table 3.4.

Table 3.4: MAT_PIECEWISE_LINEAR_PLASTICITY parameters

Parameter	LS-DYNA Symbol	Unit
Mass Density	RO	Kg/mm ³
Modulus of Elasticity	E	GPa
Poissons Ratio	PR	
Yield Stress	SIGY	GPa
Tangent Modulus	ETAN	GPa
Failure Strain	FAIL	

3.3 Methods of including rebar in reinforced concrete

3.3.1 Smearred reinforcement

In the smeared method, the reinforcement is modeled as a volume fraction of concrete, which is the volume of steel divided by the volume of concrete. This volume fraction

is modeled as a layer of elements in a RC structure. The smeared rebar method is good for small deformations where the reinforcement remains elastic.

3.3.2 Shared nodes method

In this method, the steel bars is modeled with beam or truss elements, and connected with concrete by merging the common mesh nodes. It requires the nodes of the reinforcement grid and the concrete mesh to be identical. It is easy when dealing with layers of reinforcement, but when using stirrups it is challenging.

3.3.3 Penalty methods

Unlike the shared nodes method, when the penalty method is selected the reinforcement and concrete meshes are constructed independently. LS-DYNA internally constructs a system of penalty constraints restricting the motion of the two meshes to be consistent. The keyword for connecting reinforcement to concrete in LS-DYNA is `CONSTRAINED_LAGRANGE_IN_SOLID`, which requires identifying concrete as master part and steel as slave part (Moutoussamy and Herve 2011).

In this study, the penalty method was used for linking the concrete to the steel by using LS-DYNA keyword `CONSTRAINED_LAGRANGE_IN_SOLID`.

3.4 Modeling of blast loads

The blast load can be modeled in LS-DYNA by using three methods, the empirical method, the Multi Material Arbitrary Lagrangian Eulerian (MM-ALE) method, and coupling of the empirical and MM-ALE method.

The empirical method is the simplest method, which requires less time for analysis, only modeling of the structure is required and defining the mass and coordinates of the explosion, then LS-DYNA software calculates the pressure from the explosion and apply it to the chosen structural surface as shown in Figure 3.9. The simplicity is the most important advantage of this method compared with other methods. This method also gives very good results (Tabatabaei & Volz 2012).

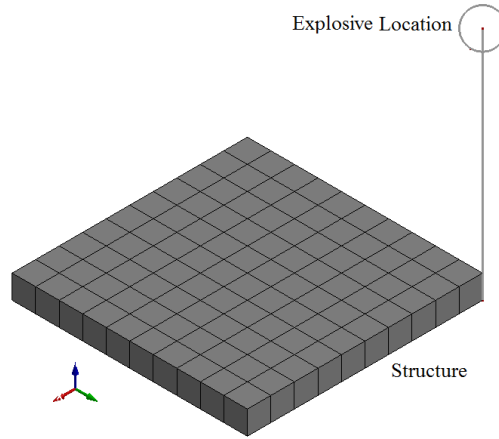


Figure 3.9: Schematic of empirical method in LS-DYNA

The Multi Material Arbitrary Lagrangian Eulerian (MM-ALE) method is a complex method requiring modeling of the structure, the explosive material and the containing air domain as shown in Figure 3.10, this results in huge number of elements need a lot of time to be analyzed and need a super computer with very high specifications. But this method gives very accurate results compared to other methods.

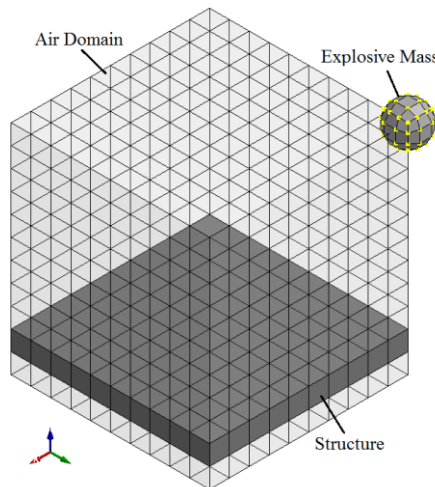


Figure 3.10: MM-ALE modeling method in LS-DYNA

Coupling of empirical method and MM-ALE method gives the benefits of both methods; it is simpler than MM-ALE and gives more accurate results than empirical method. In this method, the structure is modeled, the air domain just covering the structure is modeled, and the blast is applied as the empirical method as shown in Figure 3.11.

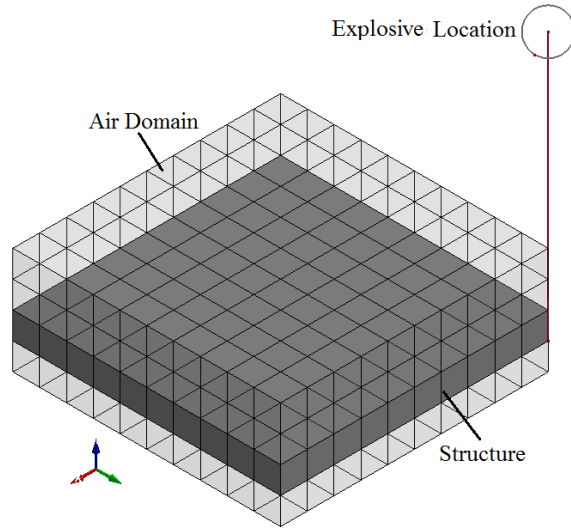


Figure 3.11: Coupling of empirical and MM-ALE method in LS-DYNA

The time of analysis depends on the size of the model and the specifications of the computer used for the processing. The computer used in this study was a personal computer with moderate specifications. The CPU was Intel core I7-2670QM@2.2 GHz (8CPUs) and the memory was 8192MB RAM.

Table 3.5 shows the number of elements and the total time of analysis for the three methods for a model in LS-DYNA software using the same computer (Tabatabaei and Volz 2012).

Table 3.5: Statistics of three blast-modeling methods (Tabatabaei and Volz 2012)

	Empirical method	MM-ALE	Coupling
No. of elements	4179	37856	12930
Time of analysis	02:13:35	84:40:03	41:42:00

In this study, the empirical method was used in modeling the blast loading where less analysis time was required and moderate computer specification but also good results can be obtained.

The blast load was applied using empirical method by using LS-DYNA keyword `LOAD_BLAST_ENHANCED`. `LOAD_BLAST_ENHANCED` uses equivalent mass of TNT located in defined coordinates to generate the blast load. Table 3.6 shows the parameters for `LOAD_BLAST_ENHANCED` keyword.

Table 3.6: LOAD_BLAST_ENHANCED keyword parameters

Parameter	LS-DYNA Symbol	Unit
Equivalent mass of TNT	M	kg
X-coordinates of point of explosion	XBO	mm
Y-coordinates of point of explosion	YBO	mm
Z-coordinates of point of explosion	ZBO	mm
Time of detonation	TBO	ms
Unit conversion flag	UNIT	
Conversion factor for time	CFT	

The blast load was applied to the interior surfaces of the structure by using LOAD_BLAST_SEGMENT_SET keyword.

Chapter 4: Model Validation

4.1 Introduction

In this chapter, verification of the model is carried out by comparing experimental results from Williamson et al. (2010) for a column subjected to blast loading with those obtained from the analysis of modeling a column with the same parameters.

4.2 Experimental test data

Extensive results were presented in Williamson et al. (2010) through conducting series of tests to investigate the behavior of concrete bridge columns under blast loads and to develop a design guidance for improving the structural performance and resistance to explosive effects for bridges. Three types of columns were tested in Williamsons study; columns designed to resist low seismic loads, high seismic loads, and blast loads.

The experimental results used in the verification process were presented in test No. 9 conducted on the column donated 3A designed to withstand low seismic loads. The column was rectangular with 30×30 in (762×762 mm) dimensions. The longitudinal reinforcement was 24 #6 bars (19.05 mm diameter) equally spaced and the transverse reinforcement was #4 bars (12.7 mm diameter) at 6 in (152.4 mm). Reinforcement detailing are shown in Figure 4.1.

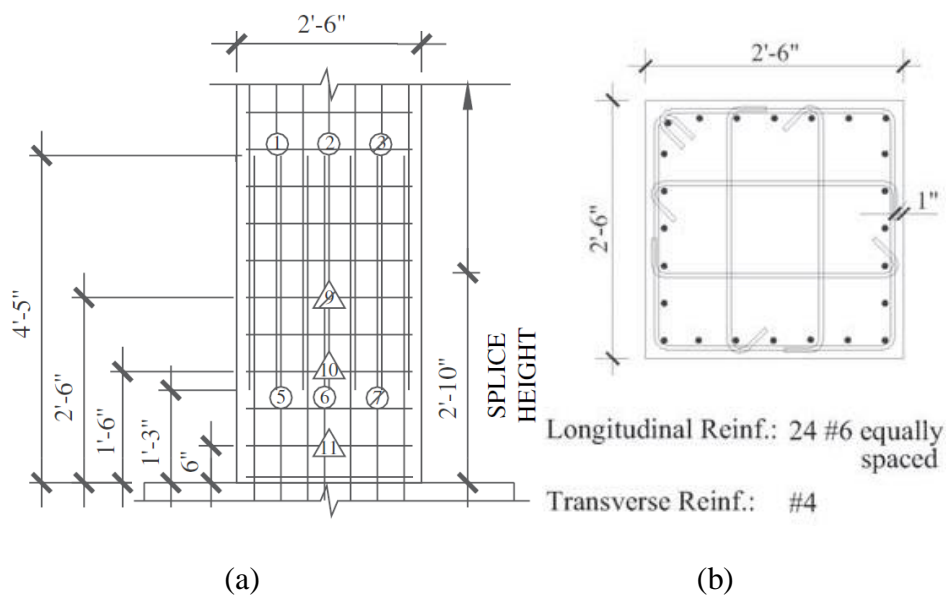


Figure 4.1: Dimensions and reinforcement details of column 3A (Williamson et al. 2010)

Concrete of 4000 psi (28 MPa) strength with a maximum aggregate size of 3/8 in (9.525 mm) was selected for the test program. Standard deformed uncoated Grade 60 (420 MPa) reinforcement bars were specified for all reinforcement.

The blast load on the column A3 resulted from the detonation of 100 lb (45 kg) of TNT at standoff distance of 41 inches (1 meter).

The tested column were placed on a pre-constructed steel frame fixed on a reinforced concrete slab to brace the tested column as shown on Figure 4.2, the explosive charge was placed on the ground. Gauges to calculate strain were placed on the steel bars before casting. The column is fixed by the frame from the top.



Figure 4.2: Field test setup (Williamson, Bayrak et al. 2010)

4.2.1 LS-DYNA model

The chosen column was modeled in LS-Prepost using material type 159 (MAT_CSCM_CONCRETE for concrete and material type 24 (MAT_PIECEWISE_LINEAR_PLASTICITY) for steel rebar, as the model under study. The elements for concrete were hexahedral elements with 25 mm dimension, and for steel reinforcement the elements were irregular hexahedral and pentahedral elements auto-meshed with maximum size of 5mm. The material properties and the blast parameters from test 9

of column A3 from (Williamson, Bayrak et al. 2010) were applied and are listed in Table 4.1 and Table 4.2.

Table 4.1: Concrete model parameters values for the verification model

Parameter	Value	Unit
Mass Density	2.5E-6	kg/mm ³
Compression Strength	0.028	GPa
Max Aggregate size	9.525	mm

Table 4.2: Reinforcement steel model parameters values for the verification model

Parameter	Value	Unit
Mass Density	7.85E-6	kg/mm ³
Modulus of Elasticity	200	GPa
Poisson's Ratio	0.30	
Yield Stress	0.42	GPa
Tangent Modulus	0.19	GPa
Failure Strain	0.30	

The blast load was applied to the column using the empirical method with the parameters as in Table 4.3.

Table 4.3: Blast load parameters values for verification model

Parameter	Value	Unit
Equivalent mass of TNT	45	kg
X-coordinates of point of explosion	1750	mm
Y-coordinates of point of explosion	375	mm
Z-coordinates of point of explosion	100	mm
Detonation Time	0	ms
Unit conversion flag	6	
Conversion factor for time	1	

The column was fixed from the bottom in all direction and from the top side against the explosion in the *x*-direction as shown in Figure 4.3.

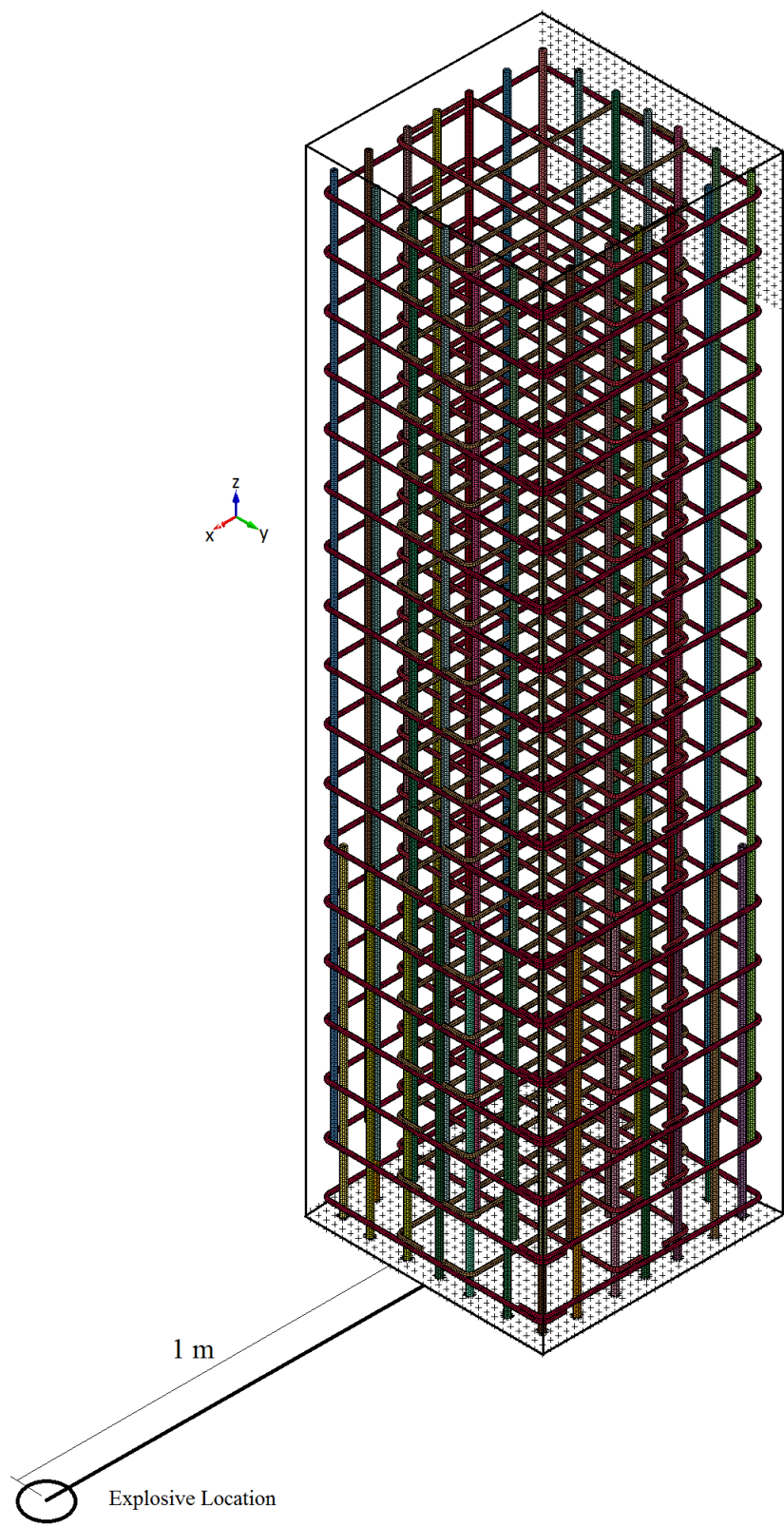


Figure 4.3: Boundary conditions and the location of the explosive

The number of nodes and elements for steel and concrete for the verification model are summarized in Table 4.4.

Table 4.4: Statistics of verification model

Material	No. of elements	No. of nodes
Steel	499,772	804,002
Concrete	144,000	154,721
Total	643,772	958,723

4.2.2 Experimental test results

The experimental test results done by Williamson et al. (2010) showed that the permanent deflection of 3 in (76.2 mm) at a height of 9 in (228.6 mm) above the ground, complete spall of the bottom 17 in (431.8 mm) of concrete cover, and flexural cracking at the mid height on the front and the back face of the columns. Figure 4.4 shows the deflection and the spall of the real test column.



Figure 4.4: Deflection and spall of test column (Williamson et al. 2010)

4.2.3 The FE analytical results

The verification model was analyzed for 1.5 milliseconds (ms), which is the time required for the blast wave to propagate throughout the column. The run time was 2:16:42 hours. The blast wave reached the column at 0.21 milliseconds and propagated

through the columns as shown in Figure 4.5. The blast wave reaches the column with a pressure of 97 MPa then the pressure decreased as shown in Figure 4.6.

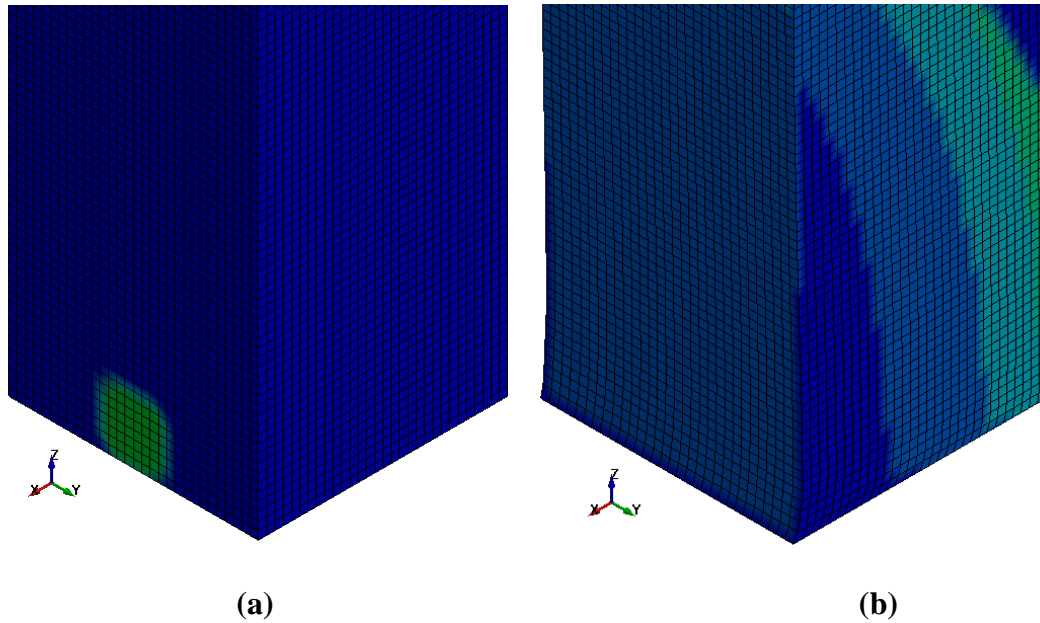


Figure 4.5: Blast wave propagation through the column at: (a) 0.21 milliseconds, (b) 0.60 milliseconds

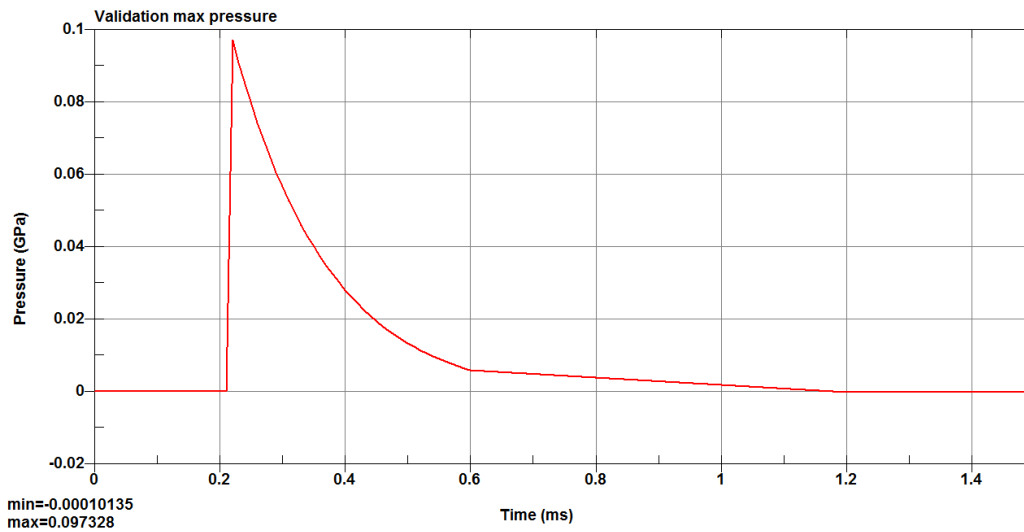


Figure 4.6: Pressure profile for the column point of contact with the blast wave

The maximum deflection of the model had a value of 73.96 mm as shown in Figure 4.7 occurred at a height from 225 mm to 250 mm above the bottom of the column as shown in Figure 4.8, which was in a very good agreement compared to 76.2 mm from the experimental test results. The shape of the deflection and spalling area for both numerical and experimental columns were nearly identical.

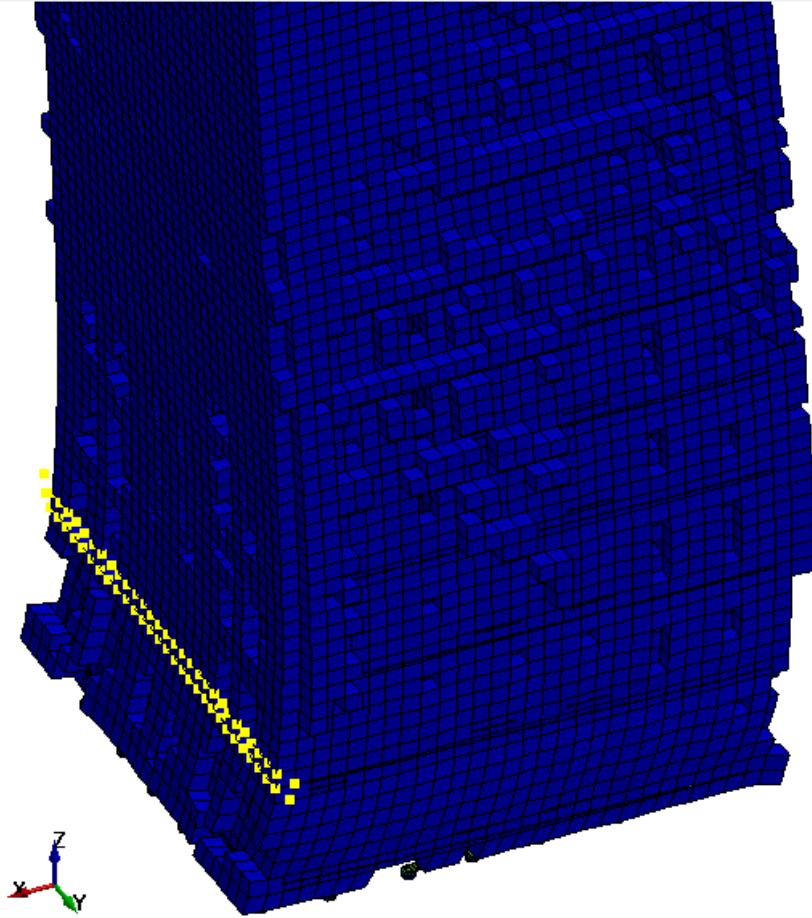


Figure 4.7: Isoperimetric view of the verification model with the deflection

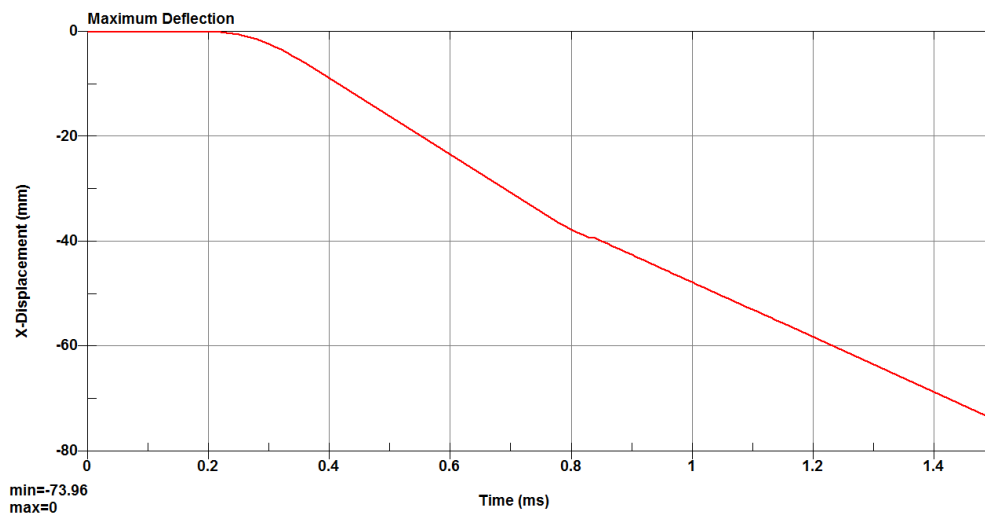


Figure 4.8: Maximum deflection in the direction of the blast versus time

Chapter 5: Numerical Model Applications

5.1 Introduction

In this chapter, three numerical applications are carried out. The basic model is a structure consisting of four columns supporting a 3×3 m one way ribbed slab and subjected to a blast load resulting from a 50 kg TNT charge located in the center of the structure. Results for stresses and deflection are recorded. The effect of increasing concrete strength and the effect of relocating the explosion are studied.

5.2 Model structure geometry

The model is a RC structure designed according to ACI-318M-11 building code provisions (ACI-318-Committee 2011). The structure consists of 4 columns with one way ribbed slab. The explosion is located in the middle of the structure as shown in Figure 5.1

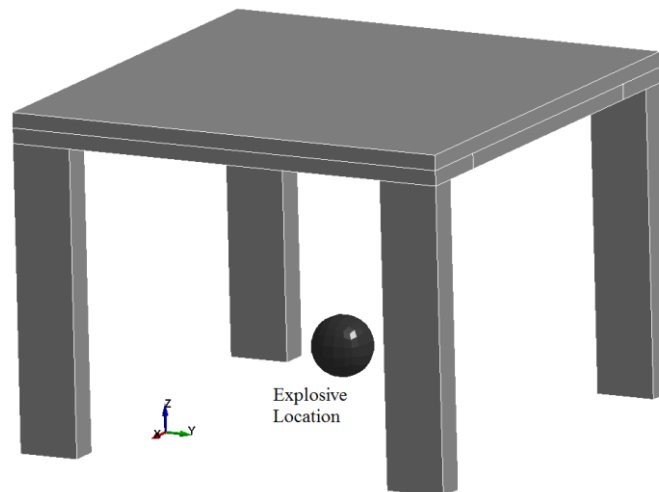
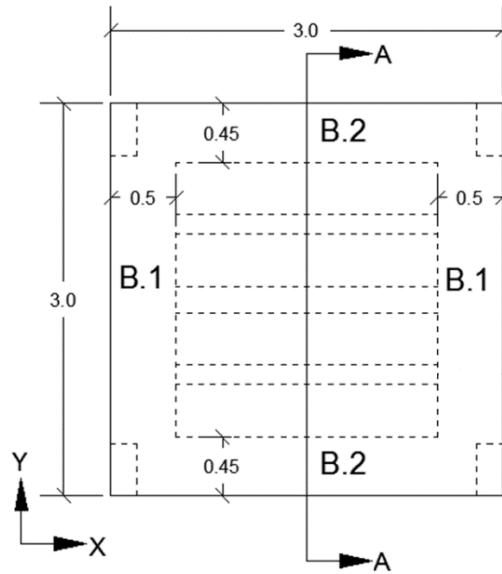
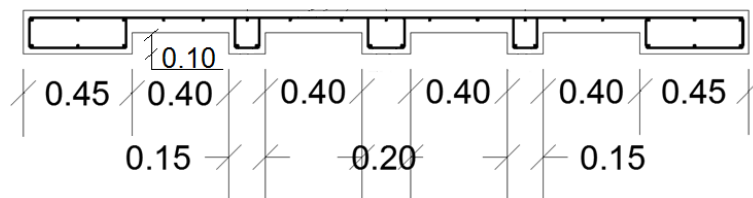


Figure 5.1: Schematic of the structure and the location of explosive

The slab is a 3 m by 3 m designed as one way ribbed slab with a total thickness of 20 cm as shown in Figure 5.2. The slab consists of two 50 cm width main beams (B.1) along the x -axis, two 45 cm width secondary beams (B.2) along the y -axis, two 15 cm width ribs, and one 20 cm middle rib along the y -axis.



(a)



(b)

Figure 5.2: Slab dimensions in meters (a) top view, (b) section A-A

The slab is supported by four columns. Each column is 200×400 mm in cross section and 2 m long as shown in Figure 5.3. The structure is fixed at the bottom of the columns in all directions.

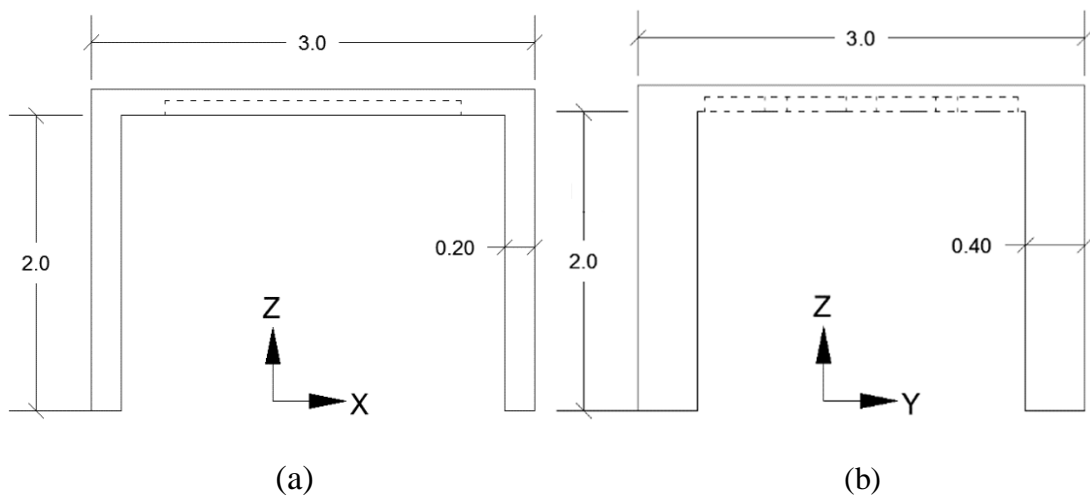


Figure 5.3: Columns Dimensions in meters: (a) Front view, (b) Side view

5.2.1 Structure reinforcement details

The main beams (B.1) are reinforced with 5 Φ 12 mm bottom bars, 3 Φ 12 mm top bars. The secondary beams (B.2) are reinforced with 3 Φ 12 mm bottom and top bars. Φ 10 mm stirrups spaced at 7.5 cm at the edges and 15 cm at the middle are applied to the beams. The top slab is reinforced with a mesh of Φ 10 mm bars at 20 cm in both directions. The ribs are reinforced with 2 Φ 12 mm bottom bars and Φ 10 mm stirrups at 15 cm. Details of slab reinforcement are shown in Figure 5.4.

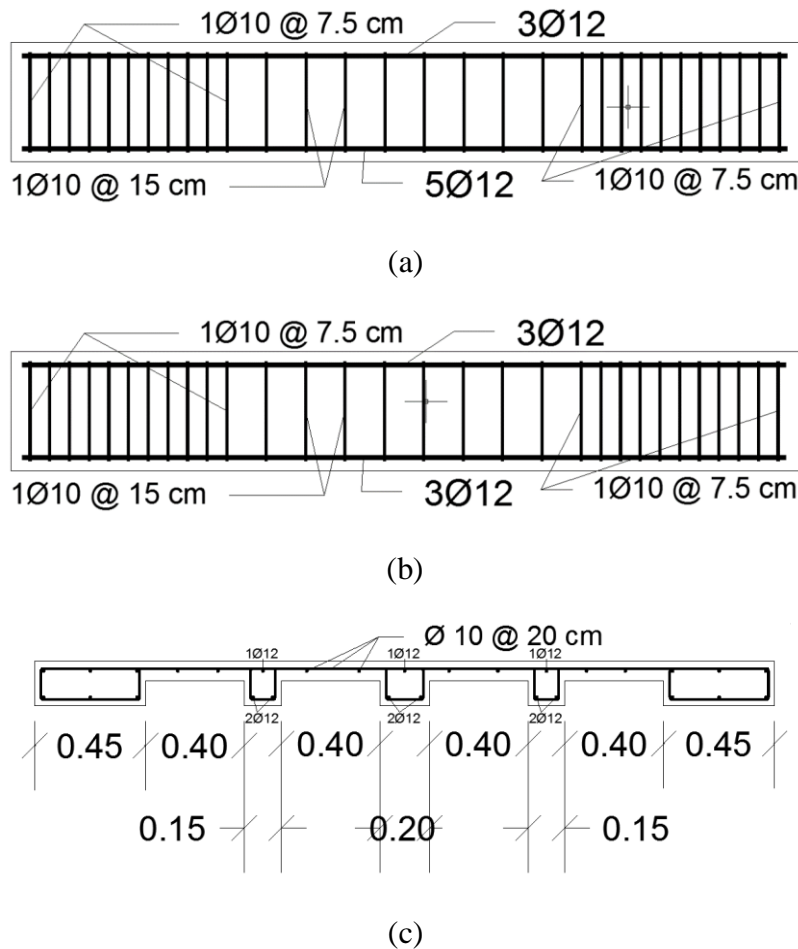


Figure 5.4: Slab reinforcement details: (a) Main beam (B.1) detailing, (b) Secondary beam (B.2) detailing, (c) Section A-A details

The columns are reinforced with 6 Φ 14 mm longitudinal steel bars and tied with Φ 10 mm ties distributed along the column every 10 cm at the bottom third and the top third and every 20 cm at the middle third as shown in Figure 5.5.

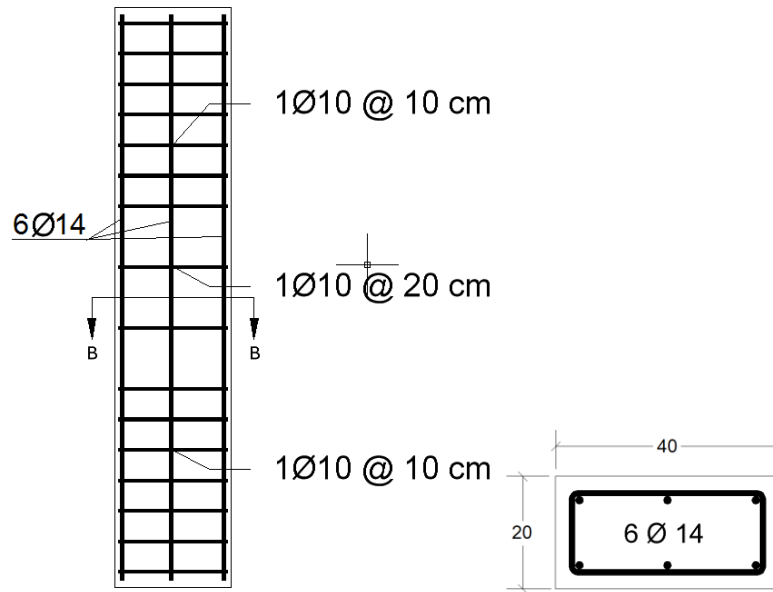


Figure 5.5: Columns reinforcement details

5.2.2 Building the model in LS-Prepost

The structure model consists of steel and concrete subjected to blast load. Steel reinforcement was first modeled. The main bars were represented as cylinder solids and the stirrups were represented as solids generated from sweeping a circular plane surface along a curve bath representing the bend steel with the hoops. The steel then meshed using auto meshing function implemented in LS-Prepost with solid irregular hexahedral and pentahedral elements with maximum size of 5 mm. Steel bars were modeled so that no intersection between bars was present. Concrete was simulated as solid meshed boxes with 25 mm solid regular hexahedral elements. Each part was modeled as separate box and then was connected by merging common nodes to create the whole structure. The model was fixed from the column bottom in all directions.

After finishing the structure geometry building, material models for concrete and steel were applied. Concrete with compressive strength of 29 MPa and steel reinforcement with yield stress of 420 MPa were used. The parameters for the material models are in Table 5.1 and

Table 5.2.

Table 5.1: Steel material model parameters values for the case study

Parameter	Value	Unit
Mass Density	7.85E-6	kg/mm ³
Modulus of Elasticity	200	GPa
Poissons Ratio	0.3	
Yield Stress	0.42	GPa
Tangent Modulus	0.19	GPa
Failure Strain	0.3	

Table 5.2: Concrete material model parameters values for the case study

Parameter	Value	Unit
Mass Density	2.5E-6	kg/mm ³
Compression Strength	0.029	GPa
Max Aggregate size	20	mm

The segments affected by the blast load were selected, and blast load was defined with the parameters in Table 5.3.

Table 5.3: Blast loading parameters values for the case study

Parameter	Value	Unit
Equivalent mass of TNT	50	kg
x-coordinates of point of explosion	0	mm
y-coordinates of point of explosion	0	mm
z-coordinates of point of explosion	500	mm
Detonation Time	0	ms
Unit conversion flag	6	
Conversion factor for time	1	

The termination time of the analysis was set to 2 ms. The number of elements and nodes for the case study are shown in Table 5.4.

Table 5.4: Statistics of the case study

Material	No. of elements	No. of nodes
Steel	337,680	682,539
Concrete	135,680	172,892
Total	473,960	855,431

5.3 Internally blasted model

The model were analyzed in LS-DYNA. The time required to finish the analysis was 01:26:17 hours. The results for every part behavior of the structure were recorded.

The blast wave reached the slab first at time 0.41 ms with a pressure of 45.7 MPa, and then reached the columns at time 0.51 ms with a pressure of 22.2 MPa as shown in Figure 5.6.

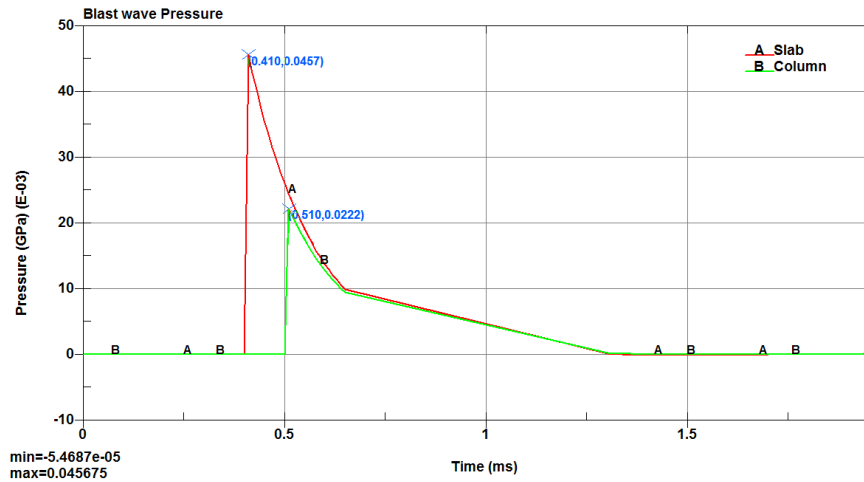


Figure 5.6: Blast wave pressure on slab and columns

The blast wave propagated through the structure members causing deformations and damages to them.

5.3.1 Stress distribution at the columns

The columns are the most important elements in the structure because they carry the whole structure. Destroying a column could cause progressive collapse of a whole building. Only the results of one column was recorded because of the symmetry of the structure. LS-DYNA uses positive sign for tension stresses and negative sign for compressive stresses.

The tension stresses of the columns in all directions increased since the blast wave effect at 0.41 ms, and reached the maximum values and remained almost constant to the end of the analysis as shown in Figure 5.7. The maximum x -axis tension stresses occurred at the bottom of the column, with a maximum value of 3.25 MPa at time 0.94 ms. In the y -direction the maximum value of the tension stresses occurred at the top of the column with a maximum value of 3.55 MPa at time 1.24 ms. in the z -direction the

maximum tension stresses occurred at the middle of the column with a maximum value of 3.39 MPa at time 1.01 ms. The maximum tension stresses occurred at outside surface of the column far from the explosion.

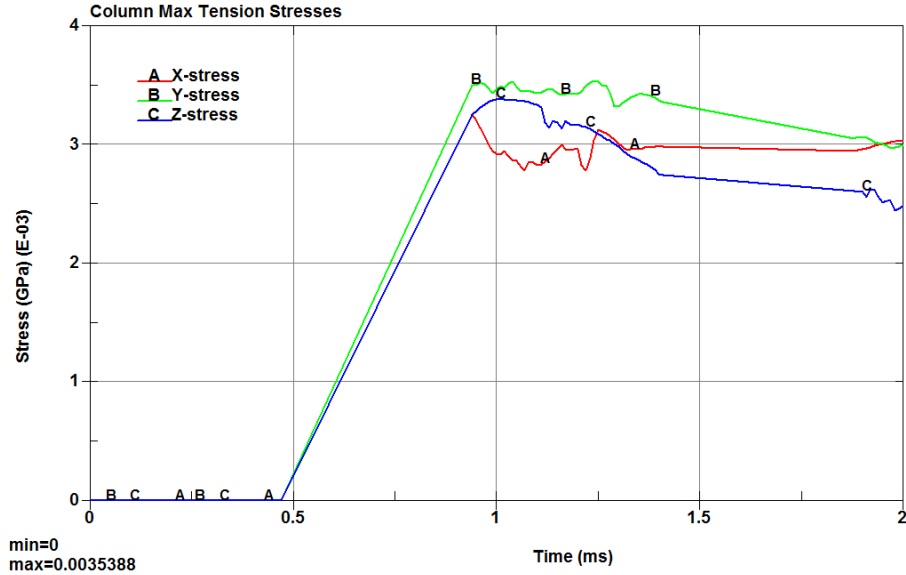


Figure 5.7: Columns tension stresses

Maximum compression stresses were recorded at the bottom of the column. The stresses increased since the blast wave effect at 0.41 ms and reached the maximum values then decreased gradually to the end of the analysis as shown in Figure 5.8. The x-axis compression stress reached a maximum value of 20.4 MPa at 0.94 ms, in the y-direction the stress reached a maximum value of 24.5 MPa at 1.20 ms, and in the z-direction the stress reached a maximum value of 28.5 MPa at 0.94 ms.

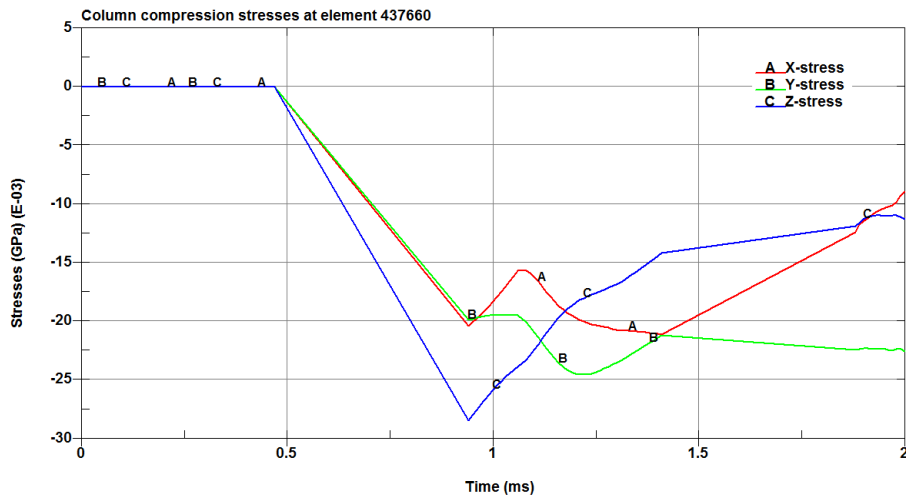


Figure 5.8: Column compression stresses

Maximum Von-Mises stress was at the bottom of the column with a maximum value of 19.93 MPa at the end of the analysis as shown in Figure 5.9.

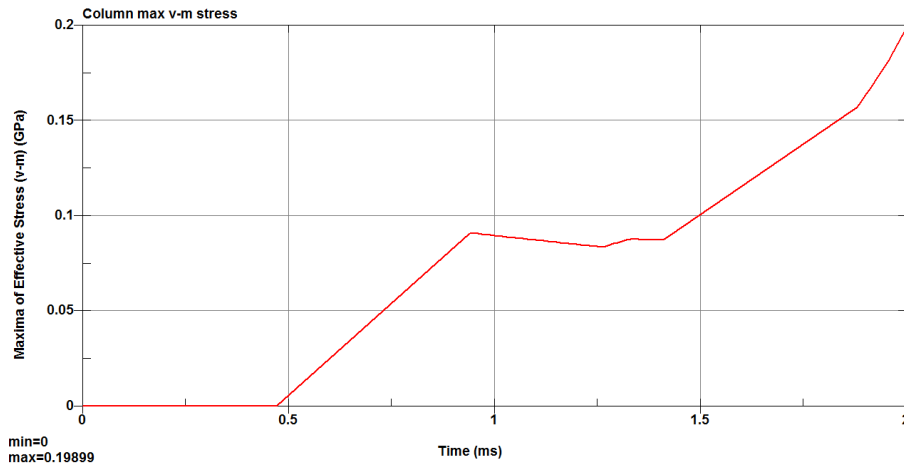


Figure 5.9: Column maximum Von-Mises stress

The columns failed at the bottom side opposite to the explosion. Elements reached a maximum value of compression stress then failed. Figure 5.10 shows the stresses of an element at the bottom of the column that reached maximum values of 1.43 MPa, 1.43 MPa, and 15.44 MPa in x , y , and z -directions respectively at time 0.94 ms before failing.

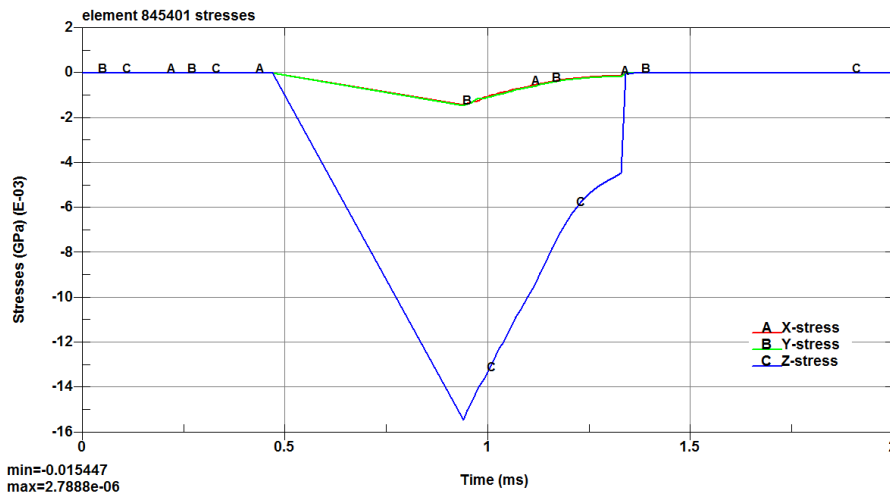


Figure 5.10: Stresses of a failed column element

5.3.2 Stress distribution at the RC slab

The slab consisted of main beams, secondary beams, ribs, and top slab. The tension and compression stresses for each member were recorded. LS-DYNA uses positive sign for tension stresses and negative sign for compressive stresses.

The x -axis and the y -axis tension stresses for most of the slab members had the same pattern. They increased since the blast wave arrival at 0.41 ms and reached the maximum values then remained almost constant to the end of the analysis. The x -axis tension stress of the top slab increased and reached the maximum value then dropped to a smaller value and remained constant to the end of the analysis. The middle rib had a different pattern in both directions, it increased suddenly at time of blast reach, then increased again to the maximum value and then remained constant until the end of the analysis, and this can be due to the location of the explosive charge below the middle rib directly. The maximum x -axis tension stress was recorded in the main beams and the minimum stress was recorded in the middle rib as shown in Figure 5.11.

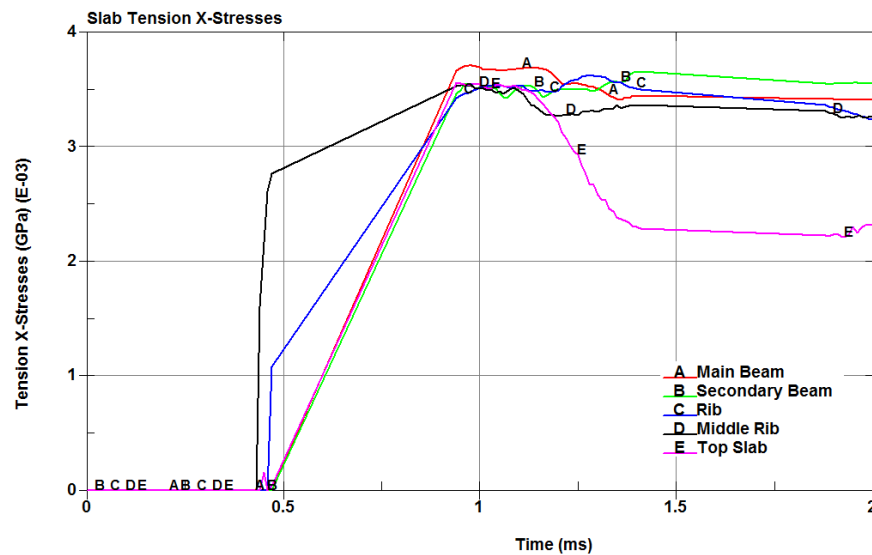


Figure 5.11: Slab members tension x -stresses

The maximum y -axis tension stress was in the secondary beam and the minimum stress was in the ribs as shown in Figure 5.12. The stresses increased at 0.41 ms, and reached the maximum value and remained almost constant to the end of the analysis.

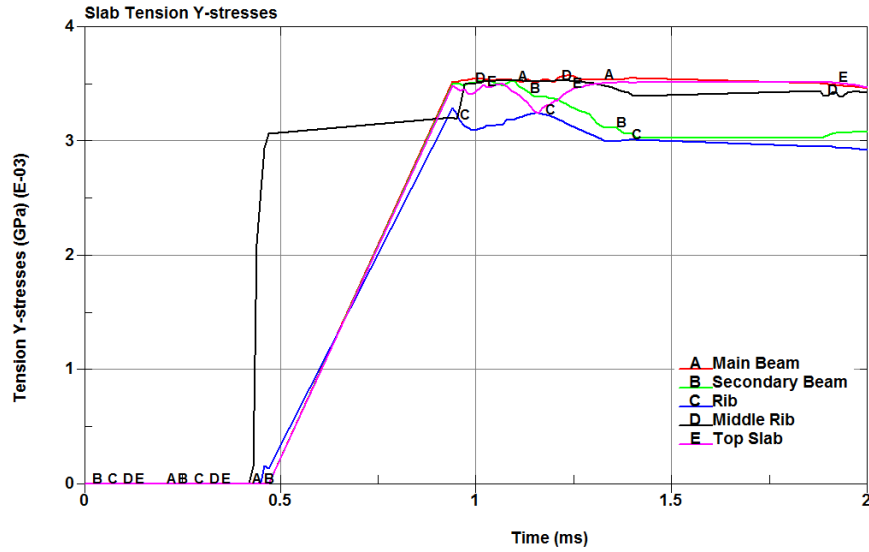


Figure 5.12: Slab members tension y-stresses

The z -axis tension stresses for the secondary beams and ribs increased since the blast wave arrival at 0.41 ms then dropped slightly, and increased again to the maximum values to remain constant until the end of the analysis. The main beam had the maximum value, it reached the maximum value then decreased and increased again slightly to the end of the analysis. The top slab z -axis stress increased immediately at the blast effect and remained constant with disturbance to the end of the analysis. The minimum z -axis tension stress was in the top slab as shown in Figure 5.13. The maximum tension stresses occurred at the top side of the slab.

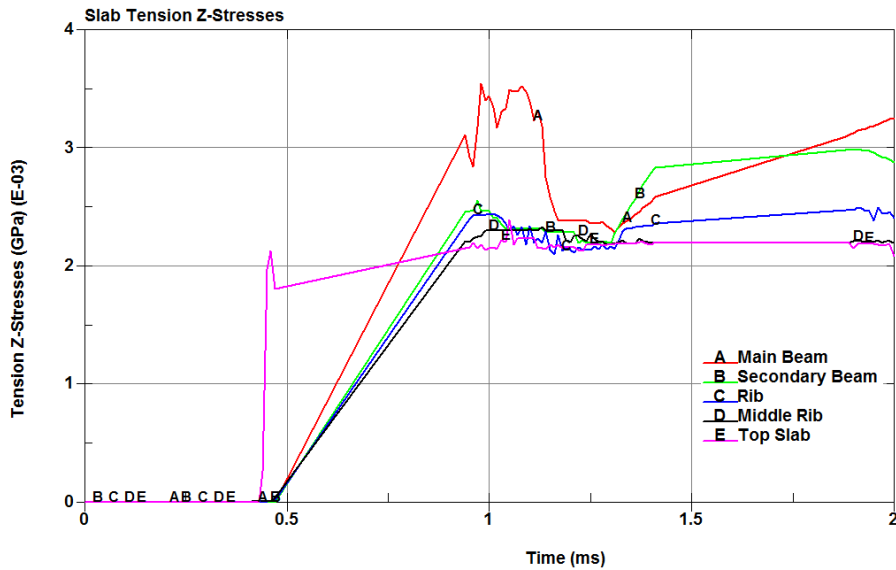


Figure 5.13: Slab members tension z -stresses

The x -axis compression stress as shown in Figure 5.14 and the y -axis compression stress as shown in Figure 5.15 had the same behavior. The stresses in the main beams, the secondary beams, and the top slab increased since the blast effect at 0.41 ms and reached the maximum values then dropped to smaller values and remained almost constant to the end of the analysis. The compression stresses of the ribs and the middle rib had different behaviors, they increased and reached their maximum values at the end of the analysis at 2.0 ms. The maximum x -axis and y -axis compression stresses were in the main beam and the minimum stresses were in the ribs.

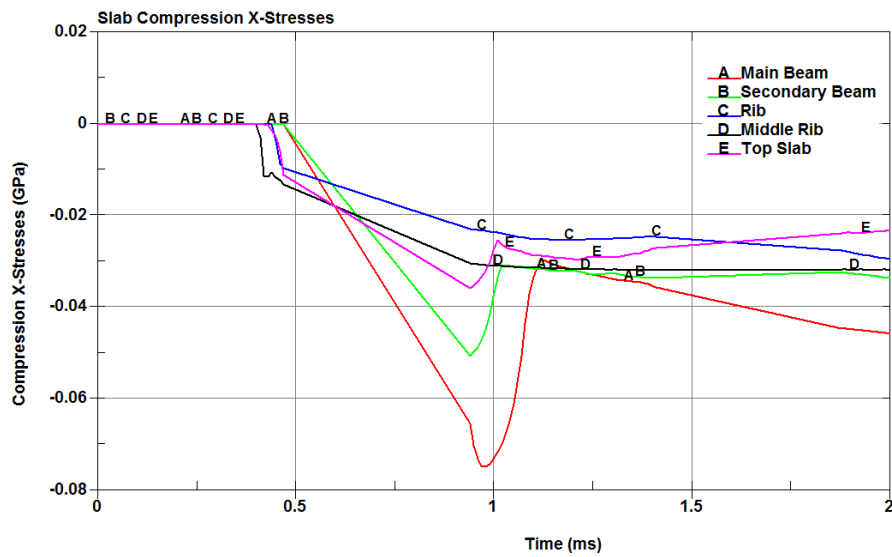


Figure 5.14: Slab members compression x -stresses

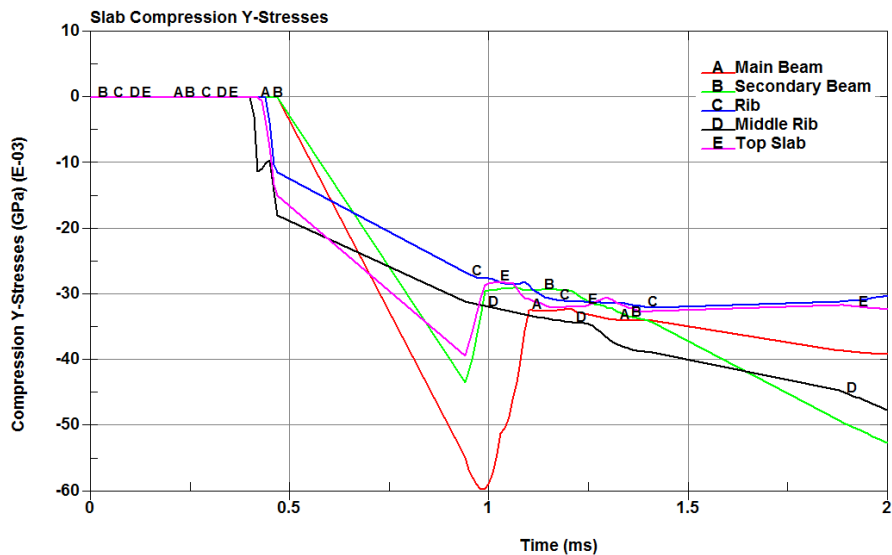


Figure 5.15: Slab members compression y -stresses

Compression stresses in z -axis for ribs, middle rib and the top slab increased immediately since the blast wave effect at 0.41 ms and reached the maximum values then dropped slightly and remained constant to the end on the analysis. For main beams and secondary beams stresses increased since the blast wave effect and reached the maximum values at the end of the analysis at 2.0 ms. The maximum z -axis compression stress was in the secondary beam and the minimum was in the ribs as shown in Figure 5.16. The maximum compression stresses occurred at the bottom side of the slab.

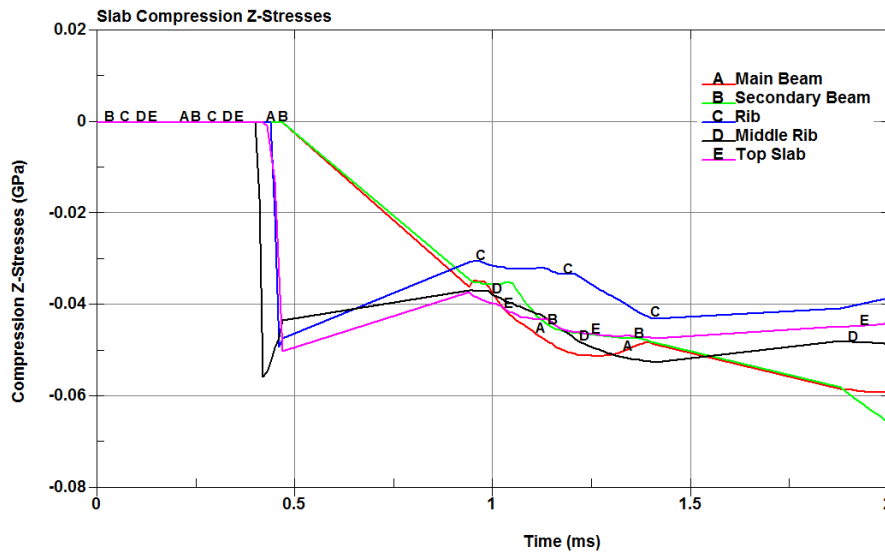


Figure 5.16: Slab members compression z -stresses

Von-Mises stresses for the slab members are shown in Figure 5.17. Maximum Von-Mises stress was recorded in main beams. The stresses increased since the blast wave effect at 0.41 ms and reached the maximum value, then dropped to a smaller value and increased again gradually to the end of the analysis. The behavior of the secondary beams were similar to that of main beams but the maximum stresses were reached at the end of the analysis. Ribs and middle rib stresses increased rapidly since the blast wave effect and reached the maximum value then remained almost constant to the end of the analysis. Top slab stress increased rapidly since the blast wave effect, then increased again gradually and reached the maximum value, dropped slightly, and remained constant to the end of the analysis. The rapid increase of the stress can be due to the location of the explosive charge in the middle of the structure and due to the

small thickness of the top slab. The main beam had the maximum values for stresses because it was affected by the deflection of the columns due to the explosion.

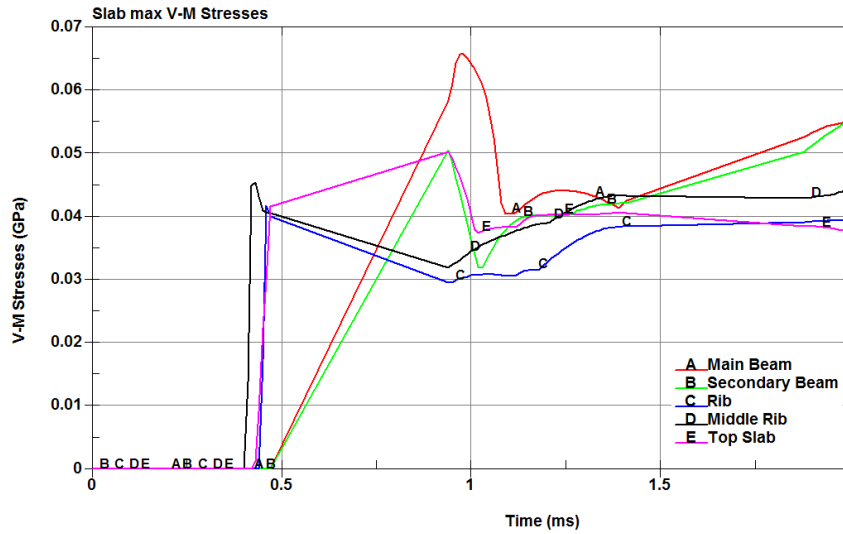


Figure 5.17: Slab members Von-Mises stresses

5.3.3 Deflections of columns

The columns gradually deformed to the outward until reaching its maximum deflection at the end of the analysis. Steel reinforcement prevented the destruction of the columns. The columns were spalled at the bottom near the supports. Figure 5.18 shows the contours of x -axis deflection and the spalling area of the columns at 2.0 ms. The structure is symmetric about the y -axis so the values to the right are negative and the values to the left are positive.

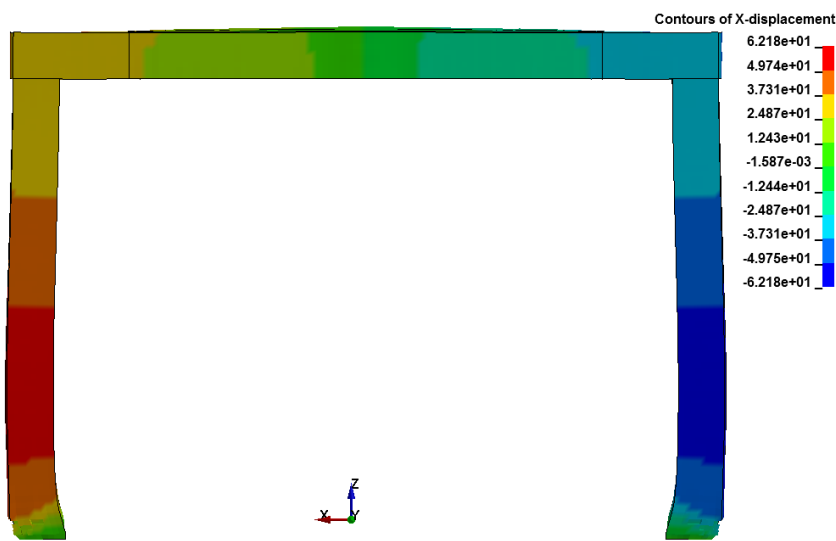


Figure 5.18: Contours of x -axis deflection

The maximum x -axis deflection occurred at the same level of the explosion center namely 500 mm from the bottom of the column. The deflection increased at 0.41 ms and reached a maximum value of 55.48 mm at 2.0 ms as shown in Figure 5.19.

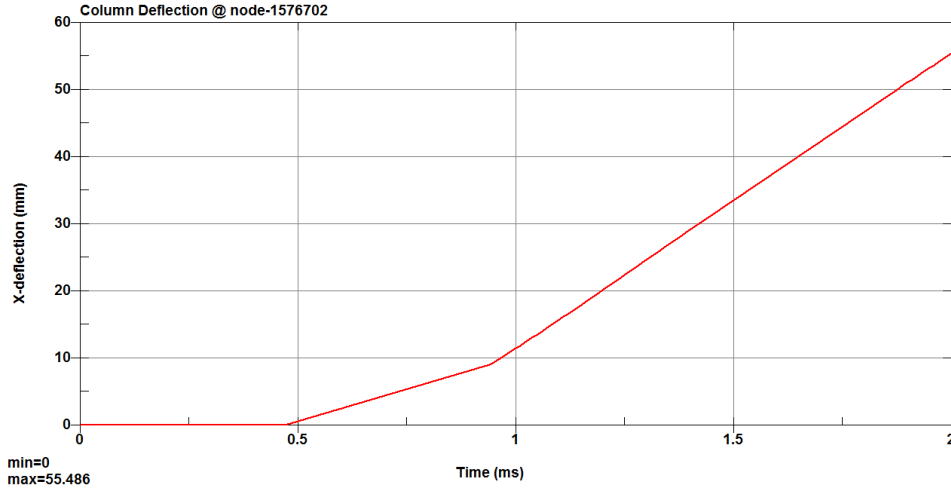


Figure 5.19: Columns x -axis deflection

The y -axis deflection was smaller than that of the x -axis. This was because the y -axis moment of inertia was greater than that of the x -axis. Figure 5.20 shows the contours of the y -axis deflection. The structure is symmetric about the x -axis so, the values to the right are negative and the values to the left are positive.

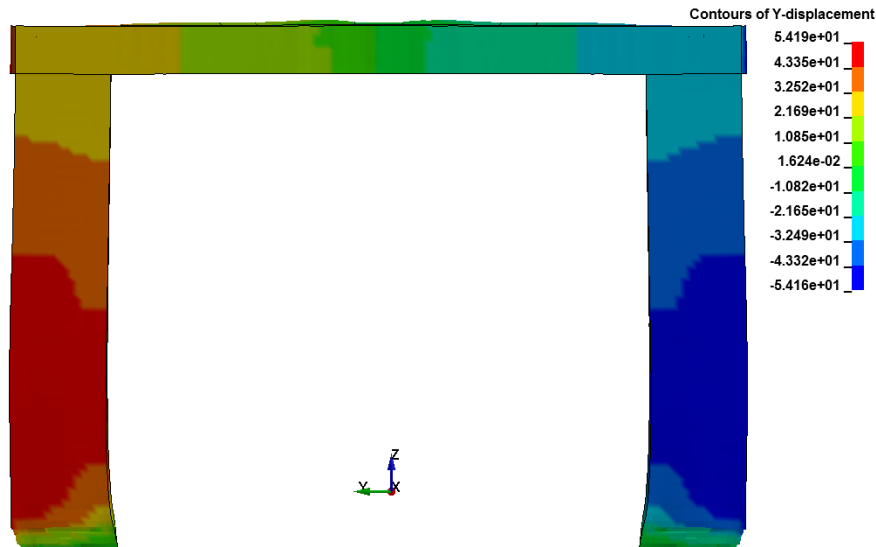


Figure 5.20: Contours of y -axis deflection

The y -axis deflection in increased at 0.41 ms and reached a maximum value of 45.3 mm at the end of the analysis at 2.0 ms as shown in Figure 5.21

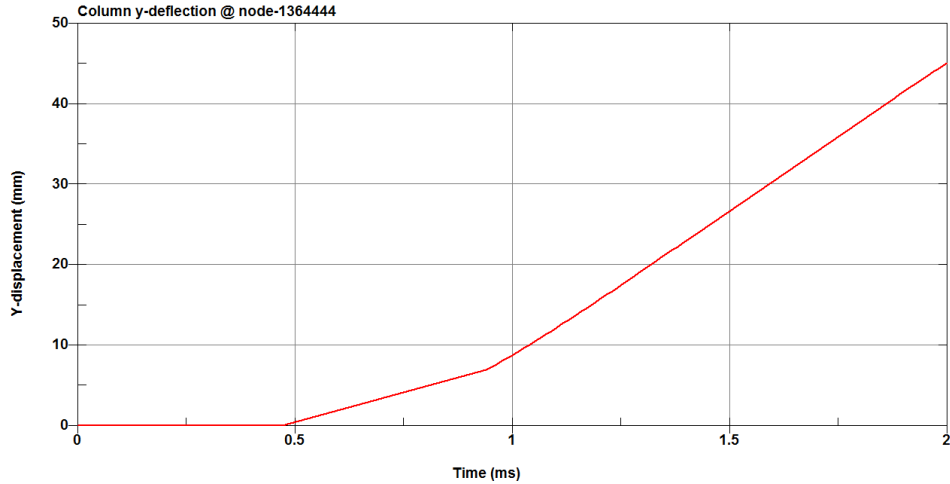


Figure 5.21: Columns y-deflection

5.3.4 Deflections of slab members

The slab deformed in the outward direction against the blast until reaching its maximum deflection at the end of the analysis. Slab members were deformed in all directions. The members started deflection since the blast wave effect at 0.41 ms and reached maximum values at the end of the analysis.

The maximum x -axis deflection was recorded in the main beams. The main beams were at the edge of the structure and were free to move in the x -direction. The minimum value were recorded in the secondary beam as shown in Figure 5.22.

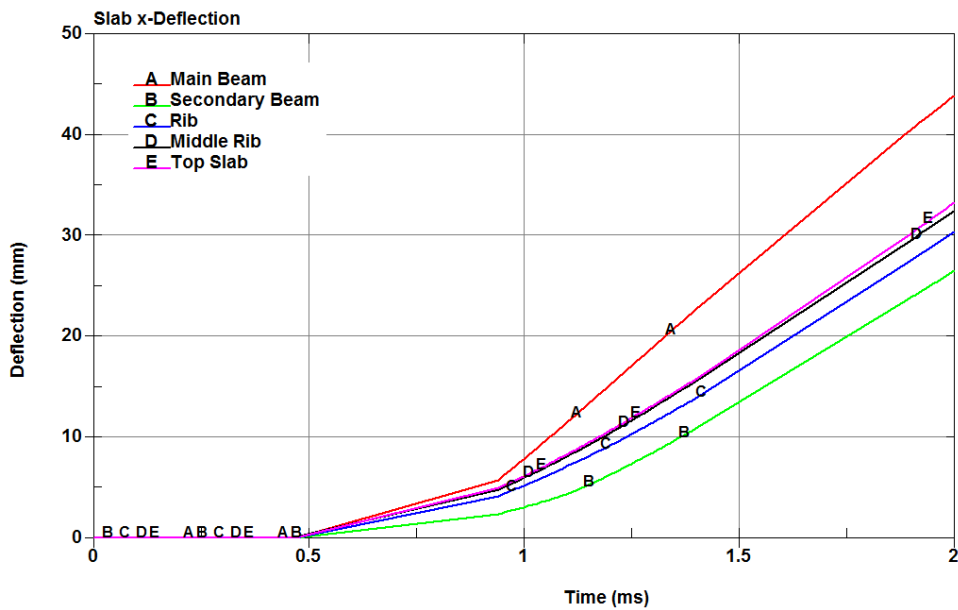


Figure 5.22: Slab members maximum x -axis deflections

Figure 5.23 shows the contours of the x -axis deflection in slab members. The structure is symmetric about the x -axis so the values to the right are positive and the values to the left are negative.

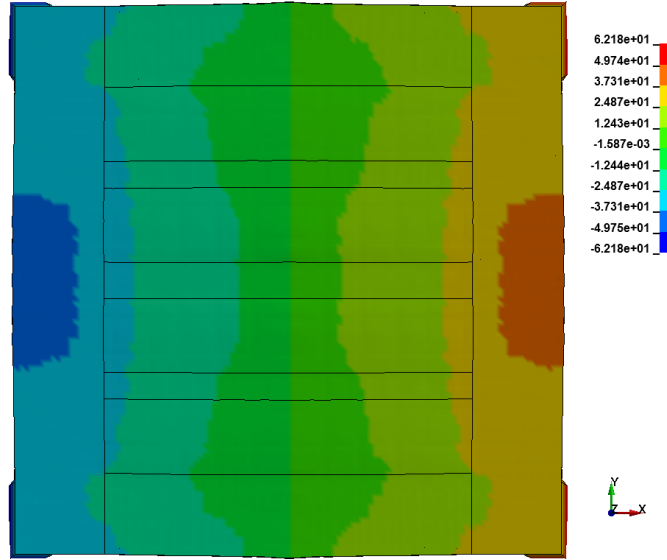


Figure 5.23: Contours of x -axis deflection for slab members

The maximum y -axis deflection was recorded in secondary beams and the minimum value were recorded in the middle rib as shown in Figure 5.24.

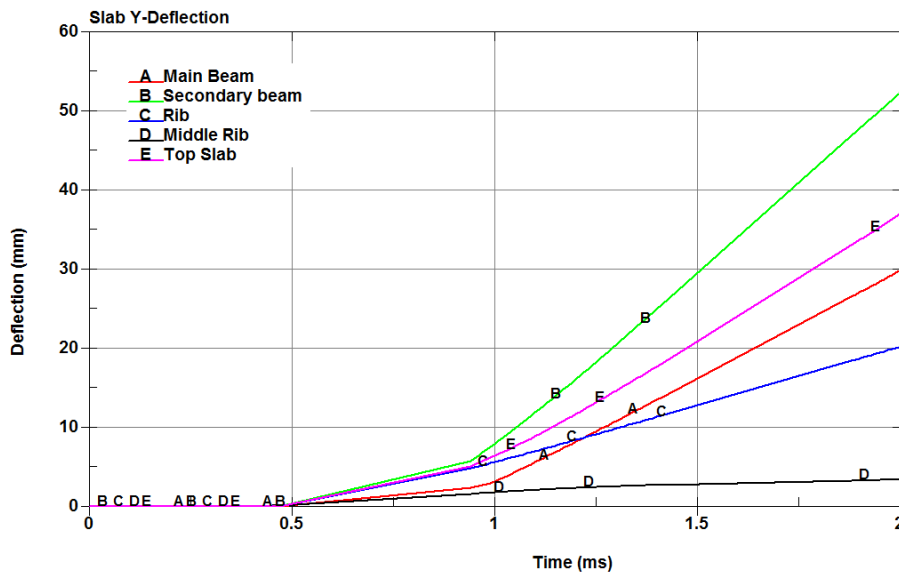


Figure 5.24: Slab members maximum y -axis deflections

Figure 5.25 shows the contours of y -axis deflection in slab members. The structure is symmetric about the x -axis so the values to the top are positive and the values to the bottom are negative.

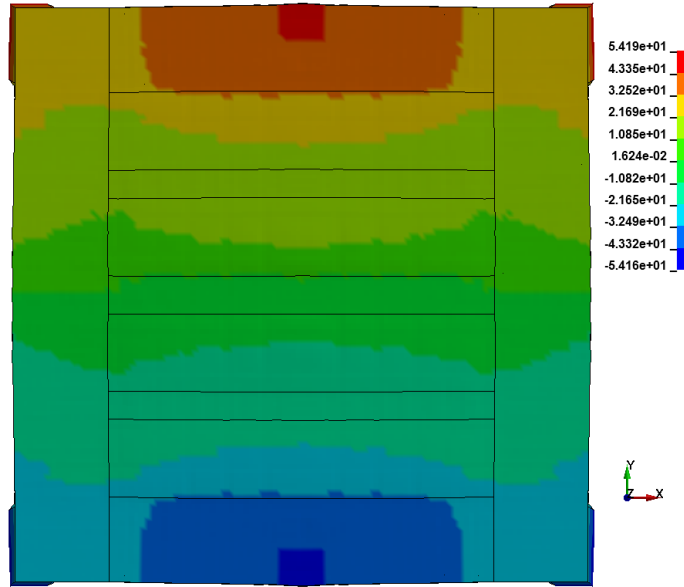


Figure 5.25: Contours of y-axis deflection for slab members

In z-direction minimum and maximum values of deflection were recorded for slab members. Minimum deflection means deflection downward in the negative z-direction and maximum deflection means upward in the positive z-direction. The minimum z-axis deflection were recorded in the edges of main beams as shown in Figure 5.26.

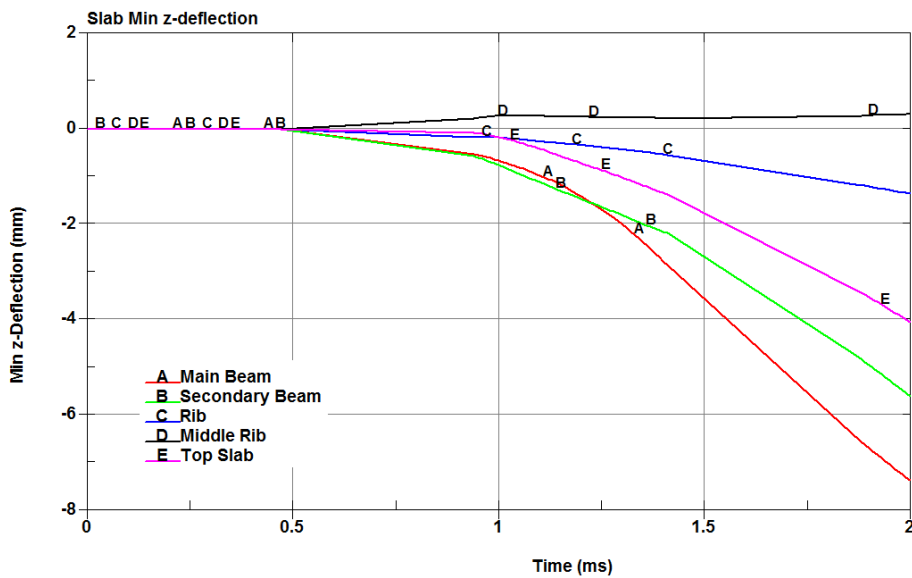


Figure 5.26: Slab members minimum z-axis deflections

The maximum z -axis deflection was recorded in top slab and the minimum value was recorded in main beams as shown in Figure 5.27.

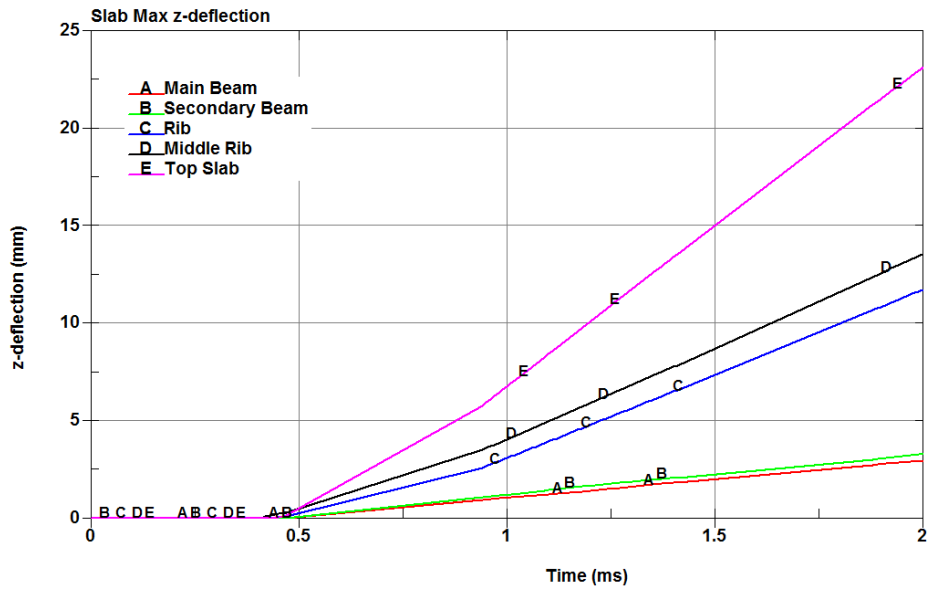


Figure 5.27: Slab members maximum z -axis deflections

Figure 5.28 shows the contours of z -deflection in slab members.

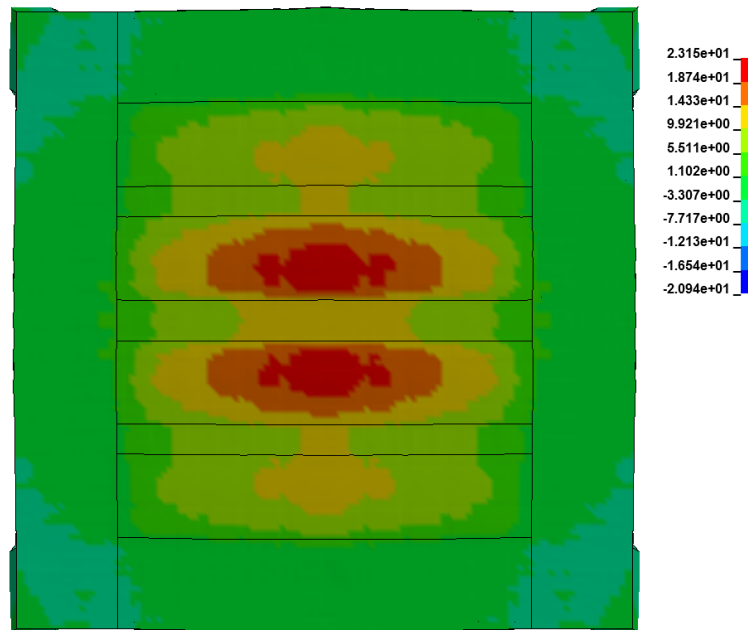


Figure 5.28: Contours of z -deflection for slab members

5.4 Effect of concrete strength on the behavior of the structure

Structural resistance to loads increases when using higher compressive strength concrete. The effect of concrete compressive strength on the behavior of a structure subjected to blast load was studied using the same previous model and changing the concrete strength to 58 MPa.

The model with the increased concrete strength was analyzed in LS-DYNA for 2.0 ms. The time required to finish the analysis were 1:24:12 hour. The behavior of every part of the structure was recorded and will be compared with the previous case.

5.4.1 Stress distribution of the columns with concrete strength of 58 MPa

The tension stresses of the columns with 58 MPa compressive strength concrete in all directions increased since the blast wave effect at 0.41 ms and reached the maximum values and then remained almost constant to the end of the analysis. The values of maximum tension stresses for columns with 58 MPa compressive strength concrete were increased when compared to those of 29 MPa compressive strength concrete as shown in Table 5.5.

Table 5.5: Comparison of column maximum tension stresses between columns with 29 MPa and 58 MPa compressive strength concrete

Direction	Column with 29 MPa strength concrete		Column with 58 MPa strength concrete		Stress increase percentage (%)
	Value (MPa)	Time (ms)	Value (MPa)	Time (ms)	
X	3.25	0.94	5.12	2.00	157.54
Y	3.55	1.24	5.36	1.12	150.98
Z	3.39	1.01	5.06	1.02	149.26

Maximum compression stresses were recorded at the bottom of the column. The stresses increased since the blast wave effect at 0.41 ms and reached maximum values then decreased gradually to the end of the analysis. The values of compression stresses for columns with 58 MPa compressive strength concrete were increased by about 175% in *x*-direction, 146% in *y*-direction, and 154% in *z*-direction when compared to those of 29 MPa compressive strength concrete as shown in

Table 5.6

Table 5.6: Comparison of column maximum compression stresses between columns with 29 MPa and 58 MPa compressive strength concrete

Direction	Column with 29 MPa strength concrete		Column with 58 MPa strength concrete		Stress increase percentage (%)
	Value (MPa)	Time (ms)	Value (MPa)	Time (ms)	
X	20.04	0.94	35.40	0.94	176.64
Y	24.5	1.20	35.9	1.04	146.53
Z	28.5	0.94	43.9	0.94	154.03

Maximum Von-Mises stress was recorded at the bottom of the column with a maximum value of 22.14 MPa at 2.00 ms at the end of the analysis as shown in Figure 5.29. The value of Von-Mises stress for 58 MPa compressive strength concrete column was 111% greater than that of 29 MPa compressive strength concrete column.

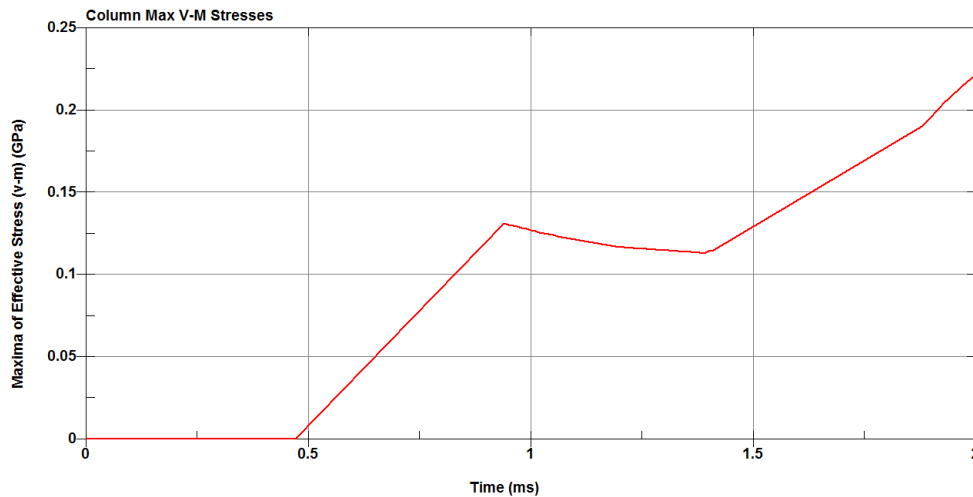


Figure 5.29: Column with 58 MPa compressive strength concrete Von-Mises stresses

The columns with 58 MPa compressive strength concrete failed at the bottom in the outside of the column opposite to the explosion, but the damage was less than the original column damage. Figure 5.30 shows the failure stresses of an element at the bottom of the column. The stresses in the x -direction and y -direction for the column with 58 MPa compressive strength concrete were close to those for the column with 29 MPa compressive strength concrete. But in the z -direction the stress was 19.65 MPa before failing but greater than that of the column with 29 MPa compressive strength concrete by 127.3%.

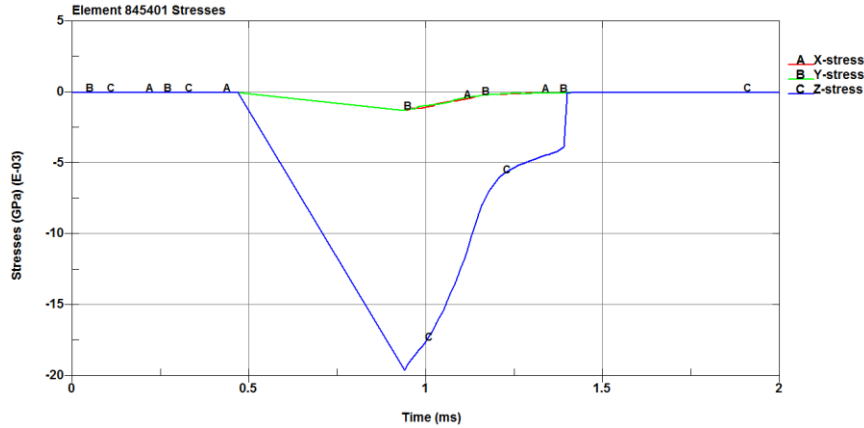


Figure 5.30: Stresses of a failed element in the column with 58 MPa concrete compressive strength

5.4.2 Stress distribution at the 58 MPa compressive strength concrete slab

The x -axis tension stress for main beams and secondary beams of the 58 MPa compressive strength concrete structure increased since the blast wave arrival at 0.41 ms and reached the maximum values and then remained almost constant to the end of the analysis. For the top slab, the ribs, and the middle rib stresses increased suddenly at the time of the blast wave arrival this was due to the location of the explosion below the middle rib, then increased gradually to the maximum value and remained constant to the end of the analysis. The maximum x -axis tension stress was in the main beams and the minimum stress was in the middle rib.

The y -axis tension stresses for the members of the slab with 58 Mpa compressive strength concrete increased except the middle rib since the blast wave arrival at 0.41 ms, reached the maximum values, and then remained almost constant to the end of the analysis. For the middle rib, the tension stress increased suddenly at the time of the blast wave arrival and reached the maximum value then remained constant to the end of the analysis. The maximum y -axis tension stress was in the secondary beams and the minimum stresses was in the ribs.

The z -axis tension stresses for the secondary beams and ribs increased since the blast wave arrival at 0.41 ms. The secondary beam reached a value then dropped slightly, and increased again to the maximum value at the end of the analysis. The ribs reached the maximum value and remained constant to the end of the analysis. The main beam stress increased and reached the maximum value then decreased and increased again

slightly to the end of the analysis. The top slab and the middle rib increased immediately at the blast arrival to the maximum values and remained constant with disturbance to the end of the analysis as shown in. The maximum z -axis tension stress was in the main beam and the minimum stress was in the top slab.

The values of tension stresses in the 58 MPa compressive strength concrete slab members were increased when compared to those of the 29 MPa compressive strength concrete slab members as shown in Table 5.7.

Table 5.7: Comparison of the tension stresses in the 58 MPa and 29 MPa strength concrete slab members

Slab member	Direction	29 MPa strength concrete slab		58 MPa strength concrete slab		Stress increase percentage (%)
		Value (MPa)	Time (ms)	Value (MPa)	Time (ms)	
Main beams	X	3.72	0.97	5.59	1.02	150.27
	Y	3.52	0.94	5.31	1.18	150.85
	Z	3.54	0.98	5.28	1.06	149.15
Secondary beams	X	3.66	1.41	5.46	1.31	149.18
	Y	3.54	1.09	5.79	1.02	163.56
	Z	3.00	1.89	5.04	2.00	168.00
Ribs	X	3.63	1.28	5.28	1.09	145.45
	Y	3.29	0.94	5.10	0.97	155.02
	Z	2.43	0.96	3.80	0.97	156.38
Middle rib	X	3.54	0.95	5.25	1.10	148.31
	Y	3.53	1.08	5.23	1.38	148.16
	Z	2.33	1.13	3.53	1.10	151.50
Top slab	X	3.56	0.93	5.31	1.04	149.16
	Y	3.49	0.94	5.27	0.95	151.00
	Z	2.4	1.05	3.25	1.23	135.42

The x -axis compression stresses in the main beams, the secondary beams and the top slab increased since the blast effect at 0.41 ms and reached the maximum values then dropped to smaller values and remained almost constant to the end of the analysis. The x -axis compression stresses of the ribs and the middle rib had a different behavior; they increased to their maximum values at the end of the analysis at 2.0 ms.

The y-axis compression stresses in the main beams and the top slab increased since the blast effect at 0.41 ms and reached the maximum values then dropped to smaller values and remained almost constant to the end of the analysis. The y-axis compression stresses of the secondary beam, the ribs, and the middle rib had a different behavior; they reached their maximum values at the end of the analysis at 2.0 ms.

The z-axis compression stresses in the main beams and in the top slab increased since the blast effect at 0.41 ms, and reached the maximum values at the end of the analysis at 2.0 ms. The compression stresses of the secondary beam, the ribs, and the middle rib had a different behavior, they increased suddenly and reached smaller values, then dropped slightly and increased to the maximum values at the end of the analysis at 2.0 ms. The values of compression stresses for the slab members with 58 MPa compressive strength concrete were increased as shown in Table 5.8.

Table 5.8: Comparison of the compression stresses in the 58 MPa and 29 MPa strength concrete slab members

Slab member	Direction	29 MPa strength concrete slab		58 MPa strength concrete slab		Stress increase percentage (%)
		Value (MPa)	Time (ms)	Value (MPa)	Time (ms)	
Main beams	X	74.8	0.97	102.27	0.95	136.72
	Y	59.7	0.98	96.58	0.95	161.78
	Z	59.7	2.00	83.65	2.00	140.12
Secondary beams	X	50.7	0.95	64.34	0.94	126.90
	Y	52.6	2.00	65.94	2.00	125.36
	Z	67.7	2.00	68.69	2.00	101.46
Ribs	X	29.6	2.00	35.36	2.00	119.46
	Y	32.1	1.41	42.67	1.41	132.93
	Z	49.3	0.46	60.18	1.41	122.07
Middle rib	X	32.1	2.00	34.32	2.00	106.92
	Y	47.6	2.00	56.97	2.00	119.68
	Z	55.8	0.42	69.04	1.41	123.73
Top slab	X	35.9	0.94	65.15	0.94	181.48
	Y	39.4	0.94	53.19	0.94	135.00
	Z	50.2	0.47	66.04	1.41	131.55

The maximum Von-Mises stress was recorded in main beams. The stress increased since the blast wave effect at 0.41 ms and reached the maximum value then dropped

to a smaller value and increased again gradually to the end of the analysis. The behavior of the secondary beams was similar to that of main beams with smaller values. Ribs and middle rib stresses increased rapidly since the blast wave effect and reached smaller values, then increased gradually to the maximum values and remained almost constant to the end of the analysis. Top slab stress increased rapidly since the blast wave effect, then increased again to the maximum value, dropped slightly, and remained constant to the end of the analysis. The stresses of the slab with 58 MPa strength concrete were greater than those of the slab with 29 MPa strength concrete.

Von-Mises stress values for the slab members with the 58 MPa strength concrete were increased when compared to those of the slab members with the 29 MPa strength concrete as shown in Table 5.9.

Table 5.9: Comparison of the Von-Mises stresses between the 29 MPa and 58 MPa strength concrete slab members

Slab member	29 MPa strength concrete slab		58 MPa strength concrete slab		Stress increase percentage (%)
	Maximum V-M stresses (MPa)	Time (ms)	Maximum V-M stresses (MPa)	Time (ms)	
Main beams	65.85	0.97	107.72	0.96	163.58
Secondary beams	55.33	2.00	81.87	0.94	147.97
Ribs	41.77	0.46	56.61	1.41	135.53
Middle rib	45.50	0.43	61.51	1.41	135.19
Top slab	50.31	0.94	88.87	0.94	176.64

5.4.3 Deflection of columns with 58 MPa compressive strength concrete

The columns deformed in the outward direction gradually until reaching its maximum deflection at the end of the analysis. Steel reinforcement prevented the destruction of the columns. The columns were spalled at the bottom near the supports. Figure 5.31 shows the contours of x -displacement and the spalling of the 58 MPa strength concrete columns at 2.0 ms. The structure is symmetric about the y -axis so the values to the left are positive and the values to the right are negative.

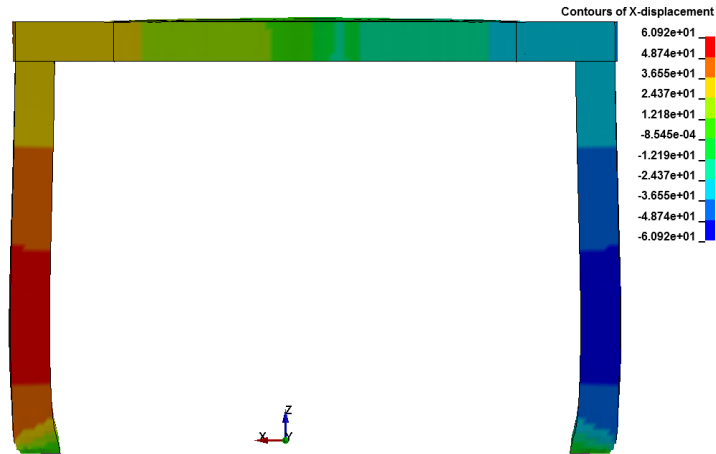


Figure 5.31: 58 MPa strength concrete structure contours of x -deflection

The maximum x -axis deflection was at the point in the same level of the explosion center namely 500 mm from the bottom of the column. The x -axis deflection increased at 0.41 ms and reached a maximum value of 55.36 mm at 2.0 ms.

The y -axis deflection was smaller than that of the x -axis. This was because the y -axis moment of inertia was greater than that of the x -axis. Figure 5.32 shows the contours of y -displacement of the structure with the 58 MPa strength concrete. The structure is symmetric about the x -axis so the values to the left are positive and the values to the right are negative.

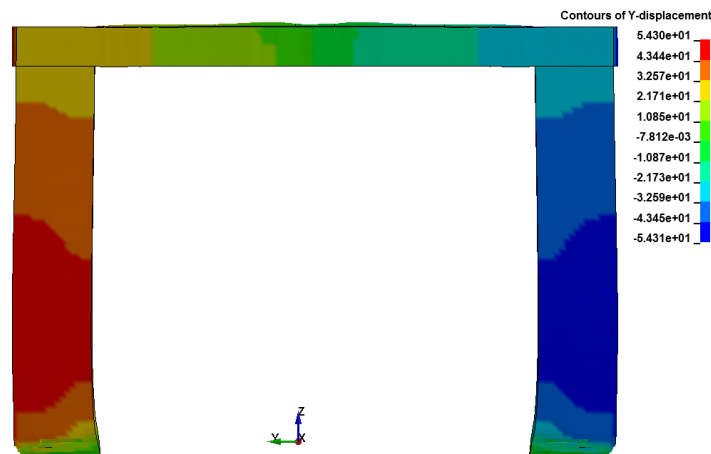


Figure 5.32: Structure with 58 MPa concrete strength contours of y -displacement

The deflection in y -direction increased at 0.41 ms and reached a maximum value of 44.37 mm at the end of the analysis at 2.0 ms. The deflection of the columns with the 58 MPa concrete compressive strength were decreased slightly when compared to that

of the columns with the 29 MPa concrete compressive strength concrete as shown in Table 5.10.

Table 5.10: Comparison of the deflection in the 58 MPa and 29 MPa strength concrete columns

Direction	29 MPa strength concrete column deflection (mm)	58 MPa strength concrete column deflection (mm)	Deflection decrease percentage (%)
X	55.48	55.36	0.22
Y	45.30	44.37	2.10

The change in the deflection of the columns was unnoticed, because of the short time of the analysis and the high rate of loading which affect the behavior of concrete.

5.4.4 Deflection of slab members with 58 MPa concrete Strength

The 58 MPa strength concrete slab deformed in the outward direction against the blast until reaching its maximum deflection at the end of the analysis. The members deflected since the blast wave effect at 0.41 ms and reached maximum values at the end of the analysis.

The maximum x -axis deflection was recorded in main beams and the minimum value was recorded in the secondary beam. Figure 5.33 shows the contours of x -axis deflection in slab members. The structure is symmetric about the y -axis so the values to the right are positive and the values to the left are negative.

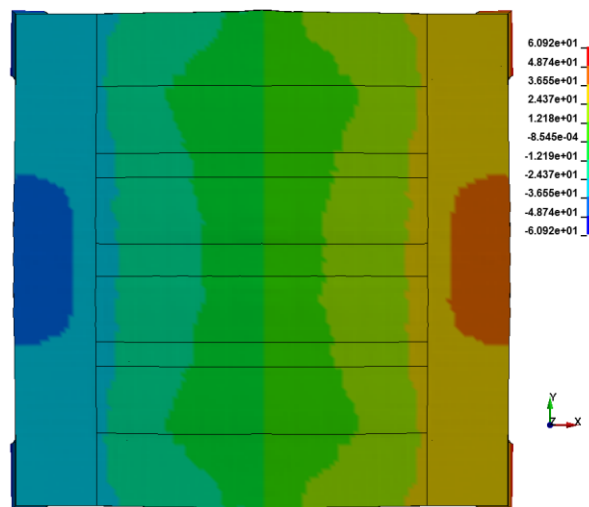


Figure 5.33: Contours of x -axis deflection for slab members with 58 MPa strength concrete

The maximum y -axis deflection was recorded in secondary beams and the minimum value was recorded in the middle rib. Figure 5.34 shows the contours of y -axis deflection in slab members. The structure is symmetric about the x -axis so the values to the top are positive and the values to the bottom are negative.

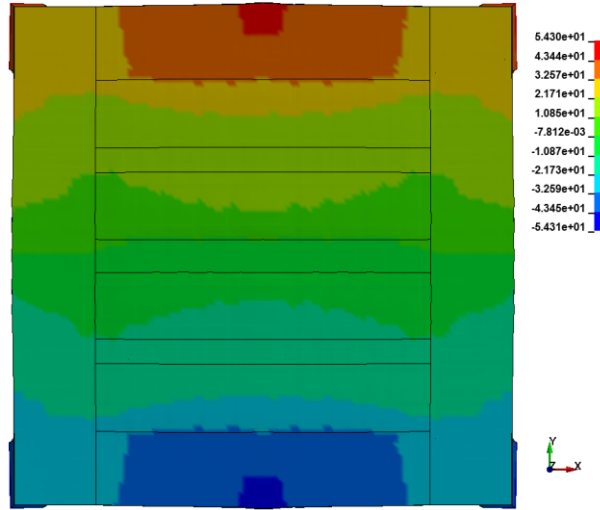


Figure 5.34: Contours of y -displacement for slab members with 58 MPa concrete strength

In z -direction minimum and maximum values of deflection were recorded for strengthened slab members. Minimum deflection means deflection downward in the negative z -direction and maximum deflection means upward in the positive z -direction. The minimum z -axis deflection was recorded in the edges of main beams and the maximum z -axis deflection was recorded in top slab. Figure 5.35 shows the contours of z -deflection in slab members.

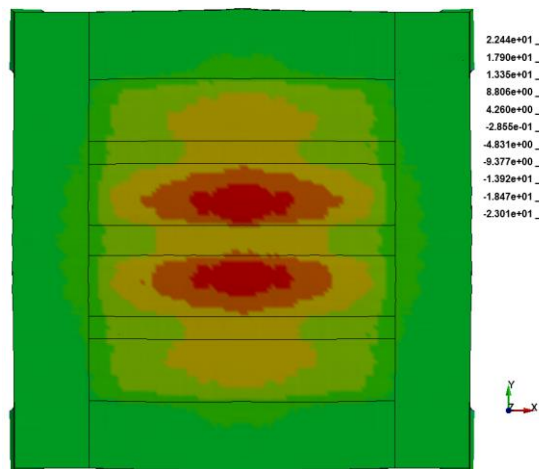


Figure 5.35: Contours of z -displacement for slab members with 58 MPa concrete strength

The high rate of loading of the blast load and the very short time of the analysis resulted in very close deflection results in all directions for all the structure's members. Table 5.11 shows the results of deflection for the slab members with 58 MPa strength concrete and for the slab members with 29 MPa strength concrete for comparison.

Table 5.11: Comparison of the deflection values for the 58 MPa and 29 MPa concrete strength slab members

Slab member	Direction	29 MPa strength concrete slab Maximum deflection (mm)	58 MPa strength concrete slab Maximum deflection (mm)	Deflection change percentage
Main beams	X	44.15	43.91	-0.54
	Y	31.15	29.88	-4.08
	Z (upward)	2.71	2.94	7.82
	Z (downward)	6.15	7.39	16.78
Secondary beams	X	27.62	26.53	-3.95
	Y	54.30	52.40	-3.50
	Z (upward)	3.87	3.28	-15.25
	Z (downward)	5.13	5.61	8.56
Ribs	X	30.04	30.39	1.15
	Y	17.73	20.21	12.27
	Z (upward)	12.25	11.74	-4.16
	Z (downward)	1.46	1.36	-6.85
Middle rib	X	31.76	32.48	2.22
	Y	3.35	3.37	0.59
	Z (upward)	14.44	13.58	-5.96
	Z (downward)	-	-	-
Top slab	X	32.75	33.29	1.62
	Y	36.79	37.00	0.57
	Z (upward)	22.44	23.15	3.07
	Z (downward)	3.81	4.06	6.16

5.5 Effect of changing the explosion location

The original model was reanalyzed with relocating the explosion outside the structure by moving the charge location by a distance of 2.5 m in y-direction as shown in Figure 5.36.

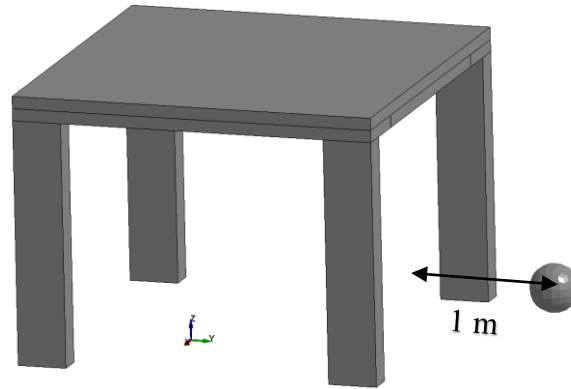


Figure 5.36: Schematic of the structure and the location of external explosion

The model with the relocated explosion was analyzed in LS-DYNA for 4.0 ms. The time required to finish the analysis were 2:56:48 hours. The results for every part behavior of the structure were recorded.

The blast wave reached the front columns first at 0.48 ms with a pressure of 25.38 MPa, and reached the slab at 0.56 ms with a pressure of 22.36 MPa, and then propagated through the structure and reached the rear columns at 2.62 ms with a pressure of 1.33 MPa as shown in Figure 5.37.

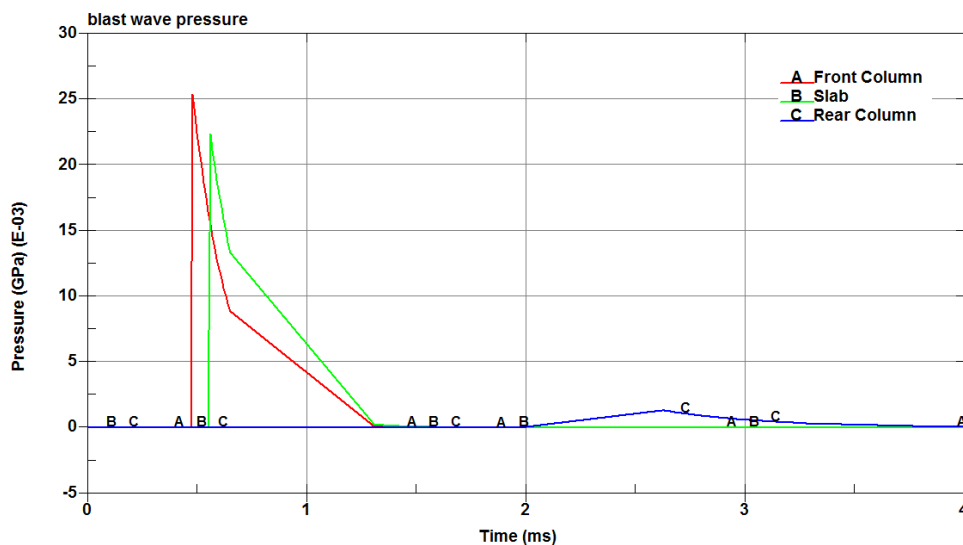


Figure 5.37: External blast wave pressure on structure

5.5.1 Stress distribution of externally blasted columns

The externally blasted structure was symmetry only about y -axis, so results for front members close to the explosion and rear members far from explosion were recorded.

The tension stresses of the front columns in all directions increased since the blast wave arrival at 0.48 ms and reached the maximum values, and remained almost constant to the end of the analysis as shown in Figure 5.38.

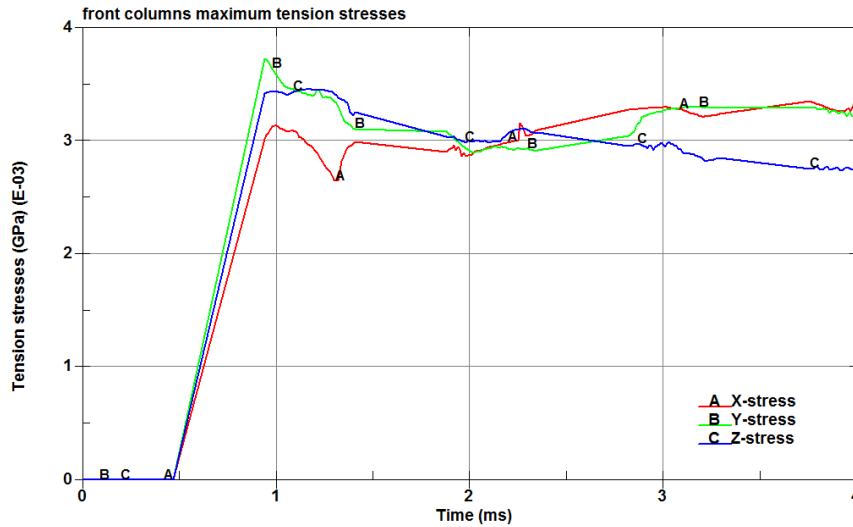


Figure 5.38: Front columns tension stresses

The compression stresses of the front columns in all directions increased since the blast wave arrival at 0.48 ms and reached the maximum values then dropped suddenly to a minor value and remained almost constant to the end of the analysis as shown in Figure 5.39.

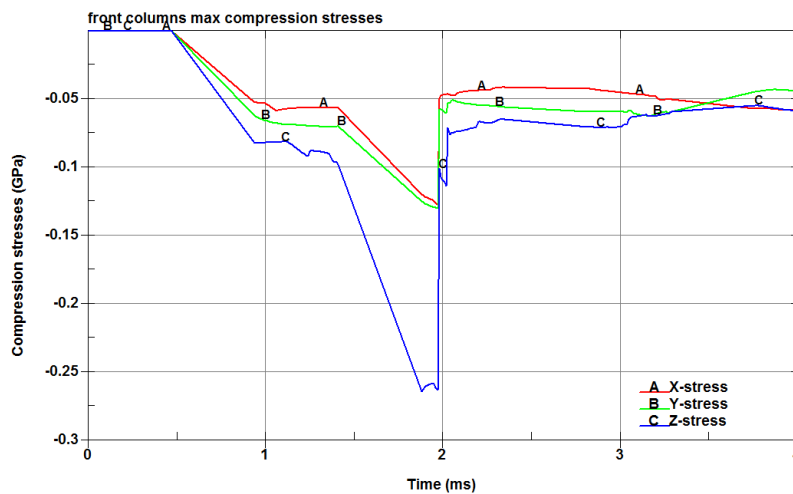


Figure 5.39: Front columns compression stresses

Maximum Von-Mises stresses in the front columns were at the bottom of the columns with a maximum value of 231.47 MPa at 1.95 ms, dropped suddenly after that to a minor value and remained almost constant to the end of analysis as shown in Figure 5.40.

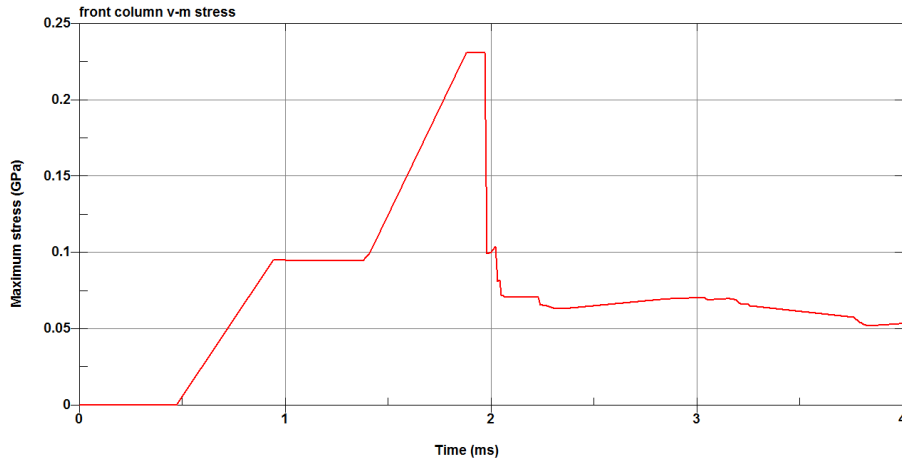


Figure 5.40: Front columns Von-Mises stresses

The tension stresses of the rear columns in all directions increased since the blast wave arrival to the structure and became disturbed when the blast wave reached it at 2.62 ms and reached the maximum values at times close to the end of the analysis as shown in Figure 5.41.

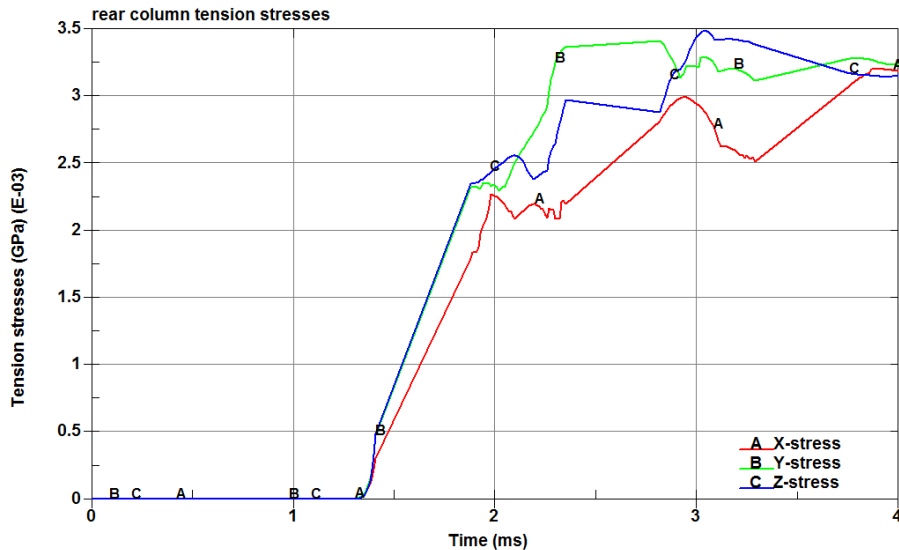


Figure 5.41: Rear columns tension stresses

The compression stresses of the rear columns in all directions increased since the blast wave arrival to the structure and continued increasing when the blast wave reached it

at 2.62 ms and reached the maximum values at the end of the analysis as shown in Figure 5.42.

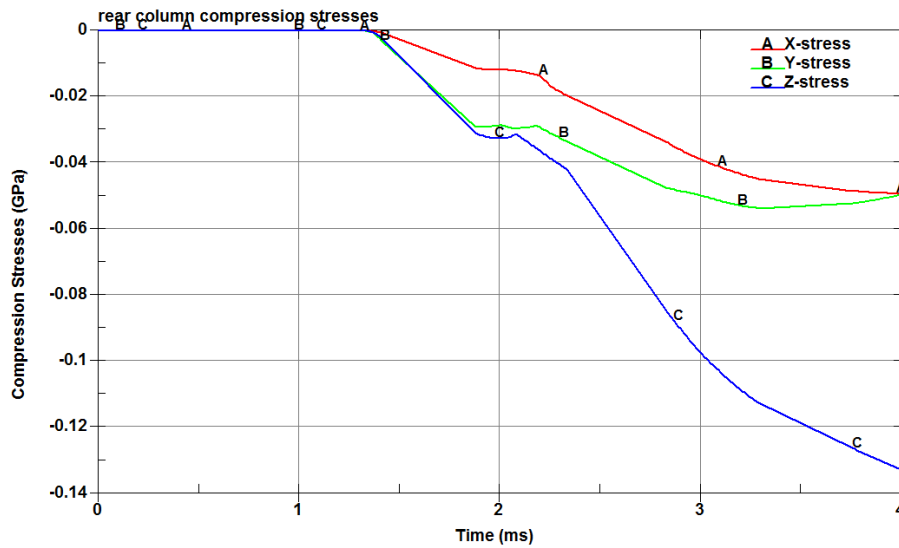


Figure 5.42: Rear columns compression stresses

Maximum Von-Mises stresses in the rear columns were at the bottom of the columns with a maximum value of 110.32 MPa at 4.00 ms at the end of the analysis as shown in Figure 5.43.

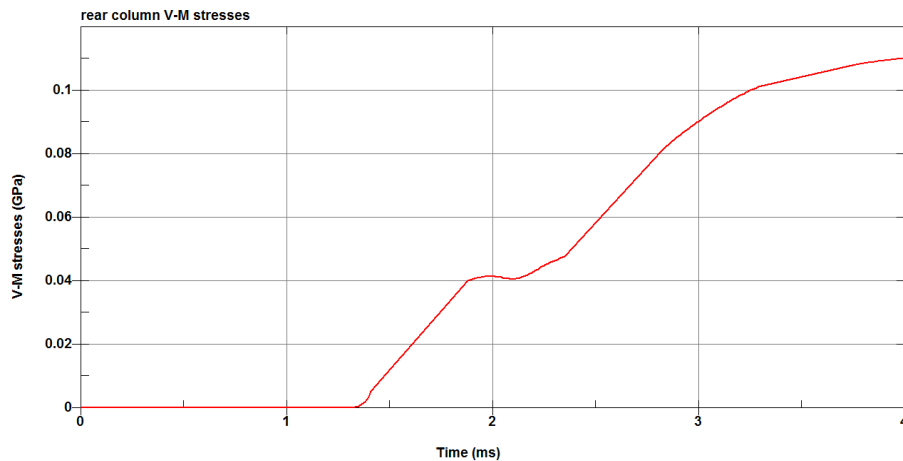


Figure 5.43: Rear columns Von-Mises stresses

The front column failed at the bottom in all sides. Elements reached maximum values of compression stresses then failed. Figure 5.44 shows the stresses of an element at the bottom of the columns that reached maximum values of 1.92 MPa, 3.20 MPa, and 23.92 MPa in x,y, and z-directions respectively at time 0.97 ms before failing.

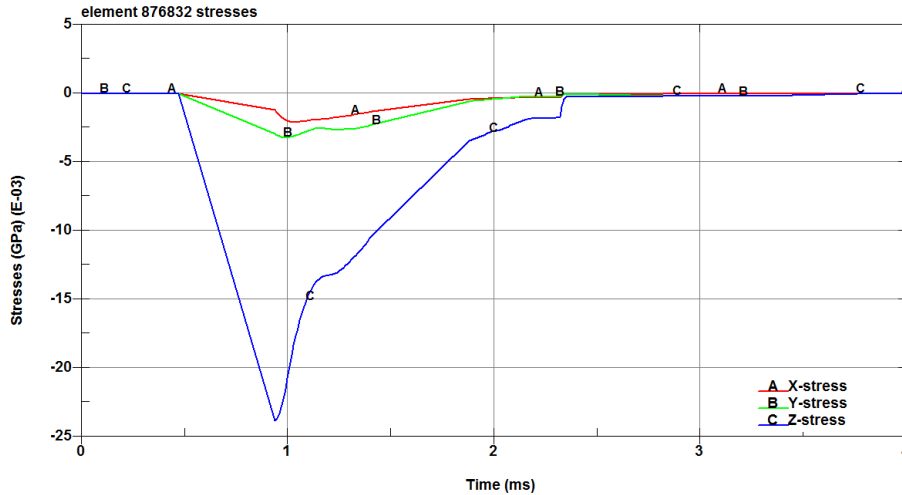


Figure 5.44: Stresses of a failed element in the front column

Table 5.12 shows the maximum stresses for the externally blasted columns.

Table 5.12: Maximum stresses value for externally blasted columns

Member	Direction	Tension stresses (MPa)		Compression stresses (MPa)	
		Value (MPa)	Time (ms)	Value (MPa)	Time (ms)
Front columns	X	3.35	3.75	127.01	1.97
	Y	3.73	0.94	130.06	1.97
	Z	3.46	1.17	264.59	1.88
Rear columns	X	3.21	3.89	49.31	3.98
	Y	3.41	2.82	53.73	3.29
	Z	3.49	3.04	132.78	4.00

5.5.2 Stress distribution of the slab members

The tension stresses for the externally blasted slab members had almost the same behavior with differences in the stresses increasing points that varied according to the arrival of the blast wave to the member.

The *x*-axis tension stress for the front top slab increased and reached the maximum value then dropped to a minor value and remained constant to the end of the analysis. For the other members the stresses increased and reached the maximum values and remained almost constant to the end of the analysis as shown in Figure 5.45.

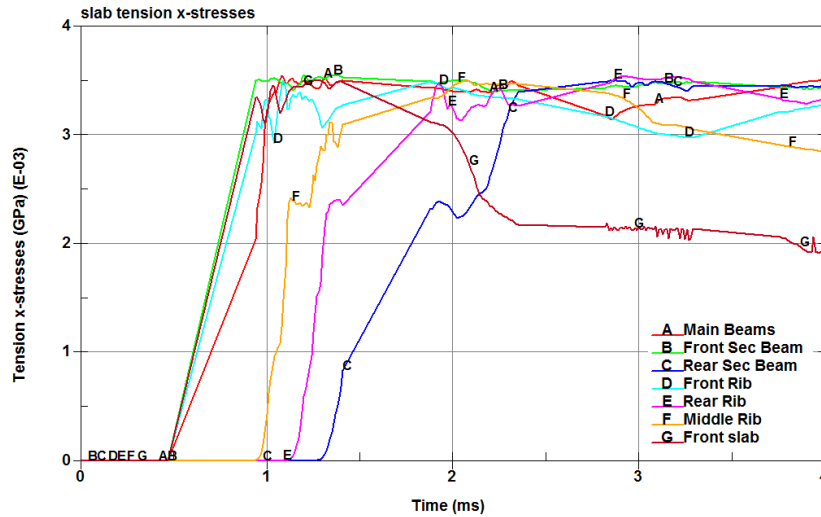


Figure 5.45: Externally blasted slab members tension x-stresses

The y-axis tension stresses for the externally blasted slab members had different patterns. For the main beams, the front secondary beams, the front rib, and the middle rib the stresses increased and reached the maximum values and remained almost constant to the end of the analysis. The stress of the rear rib increased suddenly to a large value and continued increasing and reached the maximum value at the end of the analysis. The front top slab stress increased suddenly to a large value, increased again to the maximum value, and decreased gradually to the end of the analysis. The rear secondary beam stress increased suddenly to a large value, dropped to a minor value, and increased again and reached the maximum value at the end of the analysis as shown in Figure 5.46.

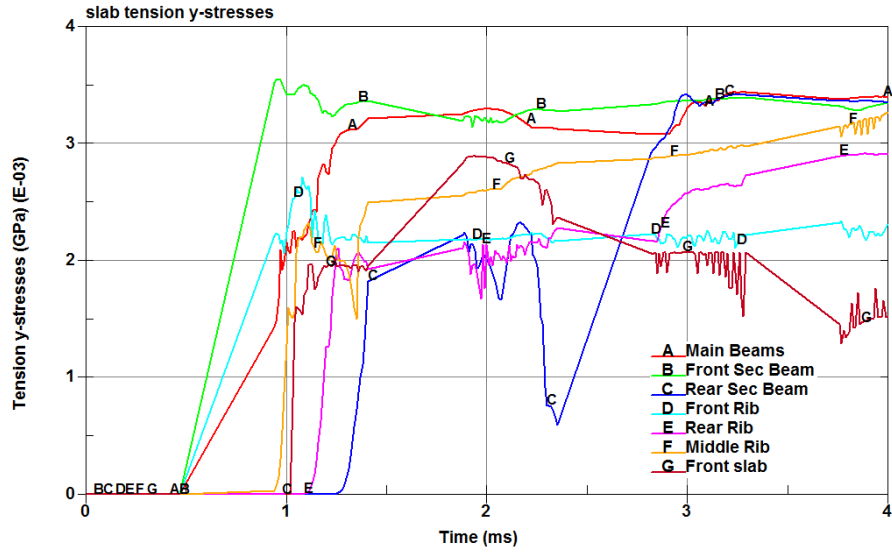


Figure 5.46: Externally blasted slab members tension y-stresses

The z-axis tension stresses for all the externally blasted members except the front top slab increased and reached the maximum values and remained constant to the end of the analysis. For the front slab the stress increased to the maximum value, dropped to a minor value, and remained constant to the end of the analysis as shown in Figure 5.47

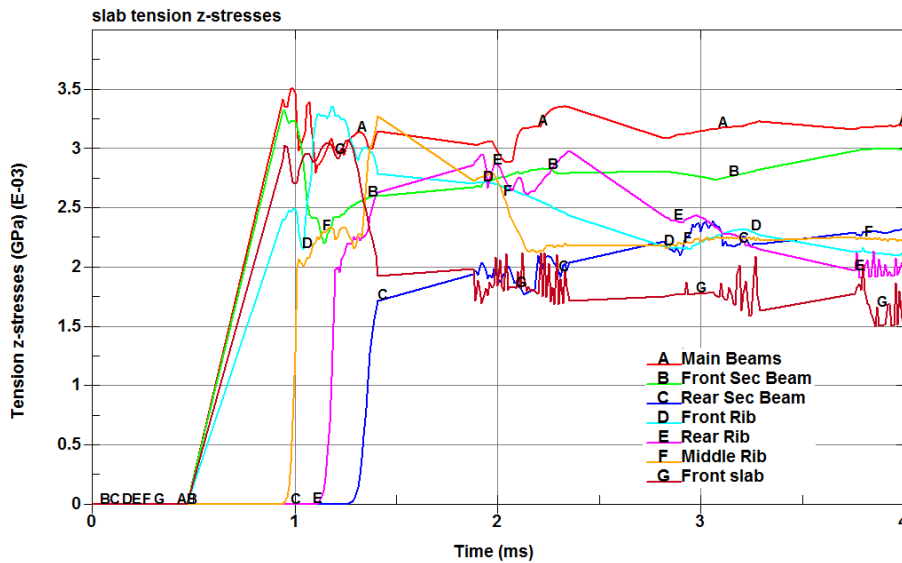


Figure 5.47: Externally blasted slab members tension z-stresses

The maximum tension stresses values for all the slab members were close to each other. The maximum tension stresses in the x-direction and in the y-direction were recorded in the front secondary beam. And in the z-direction the maximum stresses were recorded in the main beams. Tension stresses for externally blasted slab members are listed in Table 5.13.

Table 5.13: Externally blasted slab members tension stresses

Slab member	Maximum tension stress (MPa)		Time (ms)
	Direction	Value	
Main beams	X	3.55	1.08
	Y	3.44	3.27
	Z	3.52	0.99
Front secondary beams	X	3.56	1.20
	Y	3.56	0.96
	Z	3.33	0.94
Rear secondary beam	X	3.50	2.88
	Y	3.43	2.98
	Z	2.39	3.06
Front rib	X	3.51	1.09
	Y	2.72	1.08
	Z	3.36	1.18
Rear rib	X	3.54	2.91
	Y	2.92	3.88
	Z	2.98	2.35
Middle rib	X	3.50	2.07
	Y	3.27	4.00
	Z	3.28	1.41
Front top slab	X	3.51	1.28
	Y	2.90	1.98
	Z	3.07	1.26

The compression stresses for the externally blasted slab members increased since the blast wave arrival to the members in different rates and reached the maximum values.

The *x*-axis compression stress for the rear secondary beam increased since the blast wave effect on the structure and increased again in a higher rate when the blast wave reached it at 2.62 ms and reached the maximum value at the end of the analysis. The stresses for the other slab members increased and reached the maximum values, then dropped to minor values and remained constant to the end of the analysis as shown in Figure 5.48.

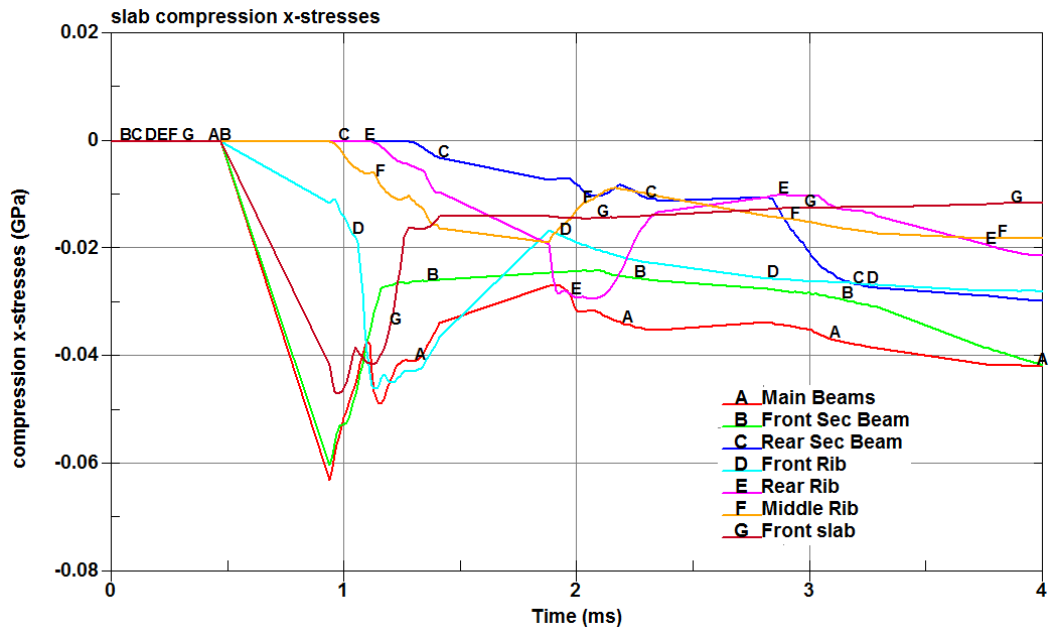


Figure 5.48: Externally blasted slab members compression x-stresses

The y-compression stresses for slab members except the front secondary beam increased and reached the maximum values, then decreased slightly gradually and remained constant to the end of the analysis. The stress of the front secondary beam increased and reached a large value, then decreased, and increased again and reached the maximum value at the end of the analysis as shown in Figure 5.49.

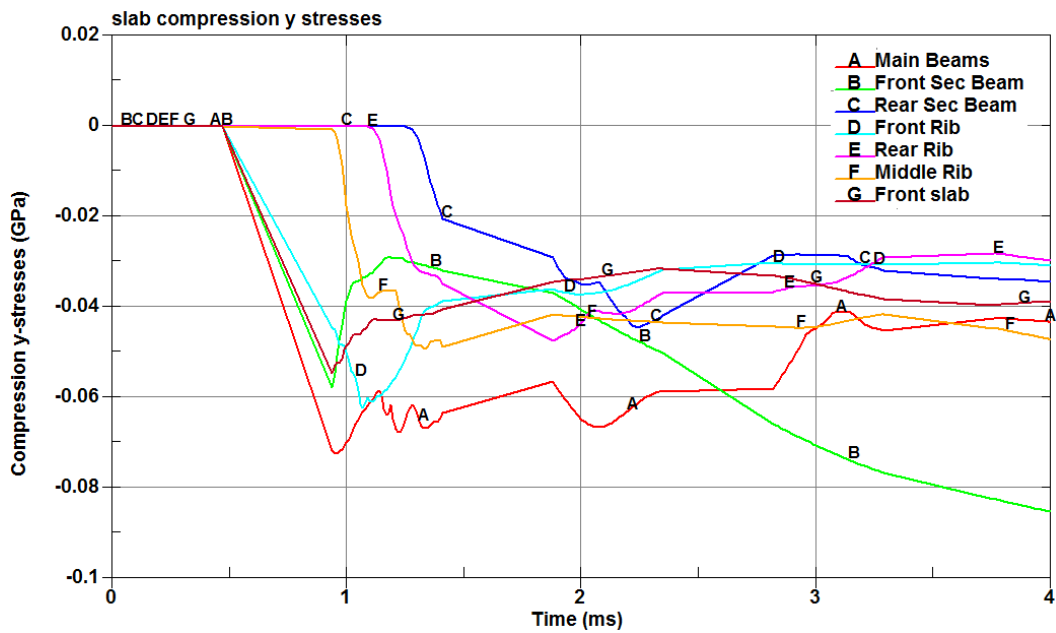


Figure 5.49: Externally blasted slab members compression y-stresses

The z -axis compression stresses for the externally blasted slab members increased gradually and reached the maximum value. For the main beam, the front rib, and the front top slab the maximum values were reached before the end of the analysis and then the stresses decreased slightly to the end of the analysis. For the other slab members the maximum values were reached at the end of the analysis as shown in Figure 5.50.

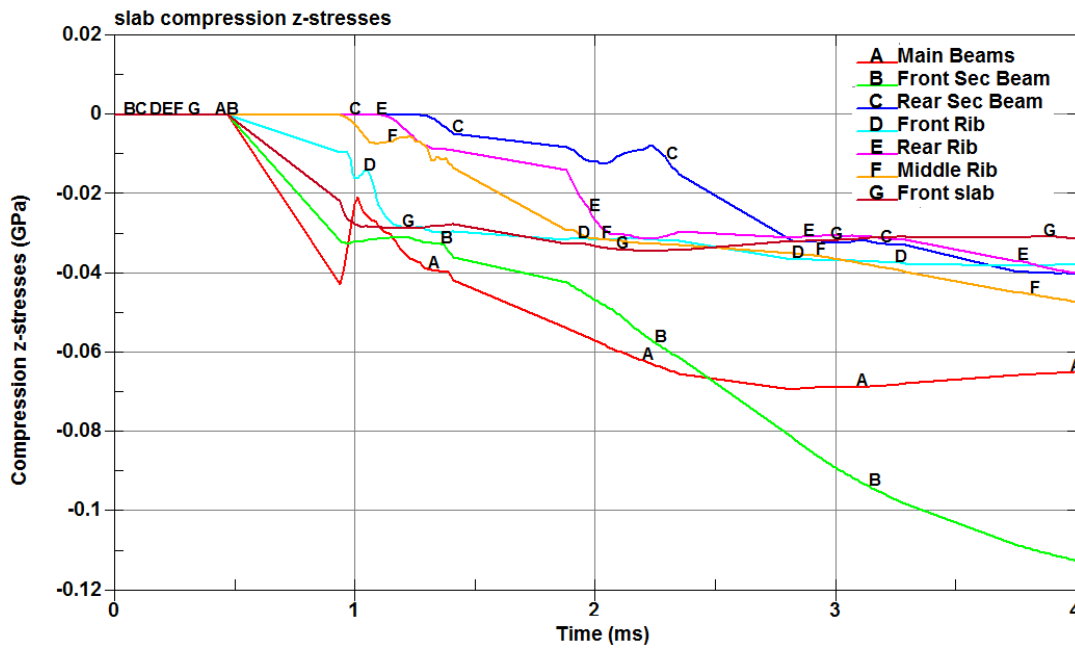


Figure 5.50: Externally blasted slab members compression z -stresses

The maximum x -axis compression stress was recorded in the main beams. And the maximum y -axis and z -axis compression stresses were recorded in the front secondary beam. Compression stresses for externally blasted slab members are shown in Table 5.14.

Table 5.14: Externally blasted slab members compression stresses

Slab member	Maximum compression stress (MPa)		Time (ms)
	Direction	Value	
Main beams	X	63.19	0.94
	Y	72.44	0.96
	Z	69.27	2.83
Front secondary beams	X	60.29	0.94
	Y	85.44	4.00
	Z	112.56	4.00
Rear secondary beam	X	29.78	4.00
	Y	44.65	2.24
	Z	40.06	3.99
Front rib	X	46.11	1.14
	Y	62.38	1.07
	Z	38.12	3.76
Rear rib	X	29.40	2.06
	Y	47.51	1.88
	Z	39.97	4.00
Middle rib	X	18.85	1.88
	Y	49.26	1.33
	Z	47.24	4.00
Front top slab	X	46.91	0.97
	Y	54.65	0.94
	Z	34.29	2.21

Von-Mises stresses for the externally blasted slab members increased since the blast wave arrival to it and reach the maximum values at different times.

The Von-Mises stress in the main beam increased to a large value then dropped and increased again gradually and reached the maximum value, then decreased to the end of the analysis. For the front secondary beam the stress increased to a large value then dropped and increased again gradually and reached the maximum value at the end of the analysis. The stress of the middle rib increased to a large value, then decreased gradually and increased and reached the maximum value at the end of the analysis. The stresses in the other slab members increased and reached the maximum values then decreased to a minor value and remained constant to the end of the analysis as shown in Figure 5.51.

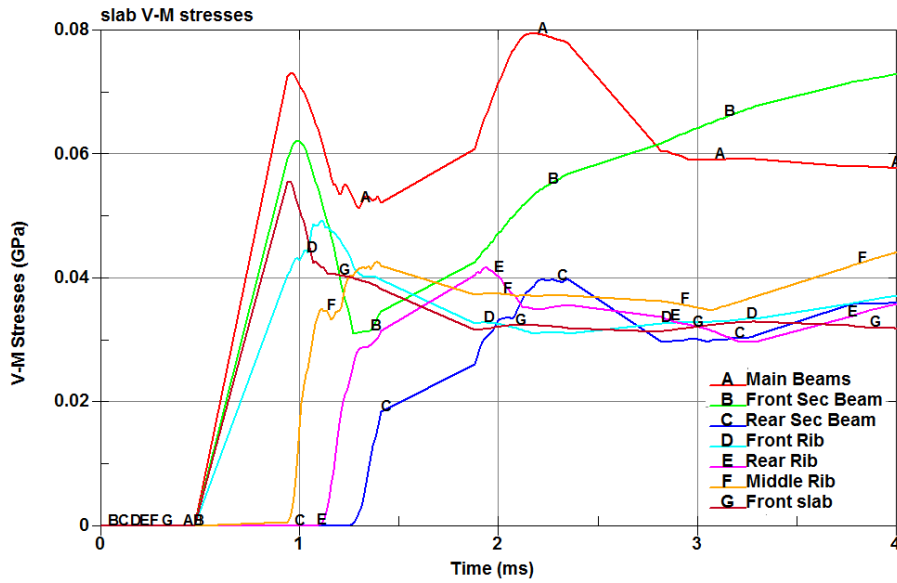


Figure 5.51: Externally blasted slab members Von-Mises stresses

The maximum Von-Mises stress was recorded in the main beams. And the minimum Von-Mises stress was recorded in the rear secondary beam. Von-Mises stresses for externally blasted slab members are shown in Table 5.15.

Table 5.15: Externally blasted slab members Von-Mises stresses

Slab member	Maximum Von- Mises stress (MPa)	Time (ms)
Main beam	79.61	2.17
Front secondary beam	73.07	4.00
Rear secondary beam	39.87	2.35
Front rib	49.32	1.11
Rear rib	41.72	1.93
Middle rib	44.21	4.00
Front top slab	55.65	0.95

5.5.3 Deflections of columns

The externally blasted structure was deformed in the negative y -direction opposite to the explosion center. The maximum deflection for all the structure members was recorded at the end of the analysis.

The maximum deflection of the front columns near the explosion was above 500 mm from the columns bottom. A maximum value 160.09 mm in the x -direction and 125.2 mm in the y -direction were recorded at the end of the analysis as shown in Figure 5.52.

The front columns deflected since the blast wave arrival at 0.48 ms

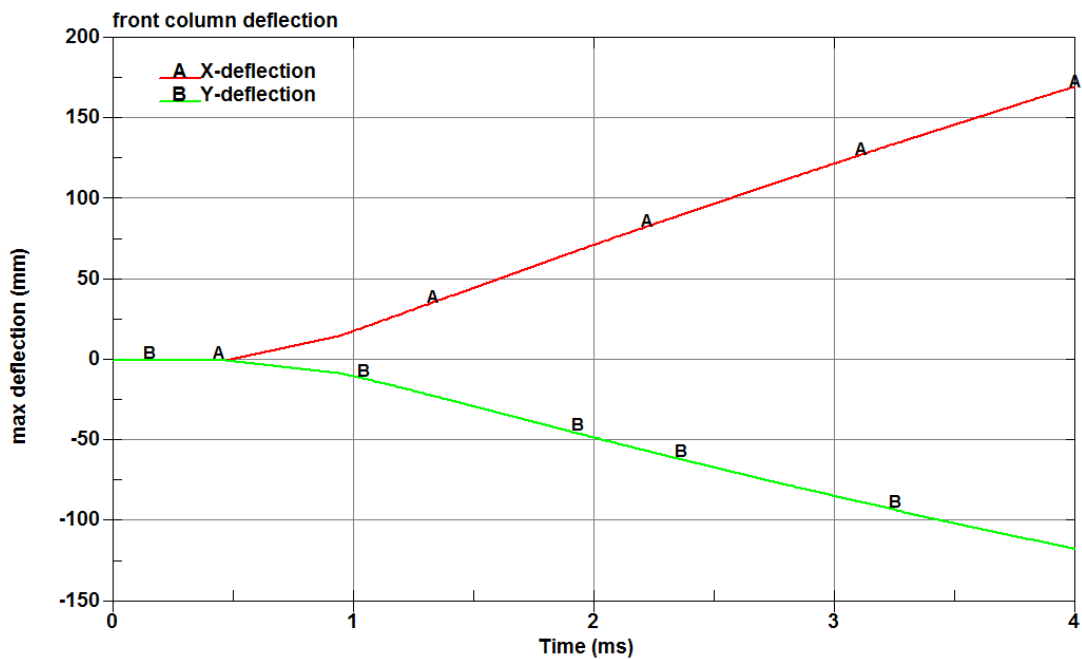


Figure 5.52: Externally blasted front columns deflection

Figure 5.53 shows the contours of the x -axis deflection and the y -axis deflection for the front column.

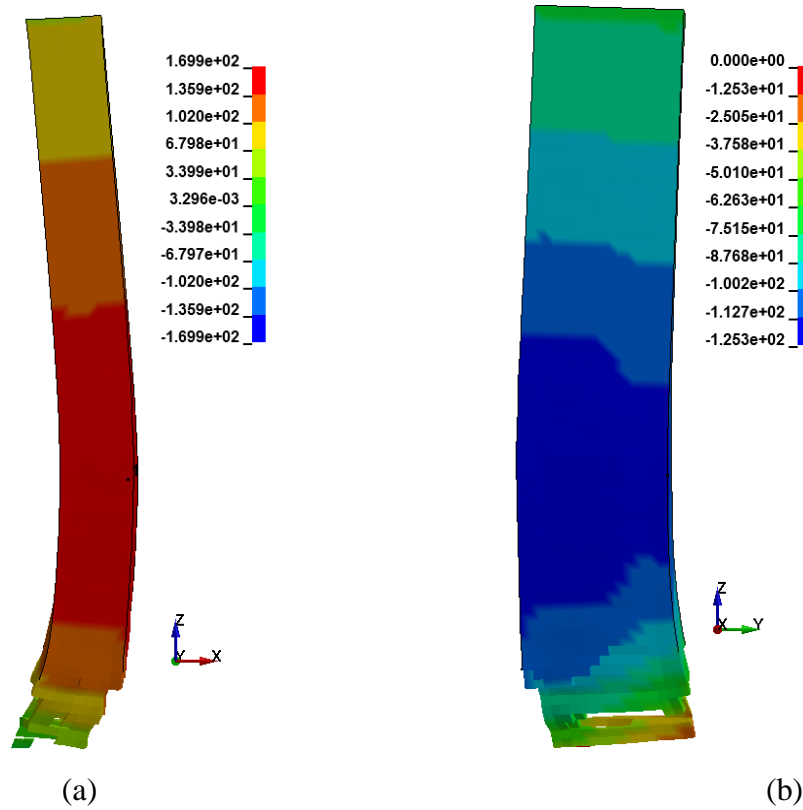


Figure 5.53: Externally blasted front columns deflection contours: (a) in x-direction, (b) in y-direction

The rear columns deflected because of the deflection of other structure members. The maximum deflection was at the top of the rear columns. The maximum x-axis deflection was 16.94 mm and the maximum y-axis deflection was 58.63 mm as shown in Figure 5.54.

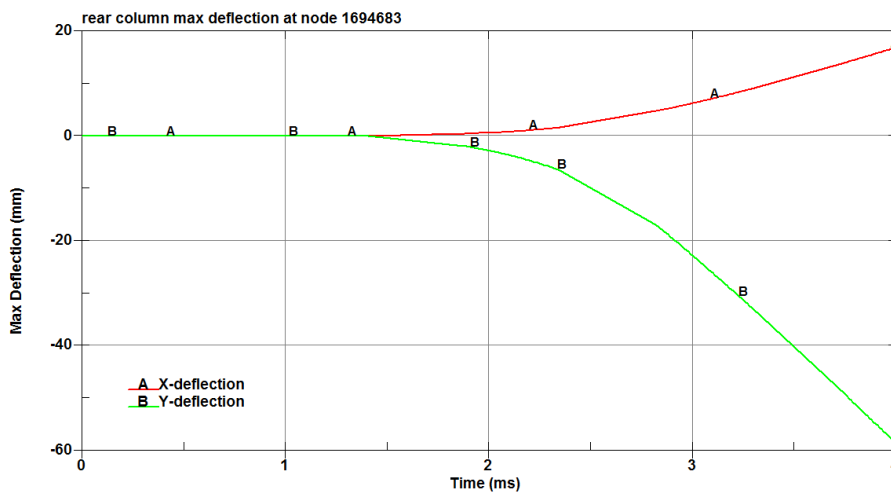


Figure 5.54: Externally blasted rear columns deflection

Figure 5.55 shows the contours of the x -axis deflection and the y -axis deflection for the rear column.

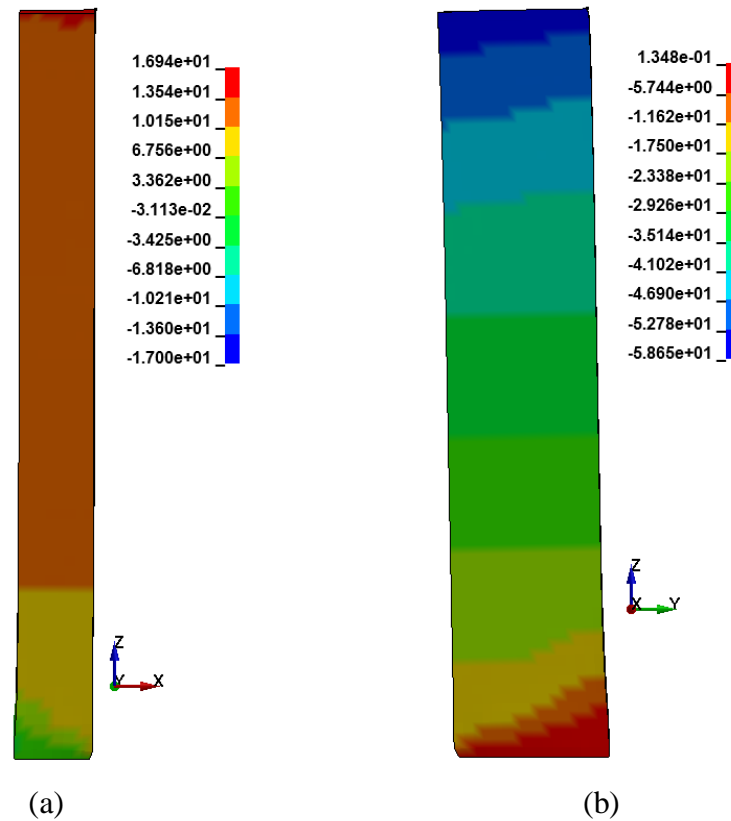


Figure 5.55: Externally blasted rear columns deflection contours: (a) in x -direction, (b) in y -direction

5.5.4 Deflection of slab members

The deformation of the externally blasted slab members increased since the blast wave arrival to the slab at 0.56 ms and reached the maximum values at the end of the analysis at 4.00 ms. The value of the deflection depended on the distance of the member from the explosion center.

The maximum x -axis deflection was in the main beam and the minimum x -axis deflection was in the rear secondary beam as shown in Figure 5.56.

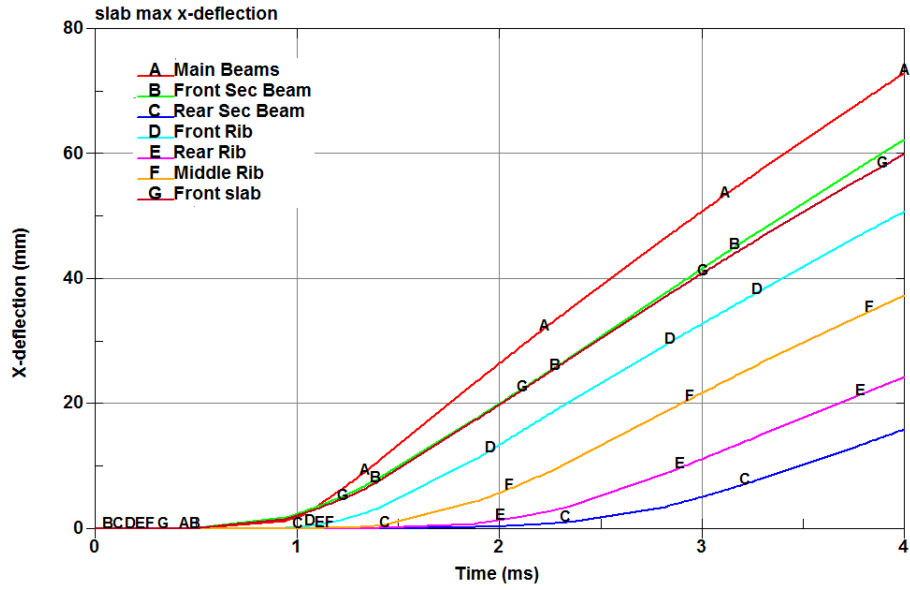


Figure 5.56: Externally blasted slab members maximum x -deflections

Figure 5.57 shows the contours of x -deflection in the externally blasted slab.

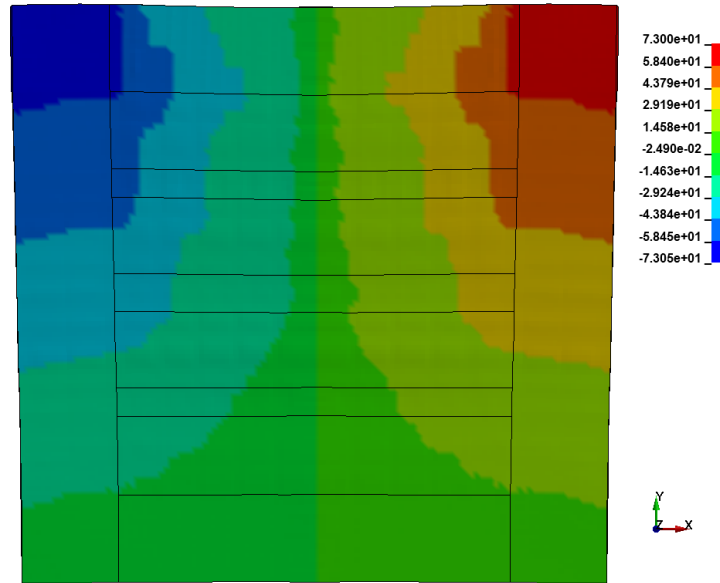


Figure 5.57: Externally blasted slab x -deflection contours

The maximum y -axis deflection was in the front secondary beam and the minimum y -axis deflection was in the rear rib as shown in Figure 5.58.

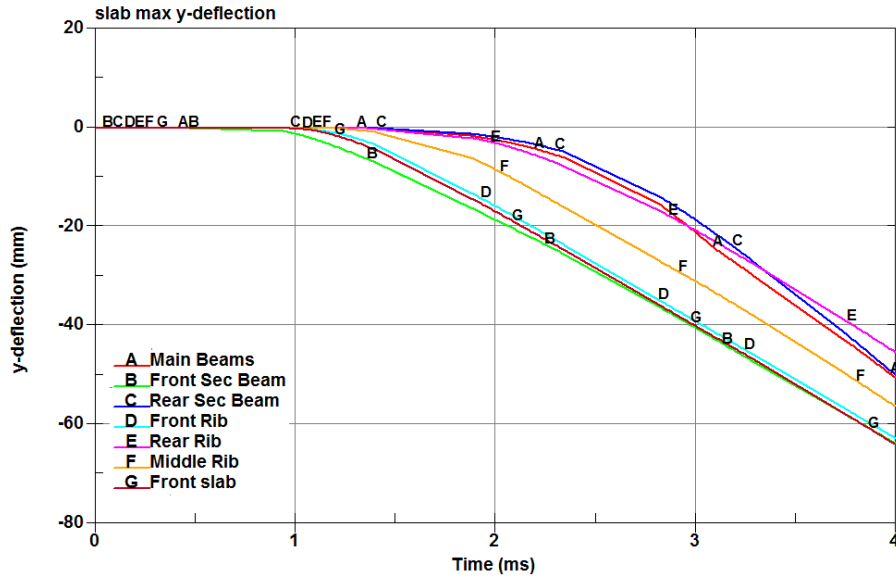


Figure 5.58: Externally blasted slab members maximum y-deflections

Figure 5.59 shows the contours of y-axis deflection in the externally blasted slab.

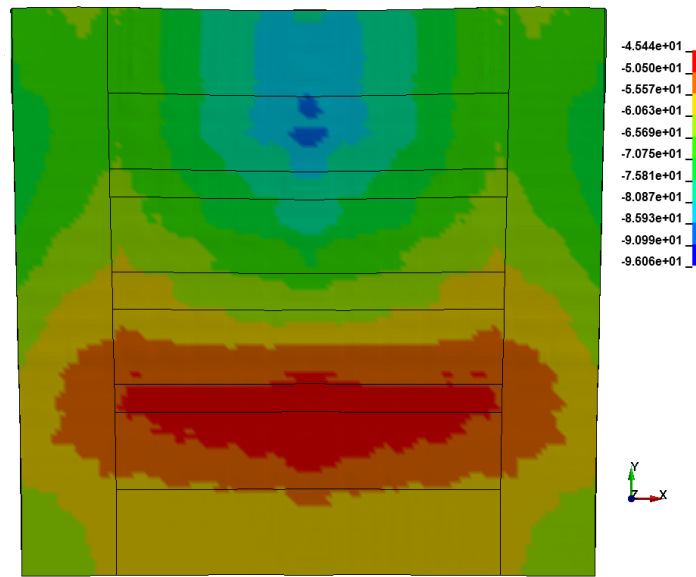


Figure 5.59: Externally blasted slab y-deflection contours

The z-axis deflection of the externally blasted members reached a maximum value in the positive z-direction in the middle of the member and reached a maximum value in the negative z-direction in the edges of the members. The members close to the explosion reached the maximum positive deflection value and decreased to a minor value at the end of the analysis but stayed positive. The members far from the explosion reached the maximum positive deflection value and decreased and reached the end of the analysis with negative deflection values. The maximum positive

deflection value was in the main beams and the minimum positive deflection value was at the rear secondary beam as shown in Figure 5.60.

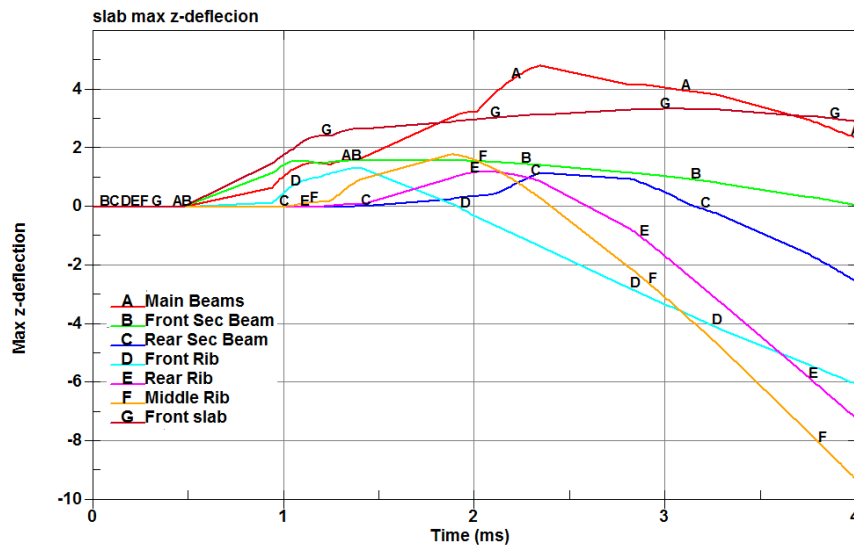


Figure 5.60: Externally blasted slab members maximum z-axis deflections

The negative z-axis deflection for the externally blasted slab members was resulted from the severe deformation of the front columns, so the members close to the explosion had the greatest values of the deflection and the members far from the explosion had the smallest values. The maximum negative z-deflection value was in the main beams and the minimum negative z-deflection value was at the rear secondary beam as shown in Figure 5.61.

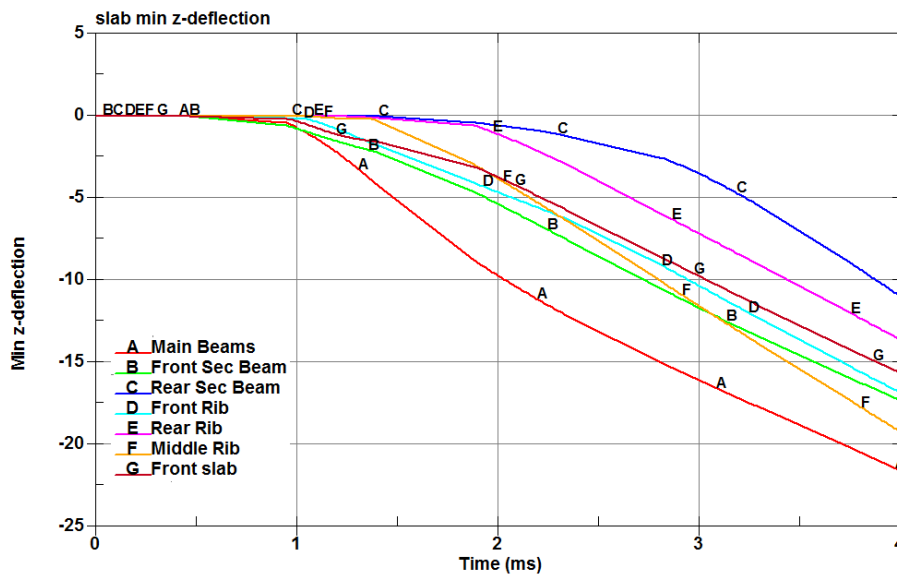


Figure 5.61: Externally blasted slab members minimum z-deflections

Figure 5.62 shows the contours of z -deflection in the externally blasted slab.

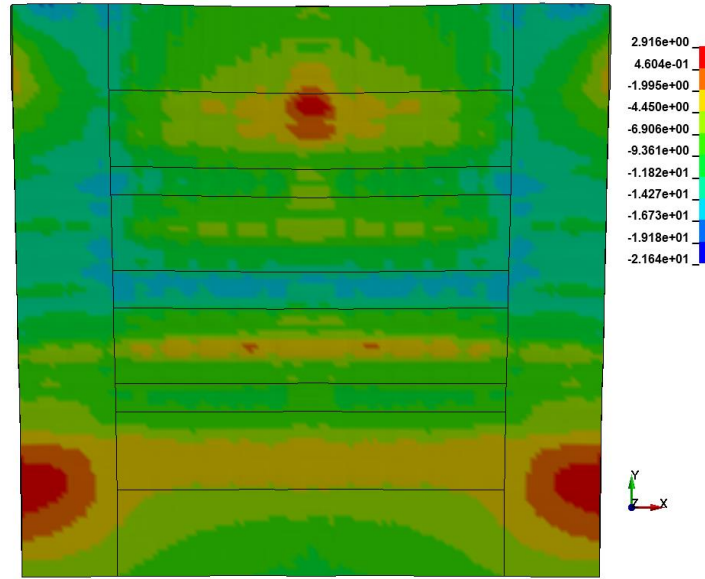


Figure 5.62: Externally blasted slab z -deflection contours

Values of deflections in all directions for the externally blasted slab members are shown in Table 5.16.

Table 5.16: Maximum deflection values for externally blasted slab members

Slab member	Deflection (mm)			
	X	Y	Z upward	Z downward
Main beams	73.00	75.45	4.84	21.64
Front Secondary beams	62.33	96.06	1.60	17.34
Rear secondary beams	15.90	59.57	1.16	10.99
Front rib	50.81	88.37	1.33	16.86
Rear rib	24.28	53.83	1.20	13.63
Middle rib	37.39	73.99	1.79	19.23
Front top slab	60.04	89.75	3.34	15.68

Chapter 6: Conclusion and recommendations

6.1 Modeling RC structure under blast loading

LS-Prepost of LS-DYNA was used to model a simple structure subjected to blast load and LS-DYNA finite element software was used to analyze it. Concrete and steel was modeled using solid elements, and the blast load was modeled using the simplest method in LS-DYNA, which is the empirical method because of its simplicity, time saving, and its need to moderate computer specifications.

A verification of the software analysis were made by comparing test results for a column from Williamson, Bayrak et al. (2010), with results of modeling and analyzing the same column in LS-DYNA. The results were satisfying.

A case study of a simple structure subjected to blast load was analyzed, and the results were recorded. A study of the effect of strengthening concrete on the behavior of a structure subjected to blast loads was conducted. And the effect of changing the blast location was studied.

6.2 Conclusions

- 1- The values of tension stresses for the columns with the 58 MPa strength concrete was increased by about 150% when compared to those of the columns with the 29 MPa Strength concrete.
- 2- The values of compression stresses for columns with 58 MPa compressive strength concrete were increased by about 175% in x -direction, 146% in y -direction, and 154% in z -direction when compared to those of 29 MPa compressive strength concrete.
- 3- The value of Von-Mises stress for 58 MPa compressive strength concrete column were 111% greater than that of 29 MPa compressive strength concrete column.
- 4- The values of tension, compression, and Von-Mises stresses in the 58 MPa compressive strength concrete slab members were increased by about 150% when compared to those of the 29 MPa compressive strength concrete slab members.
- 5- The values of deflection were decreased slightly or almost unchanged in all directions for the slab members with the 58 MPa compressive strength concrete

when compared to those of the slab members with the 29 MPa compressive strength concrete.

- 6- Changing the explosion location outside the building changed the behavior of the structure completely. The structure deflected in the negative y-direction. The members close to the explosion had the higher deflection values and affected by higher stresses.

6.3 Recommendations

Based on the achievements and work of current research, it is recommended to study several improvements that may be targeted for future work.

- 1- The reinforced concrete structure could be improved by using other material models for concrete to show better performance of the behavior of concrete.
- 2- Further studies could use beam elements for concrete to show results for moment and shear.
- 3- The model could be enhanced by using finer meshes for concrete and steel.
- 4- Other parametric studies, like the lack of stirrups and the yield strength of the longitudinal bars should be conducted to study its effect on a structure subjected to blast load.
- 5- Other methods of modeling blast loads could be verified, used and compared to determine the most reliable method.
- 6- An independent study on the behavior of reinforcement steel subjected to blast load could be conducted.
- 7- The thermal effect of the blast loads on reinforced concrete could be conducted.
- 8- Super computer could be used to provide higher specifications for modeling larger structures or the same structure for longer time, to record the progressive collapse caused by blast loads.

With further development of this work, it is believed that modeling a structure subjected to blast loads and studying thermal effects of the explosion on reinforced concrete could be very promising.

References

- ACI-318-Committee. (2011). *Building Code Requirements for Structural Concrete (ACI 318-11) and Commentary*. USA: American Concrete Institute.
- Almusallam, T. H., Elsanadedy, H., Abbas, H., Ngo, T., & Mendis, P. (2010). *Numerical analysis for progressive collapse potential of a typical framed concrete building*. *International Journal of Civil & Environmental Engineer*, 10(2), 40-46.
- Army, U., Navy, U., & Force, U. A. (1990). *Structures to resist the effects of accidental explosions*. Department of Defense. USA. 1300pp.
- Baker, W. E., Cox, P., Kulesz, J., Strehlow, R., & Westine, P. (1983). *Explosion hazards and evaluation*. Elsevier Scientific Publishing Company. (Vol. 5). 807pp.
- Borrvall, T., & Riedel, W. (2011). *The RHT concrete model in LS-DYNA*. In *Proceedings of the 8th European LS-DYNA Users Conference*, Strasbourg.
- Brode, H. L. (1955). *Numerical solutions of spherical blast waves*. *Journal of Applied physics*, 26(6), 766-775.
- Dusenberry, D. O. (2010). *Handbook for Blast Resistant Design of Buildings*. John Wiley & Sons Inc. Canada. 486pp.
- Gibson, P. (1994). *Blast overpressure and survivability calculations for various sizes of explosive charges*. Army Natick Research Development and Engineering Center. USA. 20pp
- Grote, D., Park, S., & Zhou, M. (2001). *Dynamic behavior of concrete at high strain rates and pressures: I. experimental characterization*. *International Journal of Impact Engineering*, 25(9), 869-886.
- Hussain Shah, Q., & Hasan, H. A. (2012). *LS-DYNA for beginners: an insight into Ls-Prepost and Ls-Dyna*: LAP LAMBERT Academic Publishing. Germany. 146pp.

- Jayasooriya, R., Thambiratnam, D., Perera, N., & Kosse, V. (2009). *Response and damage evaluation of reinforced concrete frames subjected to blast loading*. In Proceedings of the 34th Conference on Our World in Concrete & Structures- Conference Documentation Volume XXVIII: 123-130.
- Karlos, V., & Solomos, G. (2013). *Calculation of Blast Loads for Application to Structural Components*. Institute for the Protection and Security of the Citizen. Luxembourg. 59pp.
- Kocczaz, Z., Sutcu, F., & Torunbalci, N. (2008). *Architectural and structural design for blast resistant buildings*. In the 14th World Conference on Earthquake Engineering, Beijing, China, Beijing, China.
- Le Blanc, G., Adoum, M., & Lapoujade, V. (2005). *External blast load on structures– Empirical approach*. In 5th European LS-DYNA Users Conference, France, Birmingham, UK.
- Logan, D. (2007). *A first course in the finite element method*. Fourth edition. Thomson. Canada. 836pp.
- LS-DYNA, M. (2014a). *LS-DYNA Keyword User,s Manual Version 971*. Livermore Software Technology Corporation. Vol. I-II. California. 2444pp.
- LS-DYNA, M. (2014b). *LS-DYNA Theorys Manual Version 971*. Livermore Software Technology Corporation. California. 831pp.
- Madenci, E., & Guven, I. (2006). *The finite element method and applications in engineering using ANSYS*. Springer Science & Business Media. USA. 700pp.
- Marchand, K. A., & Alfawakhiri, F. (2004). *Facts for steel buildings 2: Blast and progressive collapse*. American Institute of Steel Construction. USA. 67pp.
- Morales Alonso, G., Franco, C., Angel, D., Galvez Diaz-Rubio, F., Erice Echávarri, B., & Sanchez Galvez, V. (2011). *Analysis of the Fracture of Reinforced Concrete Flat Elements Subjected to Explosions. Experimental Procedure and Numerical Validation*. Annals of Fracture Mechanics, 28(2), 433-438.

- Moutoussamy, L., & Herve, G. (2011). *Qualification of *Constrained_Lagrange_In_Solid command for steel/concrete interface modeling*. In 8th LS-Dyna European User Conference, France.
- Murray, Y. D. (2004). *Theory and evaluation of concrete material model 159*. In 8th International LS-DYNA users conference, Michigan, USA.
- Murray, Y. D. (2007). *Users manual for LS-DYNA concrete material model 159*. U.S. Department of Transportation. USA. 92pp.
- Ngo, T., Mendis, P., Gupta, A., & Ramsay, J. (2007). *Blast loading and blast effects on structures—an overview*. *Electronic Journal of Structural Engineering*, 7, 76-91.
- Ngo, T., Mendis, P., Hongwei, M., & Mak, S. (2004). *High strain rate behaviour of concrete cylinders subjected to uniaxial compressive impact loading*. In the Proceeding of 18th Australasian Conference on the Mechanics of Structures and Materials, Perth, Australia.
- Pereira, L., Weerheijm, J., & Sluys, L. (2013). *Damage prediction in a concrete bar due to a compression and tension pulse: A comparison of the K&C, the CSCM and the RHT material models in LS-DYNA*. In the 15th ISIEMS Conference: International Symposium on the Interaction of the Effects of Munitions with Structures, Potsdam, Germany.
- Puryear, J. M. H., Stevens, D. J., Marchand, K. A., Williamson, E. B., & Crane, C. K. (2012). *ALE Modeling of Explosive Detonation on or near Reinforced-Concrete Columns*. In the 12th International LS-DYNA Users Conference, Michigan, USA.
- Razaqpur, A. G., Tolba, A., & Contestabile, E. (2007). *Blast loading response of reinforced concrete panels reinforced with externally bonded GFRP laminates*. *Composites Part B: Engineering*, 38(5), 535-546.
- Remennikov, A. M. (2003). *A review of methods for predicting bomb blast effects on buildings*. *Journal of battlefield technology*, 6(3), 5-12.

- Schwer, L. E. (2014). *Modeling Rebar: The Forgotten Sister in Reinforced Concrete Modeling*. In the 13th International LS-DYNA Users Conference. Michigan, USA.
- Shugar, T., Holland, T., & Malvar, L. (1992). *Applications of finite element technology to reinforced concrete explosives containment structures*. Naval Civil Engineering Lab. California, USA.
- Tabatabaei, Z. S., & Volz, J. S. (2012). *A Comparison between Three Different Blast Methods in LS-DYNA®: LBE, MM-ALE, Coupling of LBE and MM-ALE*. In the 12th International LS-DYNA User Conference, Michigan, USA.
- Tai, Y., Chu, T., Hu, H., & Wu, J. (2011). *Dynamic response of a reinforced concrete slab subjected to air blast load*. Theoretical and applied fracture mechanics, 56(3), 140-147.
- Williamson, E. B., Bayrak, O., Williams, G. D., Davis, C. E., Marchand, K. A., McKay, A. E., Wassef, W. (2010). *Blast-resistant highway bridges: Design and detailing guidelines*. Transportation Research Board. Vol. 645. USA. 152pp.
- Wu, Y., Crawford, J. E., Magallanes, J. M., & Way, N. (2012). *Performance of LS-DYNA concrete constitutive models*. In the 12th International LS-DYNA Users Conference, Michigan, USA.